


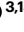
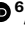



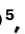







# Unlocking opioid neuropeptide dynamics with genetically encoded biosensors

Received: 28 April 2023

Accepted: 5 June 2024

Published online: 15 July 2024


 Check for updates

Chunyang Dong <sup>1,12</sup>, Raajaram Gowrishankar<sup>2,12</sup>, Yihan Jin<sup>1,13</sup>, Xinyi Jenny He <sup>3,13</sup>, Achla Gupta<sup>4</sup>, Huikun Wang<sup>5</sup>, Nilüfer Sayar-Atasoy <sup>6</sup>, Rodolfo J. Flores<sup>5</sup>, Karan Mahe<sup>1</sup>, Nikki Tjahjono<sup>1</sup>, Ruqiang Liang<sup>1</sup>, Aaron Marley<sup>7</sup>, Grace Or Mizuno<sup>1</sup>, Darren K. Lo <sup>8</sup>, Qingtao Sun <sup>9</sup>, Jennifer L. Whistler<sup>10</sup>, Bo Li <sup>9</sup>, Ivone Gomes<sup>4</sup>, Mark Von Zastrow<sup>7</sup>, Hugo A. Tejada <sup>5</sup>, Deniz Atasoy <sup>6</sup>, Lakshmi A. Devi<sup>4</sup>, Michael R. Bruchas <sup>2</sup> , Matthew R. Banghart <sup>3</sup>  & Lin Tian <sup>1,11</sup> 

Neuropeptides are ubiquitous in the nervous system. Research into neuropeptides has been limited by a lack of experimental tools that allow for the precise dissection of their complex and diverse dynamics in a circuit-specific manner. Opioid peptides modulate pain, reward and aversion and as such have high clinical relevance. To illuminate the spatiotemporal dynamics of endogenous opioid signaling in the brain, we developed a class of genetically encoded fluorescence sensors based on kappa, delta and mu opioid receptors:  $\kappa$ Light,  $\delta$ Light and  $\mu$ Light, respectively. We characterized the pharmacological profiles of these sensors in mammalian cells and in dissociated neurons. We used  $\kappa$ Light to identify electrical stimulation parameters that trigger endogenous opioid release and the spatiotemporal scale of dynorphin volume transmission in brain slices. Using in vivo fiber photometry in mice, we demonstrated the utility of these sensors in detecting optogenetically driven opioid release and observed differential opioid release dynamics in response to fearful and rewarding conditions.

Neuropeptides (NPs) are small proteins that modify neural activity, regulate brain states and control blood flow in the nervous system<sup>1–5</sup>. Neurons synthesize and release NPs in addition to fast-acting neurotransmitters (NTs) such as glutamate and GABA<sup>6</sup>. NPs activate select G-protein-coupled receptors to modulate synaptic strength, neuronal excitability and circuit dynamics. Unlike small-molecule NTs, NPs are hypothesized to be released into the extrasynaptic space and thought to be cleared by proteolysis and diffusion over a range of 100 micrometers to millimeters to affect neurons, leading to long-lasting modulatory effects<sup>6–8</sup>. A comprehensive understanding of the conditions that trigger NP release from neurons and the spatiotemporal extent of peptide release has been lacking, and yet is critical for understanding the actions of NPs at the molecular, cellular, circuit and network levels to their influence on animal behavioral states.

Among all known NPs, the opioid system is the most functionally diverse and clinically relevant family<sup>9–15</sup>. The opioid receptor family contains distinct receptor subtypes—kappa, delta and mu ( $\kappa$ OR,  $\delta$ OR and  $\mu$ OR, respectively), as well as nociception receptors—which can be activated by at least 20 endogenous opioid peptides with differential affinity and selectivity<sup>12,16,17</sup>.  $\kappa$ OR,  $\delta$ OR and  $\mu$ OR and nociception opioid receptors activate inhibitory  $G_{i/o}$  G-proteins, which leads to reductions in cellular excitability and NT secretion in receptor-expressing neurons. Opioid peptides and their receptors are widely distributed across cortical and subcortical brain regions<sup>18,19</sup>. It is thought that the diversity of opioid peptides is essential for modulating complex behavior and physiological processes, such as pain, reward, substance abuse/dependence and stress<sup>20</sup>. Opioid drugs targeting these receptors are used to treat severe pain, but prolonged use can lead to addiction and

A full list of affiliations appears at the end of the paper.  e-mail: [mbruchas@uw.edu](mailto:mbruchas@uw.edu); [mbanghart@ucsd.edu](mailto:mbanghart@ucsd.edu); [lin.tian@mpfi.org](mailto:lin.tian@mpfi.org)

overdose<sup>21</sup>. Newer efforts have isolated opioid receptors as potential targets for anxiety, depression and addiction<sup>22,23</sup>. Some of these efforts have been hindered by a lack of high-resolution methods for studying endogenous NP release *in vivo*.

Studies into NP systems, especially opioid systems, have been historically challenging due to a lack of sensitive experimental tools in the spatial and temporal domains, which can facilitate understanding the complexity and diversity of NP signaling in a circuit-specific manner. The endogenous opioid peptides have similar structures and bind to different opioid receptors with relatively lower selectivity than some NP molecules at their cognate receptors<sup>16</sup>. Physiologically relevant NP release by neurons is thought to be difficult to trigger, and the released concentration may also be at orders of magnitude lower than classical NTs (nanomolar versus micromolar or even submillimolar)<sup>24</sup>, making it extremely difficult to adequately probe the conditions to trigger the endogenous peptide release and measure the released concentration *ex vivo* and *in vivo*<sup>25</sup>. As a result, it has been exceedingly difficult to study the processes that regulate opioid NP release. Recent technological advances have begun to reveal the anatomical and spatiotemporal features of opioid signaling<sup>26,27</sup>. Transcriptomics studies have documented the distribution of opioid peptide–receptor pairs across cell types in the cortex, highlighting the substantial function of opioid signaling in mediating transcellular communication in neural circuits<sup>28</sup>. Features of peptide diffusion and clearance have been revealed by combining light-triggered photorelease of caged enkephalin with electrophysiological measurements of peptide-evoked currents in brain slices<sup>29</sup>. *In vivo*, optogenetically driven peptide release has been detected using high-speed microdialysis<sup>30</sup>. Despite these successes, it remains challenging to quantify behaviorally relevant endogenous opioid peptide release with subsecond and subregional resolution.

To bridge this gap in technology, we developed a class of genetically encoded opioid peptide indicators, κLight, δLight and μLight, based on κOR, δOR and μOR respectively. We used these sensors to systematically evaluate ligand binding-induced conformational changes at all three receptors and thereby established the binding specificity and efficacy of 14 opioid peptides and 8 opioid drugs. In acute hippocampal slices, we used κLight to determine electrical parameters that can trigger endogenous opioid peptide release and quantified the diffusion rate of dynorphin using photoactivatable peptides. Using optogenetics to stimulate opioid peptide release, we detected circuit-specific endogenous opioid signaling *in vivo*. Finally, we used these sensors to reveal rapid opioid peptide release in a subregion-specific manner in response to fear and reward conditions within the nucleus accumbens (NAc) of awake, behaving mice.

## Results

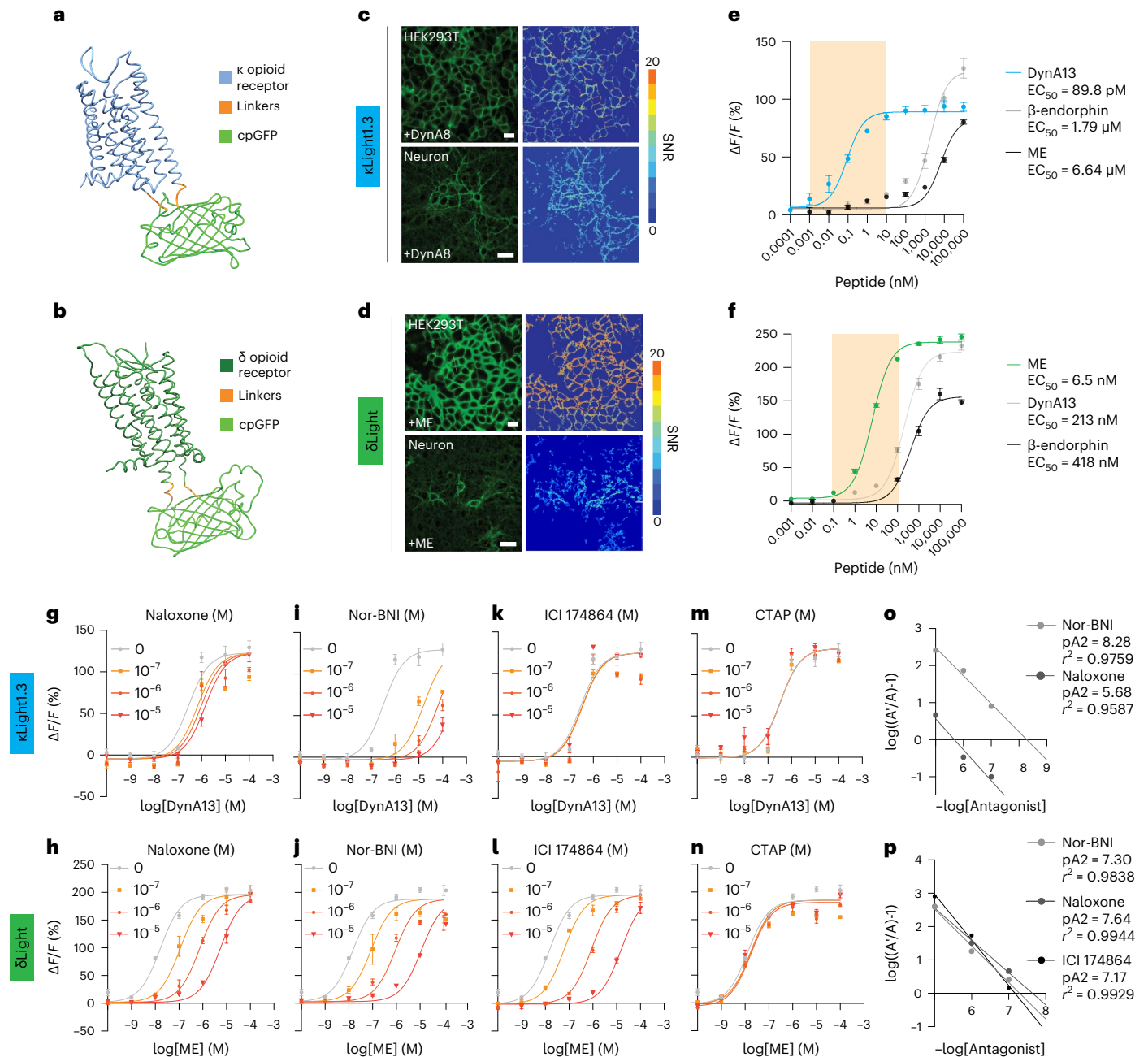
### Design and engineering of opioid biosensors

We replaced amino acids between R257 in the intracellular loop (ICL) 3 and R6.24 on the transmembrane domain (TM) 6 of the human κOR, S247 in ICL3 and K6.24 in TM6 of the human δOR, and S6.23 in TM6 and K6.24 in TM6 of human μOR, with a circularly permuted green fluorescent protein (cpGFP), to generate κLight, δLight and μLight sensors, respectively (Fig. 1a,b and Extended Data Fig. 1a,b). The dynamic range of each sensor was optimized by screening linker compositions. In total, the dynamic ranges of 698 κLight variants, 64 δLight variants and 233 μLight variants were examined in response to U50,488, met-enkephalin (ME) and DAMGO, respectively (Extended Data Fig. 1c). To promote excellent membrane localization, we fused a telencephalin (TlcnC) tag<sup>31</sup> or endoplasmic reticulum (ER) export motif (FCYENEV)<sup>32</sup> followed by a chain of GS linker and the proximal restriction and clustering (PRC) tag<sup>33</sup> to the C terminus of κLight, δLight and μLight. We named these new variants κLight1.3, δLight1 and μLight1, respectively. In addition, we mutated D3.22 of κOR and D3.32 in δOR in the binding pockets to attenuate the ligand binding, which led to two control sensors κLight0 and δLight0.

When transiently expressed in mammalian HEK293 cells and dissociated neuronal cultures, we observed excellent membrane expression of κLight1.3, δLight and μLight. All three sensors were activated by their endogenous receptor agonists (100 μM), dynorphin A1-8 (DynA8), ME and β-endorphin, respectively (signal-to-noise ratios (SNR) values for κLight1.3 (HEK) = 7.5 ± 0.45; κLight1.3 (neuron) = 5.6 ± 0.2; δLight (HEK) = 16 ± 0.62; δLight (neuron) = 8.9 ± 0.43; μLight (HEK) = 4.7 ± 0.26) (Fig. 1c,d and Extended Data Fig. 1d). The ligand-induced responses (κLight1.3 change in fluorescence ( $\Delta F/F$ ); neuron) = 151% ± 5.1%; δLight  $\Delta F/F$  (neuron) = 123% ± 19.4%; μLight  $\Delta F/F$  (neuron) = 19.6% ± 3.2%) were blocked by naloxone (1 mM), which is an antagonist for all three receptors (Extended Data Fig. 1e).

To eliminate response variability due to inconsistent expression level of sensors via transient transfection, we developed HEK293T cell lines stably expressing κLight1.3, δLight and μLight. Using these cell lines, we characterized the promiscuity of endogenous opioid peptides on activating sensors<sup>34</sup>. First, all three sensors have consistent excitation peak wavelengths at 495 nm and emission peaks at 515 nm (Extended Data Fig. 1f). Second, *in situ* titration showed that all three sensors can be activated by three distinct endogenous opioid peptides but with different potency and efficacy. κLight1.3 responded to dynorphin A1-13 (DynA13) with an apparent half maximal effective concentration ( $EC_{50}$ ) of 89.8 pM, which is three magnitudes higher than β-endorphin and ME. However, at higher concentrations (>10 μM), κLight1.3 displayed higher fluorescence changes to β-endorphin, followed by DynA13 and ME ( $\Delta F/F$  (κLight - DynA13) = 93.6% ± 3.9%;  $\Delta F/F$  (κLight - β-endorphin) = 126.9% ± 8.6%;  $\Delta F/F$  (κLight - ME) = 80.3% ± 1.8%; Fig. 1e). δLight was activated by ME with an  $EC_{50}$  of 6.5 nM, which is two orders of magnitude greater than DynA13 and β-endorphin, and had higher fluorescence efficacy compared to these two peptides ( $\Delta F/F$  (δLight - DynA13) = 232.6% ± 6.8%;  $\Delta F/F$  (δLight - β-endorphin) = 147.9% ± 4.1%;  $\Delta F/F$  (δLight - ME) = 246.1% ± 4.6%; Fig. 1f). In contrast, we did not observe apparent responses of control sensors when the binding pocket was ablated (κLight0 or δLight0; Extended Data Fig. 1g,h). To further examine the selectivity for κLight1.3 and δLight in the context of neurons, we infected dissociated hippocampal neurons with AAV9-*hSyn*-κLight1.3 and AAV9-*hSyn*-δLight, respectively. We performed *in situ* titration in dissociated hippocampal neurons in the same context as in the HEK293T stable cell line. Expectably, the selectivity of both sensors in neurons is consistent to that in HEK293T cells (Extended Data Fig. 1i,j). However, all three endogenous opioid peptides showed similar sensor potency and efficacy for μLight activation (Extended Data Fig. 2a), suggesting that further improvement and engineering are required. Together, at presumed physiological conditions (pM–100 nM), both κLight1.3 and δLight are selective and sensitive to endogenous opioid peptides.

Next, we sought to determine the selectivity of antagonists acting on κLight1.3 and δLight. By running the *in situ* titration in antagonist mode<sup>35</sup> using the same HEK293T stable cell lines, we were able to determine the selectivity of antagonists acting on κLight1.3 and δLight. In addition to naloxone, we chose nor-binaltorphimine (Nor-BNI), ICI 174864 and CTAP, which selectively antagonize κOR, δOR and μOR, respectively. As expected, increasing the concentration of naloxone (100 nM to 10 μM) shifted the apparent  $EC_{50}$  to the right for DynA13 and ME for κLight1.3 and δLight, respectively: naloxone inhibited δLight with twofold greater affinity than κLight ( $pA_2$  (δLight - naloxone) = 7.64,  $pA_2$  (κLight - naloxone) = 5.68). Nor-BNI displayed slightly higher affinity in blocking κLight than δLight ( $pA_2$  = 8.28 and 7.3, respectively; Fig. 1g–j,o,p). We did not observe apparent antagonism of κLight by ICI 174864, whereas it effectively inhibited activation of δLight by ME ( $pA_2$  δLight - ICI 174864 = 7.17; Fig. 1k,l,o,p). The μOR-selective antagonist CTAP did not affect the  $EC_{50}$  of DynA13 or ME in either κLight or δLight, respectively (Fig. 1m–p).

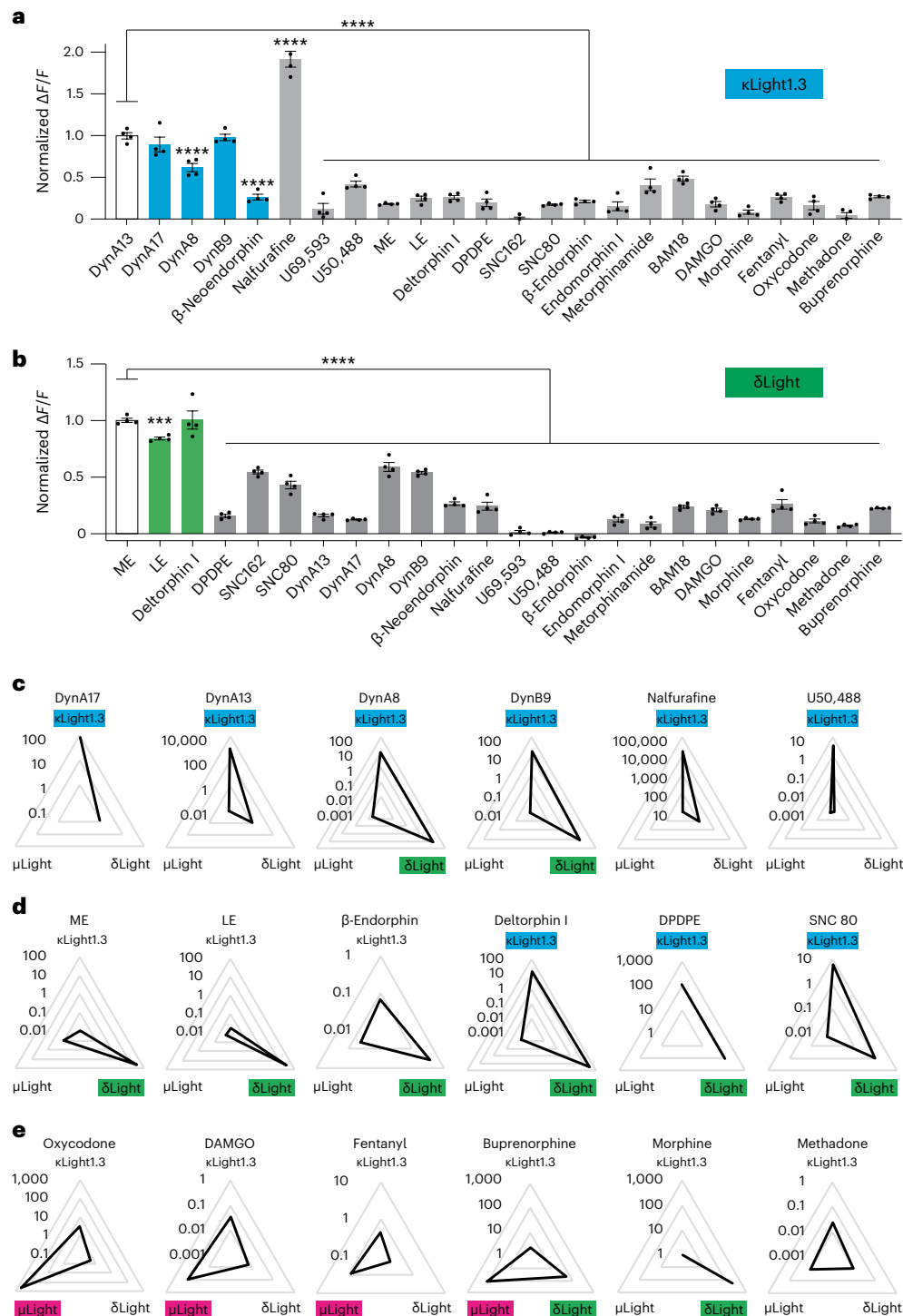


**Fig. 1 | Development of the opioid sensors.** **a, b**, Simulated structure of  $\kappa$ Light1.3 (**a**) and  $\delta$ Light (**b**). **c, d**, Representative images of four independent transient transfections of  $\kappa$ Light1.3 (**c**) and  $\delta$ Light (**d**) in HEK293T cells and cultured hippocampal neurons. Heat map indicates SNR upon addition of DynA8 (100  $\mu$ M) or ME (100  $\mu$ M). Scale bar, 20  $\mu$ m (cells) and 50  $\mu$ m (neurons). **e, f**, In situ titration of  $\kappa$ Light1.3 (**e**) and  $\delta$ Light (**f**)-expressing HEK293T cells respond to ligands in a concentration-dependent manner (DynA13, blue;  $\beta$ -endorphin, gray; ME, black). Error bars represent the s.e.m. The highlighted area corresponds to a concentration range from 1 pM to 10 nM or 100 pM to 100 nM. Dyn, dynorphin. **g, h**, Schild plot of  $\kappa$ Light1.3 (**g**) and  $\delta$ Light (**h**) dose response with 100 nM, 1  $\mu$ M and 10  $\mu$ M of naloxone. **i, j**, Schild plot of  $\kappa$ Light1.3 (**i**) and  $\delta$ Light (**j**) dose response with 100 nM, 1  $\mu$ M and 10  $\mu$ M of Nor-BNI. **k, l**, Schild plot of  $\kappa$ Light1.3 (**k**) and  $\delta$ Light (**l**) dose response with 100 nM, 1  $\mu$ M and 10  $\mu$ M of ICI 174864. **m, n**, Schild plot of  $\kappa$ Light1.3 (**m**) and  $\delta$ Light (**n**) dose response with 100 nM, 1  $\mu$ M and 10  $\mu$ M of CTAP. **o**, Combined Schild regression with Nor-BNI and naloxone on  $\kappa$ Light1.3. **p**, Combined Schild regression with Nor-BNI, naloxone and ICI 174864 on  $\delta$ Light. **e–o**,  $n = 4$ . Error bars represent the s.e.m.

### Selectivity and pharmacology of the opioid biosensors

We next used a low concentration (10 nM) of a broad panel of endogenous and synthetic ligands to evaluate their rank order of response for inducing sensor fluorescence. We found that known  $\kappa$ OR-selective endogenous peptides induced significantly greater fluorescence changes at  $\kappa$ Light compared to  $\delta$ OR-selective or  $\mu$ OR-selective ligands. Among the dynorphin peptides, the shorter-form dynorphin DynA8 induced lower activation of  $\kappa$ Light compared to DynA13. Interestingly, nalfurafine, a synthetic  $\kappa$ OR agonist, elicited an almost twofold greater

fluorescence change compared to the dynorphins (Fig. 2a). For  $\delta$ Light cells, enkephalins and  $\delta$ OR-selective agonists elicited larger responses compared to other ligands; deltorphin I displayed similar efficacy as ME and LE for  $\delta$ Light activation (Fig. 2b). Endogenous opioid peptide agonists at  $\mu$ OR, including  $\beta$ -endorphin, endomorphin, metorphinamide and BAM18, displayed various efficacies for  $\kappa$ Light1.3 and  $\delta$ Light activation, although to a much smaller extent compared to  $\kappa$ OR-specific and  $\delta$ OR-specific peptides. Notably, U50,488 and U69,593 selectively activated  $\kappa$ Light over  $\delta$ Light, while SNC80 and SNC162 activated  $\delta$ Light



**Fig. 2 | Pharmacological characterization of  $\kappa$ Light and  $\delta$ Light.** **a**, Normalized  $\Delta F/F$  of  $\kappa$ Light1.3 upon addition of the listed compounds (10 nM).  $\Delta F/F$  of all compounds are normalized to DynA13 (DynA13:  $1 \pm 0.03$ , DynA17:  $0.89 \pm 0.08$ , DynA8:  $0.61 \pm 0.04$ , DynB9:  $0.97 \pm 0.03$ ,  $\beta$ -neoendorphin:  $0.26 \pm 0.03$ , nalfurafine:  $1.91 \pm 0.09$ , U69,593:  $0.12 \pm 0.06$ , U50,488:  $0.42 \pm 0.03$ , ME:  $0.18 \pm 0.005$ , LE:  $0.24 \pm 0.02$ , deltorphin I:  $0.26 \pm 0.02$ , DPDPE:  $0.19 \pm 0.04$ , SNC162:  $0.009 \pm 0.02$ , SNC 80:  $0.17 \pm 0.008$ ,  $\beta$ -endorphin:  $0.21 \pm 0.01$ , endomorphin I:  $0.15 \pm 0.05$ , metorphinamide:  $0.41 \pm 0.06$ , BAM18:  $0.48 \pm 0.03$ , DAMGO:  $0.17 \pm 0.03$ , morphine:  $0.08 \pm 0.02$ , fentanyl:  $0.26 \pm 0.02$ , oxycodone:  $0.16 \pm 0.04$ , methadone:  $0.04 \pm 0.03$ , buprenorphine:  $0.27 \pm 0.01$ ;  $n = 4$  wells each. \*\*\*\* $P < 0.0001$ , one-way analysis of variance (ANOVA) compared to DynA13 with Sidak's multiple-comparisons test). Error bars represent the s.e.m. **b**, Normalized  $\Delta F/F$  of  $\delta$ Light upon addition of the listed compounds (10 nM).

$\Delta F/F$  of all compounds were normalized to ME (ME:  $1 \pm 0.01$ , LE:  $0.84 \pm 0.01$ , deltorphin I:  $1 \pm 0.07$ , DPDPE:  $0.15 \pm 0.01$ , SNC162:  $0.54 \pm 0.02$ , SNC80:  $0.42 \pm 0.03$ , DynA13:  $0.15 \pm 0.01$ , DynA17:  $0.12 \pm 0.004$ , DynA8:  $0.58 \pm 0.03$ , DynB1-9:  $0.53 \pm 0.01$ ,  $\beta$ -neoendorphin:  $0.26 \pm 0.01$ , nalfurafine:  $0.24 \pm 0.03$ , endomorphin I:  $0.12 \pm 0.014$ , U50,488:  $0.009 \pm 0.004$ ,  $\beta$ -endorphin:  $-0.03 \pm 0.004$ , endomorphin I:  $0.12 \pm 0.01$ , metorphinamide:  $0.07 \pm 0.02$ , BAM18:  $0.23 \pm 0.01$ , DAMGO:  $0.2 \pm 0.01$ , morphine:  $0.12 \pm 0.005$ , fentanyl:  $0.25 \pm 0.04$ , oxycodone:  $0.11 \pm 0.01$ , methadone:  $0.06 \pm 0.006$ , buprenorphine:  $0.22 \pm 0.003$ ;  $n = 4$  wells each. \*\*\*\* $P < 0.0001$ , \*\*\* $P = 0.0006$ , one-way ANOVA compared to DynA13 with Dunnett's multiple-comparisons test). Error bars represent the s.e.m. **c-e**, log s-slope values (in  $nM^{-1}$ ) of  $\kappa$ OR (c),  $\delta$ OR (d) and  $\mu$ OR (e)-specific ligands plotted in triangle plots ( $\kappa$ Light, blue;  $\delta$ Light, green;  $\mu$ Light, magenta). Higher s-slope values are located on the outer triangle. Enk, enkephalin.

over  $\kappa$ Light, confirming the sensors' specificity to receptor-specific small-molecule agonists (Fig. 2a,b).

We then used radar plots to compare the proportionality constant (s-slope) of various receptor-selective ligands for activating each sensor (Fig. 2c–e and Extended Data Table 1). The s-slope is a constant that links the variables of dynamic range ( $\Delta F/F_{\max}$ ) and  $EC_{50}$  of a given sensor response to a drug, defined as  $\Delta F/F_{\max}/EC_{50}$ . It highlights both the efficacy and potency of drugs on sensor responses<sup>36</sup>. By plotting s-slope values of individual ligands on three sensors as a radar plot, we found that the long forms of dynorphin are more potent in activating  $\kappa$ Light1.3 than the short forms, the latter of which displayed considerable activity at  $\delta$ Light as well. Both nalfurafine and U50,488 were selective for  $\kappa$ Light1.3 (Fig. 2c). The enkephalins (both ME and Leu-Enk (LE)), as well as  $\beta$ -endorphin, were highly selective for  $\delta$ Light, whereas deltorphin I and DPDPE displayed similar s-slopes for  $\kappa$ Light1.3 and  $\delta$ Light. Despite low efficacy at  $\kappa$ Light1.3, the s-slope of SNC80 was slightly higher at  $\kappa$ Light1.3 than that at  $\delta$ Light (Fig. 2d). Notably,  $\mu$ Light was insensitive to morphine, whereas the latter induced slight fluorescence increases at  $\kappa$ Light1.3 and  $\delta$ Light. In contrast, methadone activated all three sensors with similar efficacy and potency. Buprenorphine activates all three sensors but showed higher potency for  $\mu$ Light and  $\delta$ Light. On the other hand, other  $\mu$ OR-selective synthetic drugs, including DAMGO, fentanyl and oxycodone, engaged  $\mu$ Light with higher s-slopes compared to  $\kappa$ Light1.3 and  $\delta$ Light (Fig. 2e). Interestingly, oxycodone and buprenorphine suppressed, rather than enhanced,  $\mu$ Light fluorescence; thus, the s-slope was calculated using the absolute  $\Delta F/F_{\max}$  (Extended Data Fig. 2b).

To determine whether the insertion of cpGFP perturbs the ligand binding properties of these receptor-based opioid sensors, we first assessed the binding profile of both sensors and their corresponding receptors, followed by examining the ability of  $\kappa$ Light1.3 and  $\delta$ Light to engage G-protein and  $\beta$ -arrestin pathways coupled to  $\kappa$ OR and  $\delta$ OR, respectively. We conducted a radioligand binding assay using cells expressing each sensor and a panel of ligands that includes several endogenous peptides<sup>16,37,38</sup>. For cells stably expressing  $\mu$ Light, endogenous opioid peptides displaced [<sup>3</sup>H] diprenorphine binding with nM  $IC_{50}$  except for metorphamide ( $\mu$ M  $IC_{50}$ ). Specific binding detected in the presence of these peptides ranged from 34%  $\pm$  2% for peptide F to 82%  $\pm$  2% with BAM18. In the case of synthetic agonists, we see that DAMGO and oxycodone have nM  $IC_{50}$  while morphine and fentanyl have  $\mu$ M  $IC_{50}$ . Interestingly, in the case of fentanyl, we found that it exhibits nM  $IC_{50}$  in CHO cells stably expressing  $\mu$ ORs (Extended Data Table 2). For cells stably expressing  $\delta$ Light, the endogenous opioid peptides and the synthetic agonists displaced [<sup>3</sup>H] diprenorphine binding with nM  $IC_{50}$  except for peptide E ( $\mu$ M  $IC_{50}$ ). Specific binding detected in the presence of the endogenous peptides ranged from 32%  $\pm$  3% for BAM18 to 77%  $\pm$  4% with ME (Extended Data Table 2). For cells stably expressing  $\kappa$ Light1.3, the endogenous opioid peptides and the synthetic agonist U69,593 displaced [<sup>3</sup>H] diprenorphine binding with nM  $IC_{50}$ . Specific binding detected in the presence of the endogenous peptides ranged from 10%  $\pm$  5% for ME to 76%  $\pm$  2% with DynB13 (Extended Data Table 2). We next compared binding parameters of sensors with those of receptors as previously reported under similar conditions<sup>16</sup>. Using s-slope analysis, we found that binding parameters of sensors and receptors correlated in all three cases (Extended Data Fig. 2c–e). A positive correlation, especially for  $\kappa$ Light and  $\delta$ Light, suggested that both radioligand binding assay and fluorescence assay can report peptides' efficaciousness similarly. Where  $\mu$ Light shows a negative correlation to  $\mu$ OR indicates that the dynamic range and affinity of  $\mu$ Light still needs improvement to reliably report binding profiles for endogenous peptides.

Besides comparing the sensors with radioligand binding, we assessed the signaling conductivity directly on  $\kappa$ Light1.3 and  $\delta$ Light. By implementing NanoBiT assay, we measured luminescence values indicating the elevation of  $\beta$ -arrestin1 upon addition of DynA17 comparing

between  $\kappa$ Light1.3 and  $\kappa$ OR, and addition of DADLE comparing between  $\delta$ Light and  $\delta$ OR. Unsurprisingly, the addition of cpGFP eliminated the  $\beta$ -arrestin1-recruiting capability of  $\kappa$ Light1.3 and  $\delta$ Light (Extended Data Fig. 2f). On the other hand, we assessed the DynA17 inhibition of forskolin-induced cAMP elevation by applying the GloSensor assay onto  $\kappa$ Light1.3 and  $\kappa$ OR, and same paradigm for DADLE inhibition onto  $\delta$ Light and  $\delta$ OR. The result indicates that neither  $\kappa$ Light1.3 nor  $\delta$ Light is able to reduce the ligand-induced elevation of cAMP signals (Extended Data Fig. 2g).

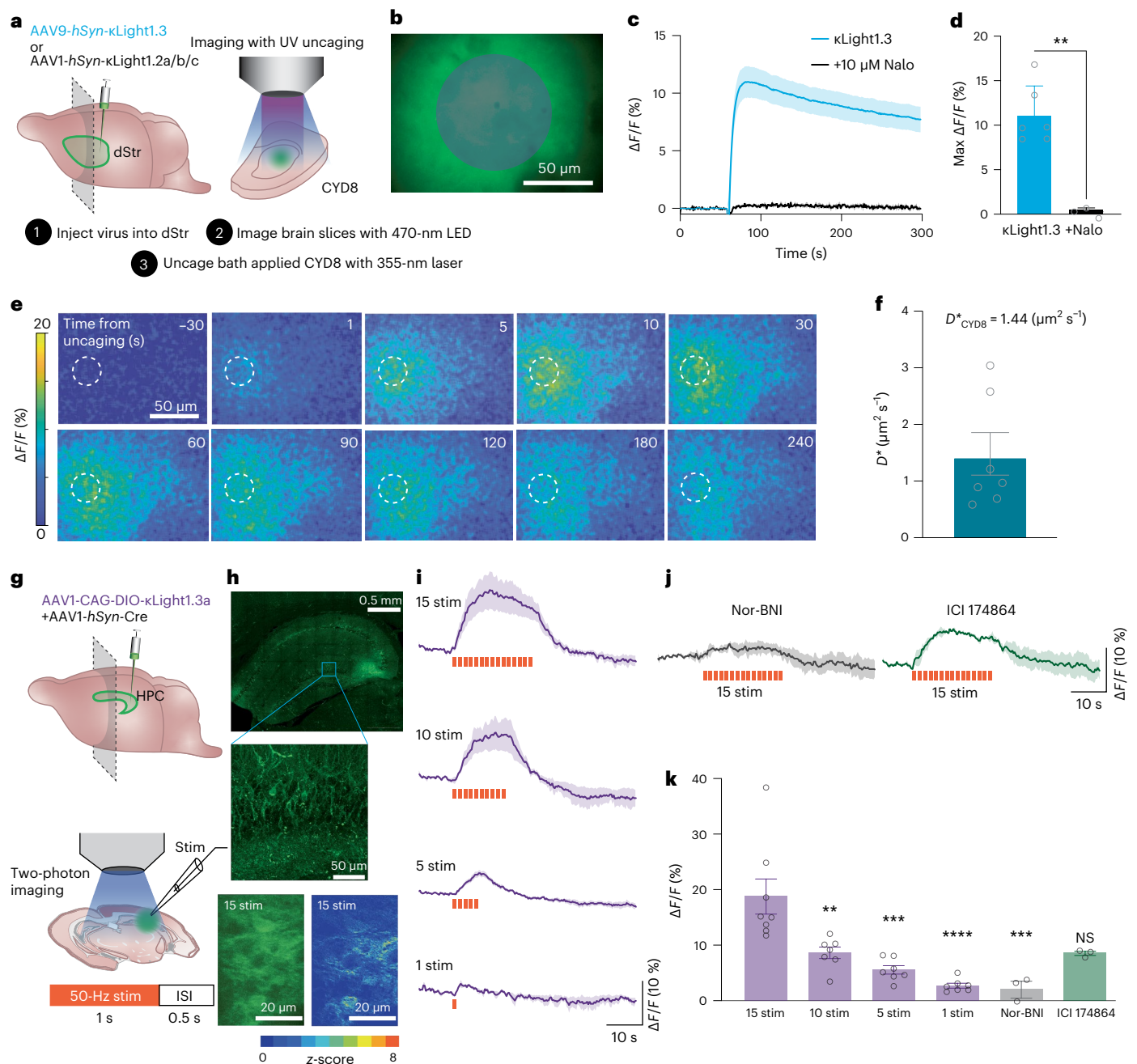
Together, these data suggest that the cpGFP insertion eliminated the signaling conductivity of the receptors and is not likely to perturb the binding pockets of the parent receptor. Our studies demonstrate that peptide binding to an opioid sensor triggers fluorescence changes that correlate with the binding of the peptide to the receptor, making the sensors serve as useful tools to quantify differences in ligand-driven conformational changes between peptides.

### Imaging dynorphin diffusion in brain tissue with $\kappa$ Light

Photoactivatable or 'caged' synthetic variants of opioid NPs or photo-sensitive nanovesicles can be activated with millisecond precision using short flashes of light and have been optimized for spectrally orthogonal use with GFP-based probes<sup>39</sup>. The spatiotemporal scale over which NP volume transmission occurs in brain tissue has been determined by combining photoactivatable NPs or nanovesicles, electrophysiological recording or cell-based NP biosensors. We thus asked whether  $\kappa$ Light can report opioid peptide volume transmission in brain tissue using photo-uncaging experiments.

To choose the most appropriate  $\kappa$ Light variant that balances dynamic range and sensitivity, we first examined the responses and kinetics of various  $\kappa$ Light variants using photoactivatable DynA8 (CYD8)<sup>29</sup>. We injected AAV9-*hSyn*- $\kappa$ Light1.x (top  $\kappa$ Light variants including 1.2a, 1.2b, 1.2c and 1.3) into the dorsal striatum (dStr) of C57 mouse pups (postnatal day (P)0–P3) and prepared the brain slices after 3 weeks of expression (Fig. 3a). On the day of imaging, CYD8 was circulated in the bath and photo-uncaged with a 50-ms flash of 355-nm laser light over an area of 3,800  $\mu$ m<sup>2</sup>, while imaging the responses of  $\kappa$ Light with a 473-nm LED within the same region (Fig. 3b). Among all the  $\kappa$ Light variants tested (Extended Data Fig. 3a),  $\kappa$ Light1.3 yielded the greatest response ( $\Delta F/F = 11\% \pm 1.4\%$ ; Fig. 3c,d), followed by  $\kappa$ Light1.2a ( $\Delta F/F = 9.09\% \pm 0.81\%$ ),  $\kappa$ Light1.2c ( $\Delta F/F = 6.84\% \pm 0.65\%$ ) and  $\kappa$ Light1.2b ( $\Delta F/F = 5.1\% \pm 0.51\%$ ; Extended Data Fig. 3b,c). The uncaging response was completely blocked by the presence of naloxone (0.5%  $\pm$  0.1%; Fig. 3d), confirming that the fluorescence change is due to ligand-dependent sensor activation, as opposed to being an artifact of the ultraviolet (UV) light flash. While  $\kappa$ Light1.3 had the greatest  $\Delta F/F$ , we noticed that its response was slow to decay in comparison to  $\kappa$ Light1.2a ( $\tau_{\text{off}} - \kappa$ Light1.3 = 202.1 s,  $\tau_{\text{off}} - \kappa$ Light1.2a = 179.7 s,  $\tau_{\text{off}} - \kappa$ Light1.2b = 246.1 s,  $\tau_{\text{off}} - \kappa$ Light1.2c = 165.0 s; Fig. 3c and Extended Data Fig. 3b), presumably due to the higher affinity for dynorphins that results in slower peptide dissociation (Extended Data Fig. 3d).

We next examined whether sensor expression might alter the ability of peptide ligands to engage endogenous opioid receptors. For this experiment, we used  $\kappa$ Light1.2a, which exhibited faster decay kinetics than  $\kappa$ Light1.3 upon DynA8 photorelease (Extended Data Fig. 3b), yet still produced a relatively large  $\Delta F/F$ . Adeno-associated viruses (AAVs) encoding  $\kappa$ Light1.2a or GFP control were injected into the hippocampus of C57 pups (P0–P3) and allowed to express for a minimum of 3 weeks before acute slices were prepared for electrophysiology (Extended Data Fig. 3e). Parvalbumin interneurons in the CA1 region of the hippocampus express  $\mu$ OR and  $\delta$ OR, which act presynaptically to suppress synaptic transmission<sup>40</sup>. Although DynA8's primary target is  $\kappa$ OR, it also binds to  $\mu$ OR and  $\delta$ OR (for example, Fig. 2b and Extended Data Table 1)<sup>41</sup>. This allowed us to ask whether the activation of  $\mu$ OR and  $\delta$ OR by DynA8 is altered by the expression of  $\kappa$ Light1.2a. To assay opioid receptor function, we recorded inhibitory



**Fig. 3 |  $\kappa$ Light1.3 characterization in acute brain slices.** **a**, Schematics shows imaging of striatal acute brain slices and photo-uncaging CYDS with a 355-nm laser. **b**, Time-lapse images (semitransparent gray circle shows the field of UV illumination). Scale bar, 50  $\mu$ m. **c**, Response of  $\kappa$ Light1.3 to CYDS photo-uncaging (blue,  $n = 6$  slices) in the absence and presence of naloxone (Nalo, 10  $\mu$ M; black,  $n = 3$  slices). Solid lines represent the mean, and the shaded areas represent the s.e.m. **d**, Quantification of the peak  $\Delta F/F$  evoked by CYDS photo-uncaging.  $\kappa$ Light1.3 (blue);  $11.1\% \pm 1.36\%$ ,  $n = 6$ , +naloxone (black);  $0.51\% \pm 0.12\%$ ,  $n = 3$ ,  $P = 0.0011$ , two-tailed unpaired  $t$ -test. **e**, Time course of  $\kappa$ Light1.2a after CYDS (5  $\mu$ M) photo-uncaging in the dStr. The dashed circle indicates the site of UV illumination. Heat map indicates  $\Delta F/F$  (%). Scale bar, 50  $\mu$ m. **f**, Summary of experiments determining the apparent diffusion coefficient,  $n = 7$  slices from 4 mice.  $D^* = 1.439 \pm 0.37 \mu\text{m}^2 \text{s}^{-1}$ . **g**, Schematics show local electrical stimulation of hippocampal slice with trains of 1-s, 50-Hz stimuli with a 0.5-s interstimulus interval. HPC, hippocampus; ISI, interstimulation interval. **h**, Representative image showing expression of  $\kappa$ Light1.3a in CA3 (top; scale bar,

0.5 mm) and zoomed in to visualize the localization of localization  $\kappa$ Light1.3a to the membranes of neuronal processes in the dentate gyrus (middle; scale bar, 50  $\mu$ m). Representative two-photon field of view from 15 stimulations (bottom) indicating the averaged intensity across all frames and z-score of responses in the representative field of view; scale bar, 20  $\mu$ m. **i, j**, Average  $\kappa$ Light1.3a responses to various electrical stimulation in the absence (**i**) and presence (**j**) of antagonists, Nor-BNI (gray) and ICI174864 (green). Solid lines represent the mean, and shaded areas represent the s.e.m. **k**, Bar graph summarizing the peak fluorescence response to each stimulation condition. 15 stim ( $n = 8$  slices):  $14.3\% \pm 2.4\%$ , 10 stim ( $n = 7$  slices):  $6.62\% \pm 0.8\%$ , 5 stim ( $n = 7$  slices):  $4.28\% \pm 0.6\%$ , 1 stim ( $n = 7$  slices):  $2.12\% \pm 0.3\%$ , Nor-BNI (100  $\mu$ M,  $n = 3$  slices):  $1.57\% \pm 1.2\%$ , ICI174864 (100  $\mu$ M,  $n = 3$  slices):  $6.44\% \pm 0.3\%$ . Ordinary one-way ANOVA with Bonferroni's multiple-comparisons test, individual conditions compared to 15 stim, 15 stim versus 10 stim:  $**P = 0.044$ , 15 stim versus 5 stim:  $***P = 0.0001$ , 15 stim versus 1 stim:  $****P < 0.0001$ , 15 stim versus Nor-BNI:  $***P = 0.0002$ , 15 stim versus ICI174864: not significant (NS),  $P = 0.0525$ . Error bars represent the s.e.m.

postsynaptic currents (IPSCs) in pyramidal cells, evoked with a stimulation protocol that favors  $\mu$ OR-sensitive and  $\delta$ OR-sensitive parvalbumin synapses<sup>40</sup> (Extended Data Fig. 3f). Photorelease of DynA8 using 5-ms flashes of 355-nm light produced a rapid, power-dependent reduction in IPSC amplitude that reversed over the course of several minutes (Extended Data Fig. 3g,h). Compared to GFP control,  $\kappa$ Light1.2a expression altered neither the degree of IPSC suppression, nor the time course of IPSC recovery in response to DynA8 photorelease across all light power densities examined (Extended Data Fig. 3i,j). These results suggest that  $\kappa$ Light1.2a expression does not result in sufficient ligand buffering as to perturb the activation of endogenous opioid receptors.

We next measured the spread of DynA8 in space and time. AAV1-*hSyn*- $\kappa$ Light1.2a was injected into dStr and imaging was performed 3 weeks after injection (Fig. 3a). Small volumes of DynA8 were rapidly photoreleased using a focused 25- $\mu$ m-diameter spot of 355-nm light (Fig. 3e) while monitoring sensor activation at distances of up to 125  $\mu$ m away. We observed that the peak  $\Delta F/F$  decreased with increased time from uncaging and with distance from the uncaging site (Extended Data Fig. 4a). For each video frame after uncaging, we plotted the fluorescence profile as a function of distance from the uncaging spot and extracted the  $\Delta F/F$  half-width, which was used to compute an effective diffusion coefficient ( $D^*$ ) of  $1.4 \pm 0.4 \mu\text{m}^2 \text{s}^{-1}$  ( $n = 7$  slices from four mice) for DynA8 in dStr (Extended Data Fig. 4b–d). These results suggest that DynA8 can reach receptors over 100  $\mu$ m away from release sites within several seconds of release in the dStr.

### Two-photon imaging of dynorphin release via electrical stimulation

It has been historically difficult to determine the electrical parameters that can effectively trigger the release of endogenous opioid peptides in brain tissue. We thus examined if  $\kappa$ Light can detect endogenous opioid peptide release triggered by electrical stimulation *in vivo*. To do so, we first improved the basal fluorescence of  $\kappa$ Light1.3 by integrating CYKIWRNFKGK as linker 1 and SVISKAKIRTV as linker 2 derived from the oxytocin sensor MTRIA<sub>Or</sub><sup>42</sup> (Extended Data Fig. 3a). This new variant, named  $\kappa$ Light1.3a, displayed a similar dynamic range ( $\kappa$ Light1.3 at 155%  $\pm$  11.6%,  $\kappa$ Light1.3a at 152%  $\pm$  29.5%,  $P = 0.92$ , unpaired  $t$ -test), but  $>2\times$  the basal brightness compared to  $\kappa$ Light1.3 ( $\kappa$ Light1.3 at  $25 \pm 0.08$ ,  $\kappa$ Light1.3a at  $61.8 \pm 7.6$ ,  $P = 0.0075$ , unpaired  $t$ -test; Extended Data Fig. 4e,f). To validate that  $\kappa$ Light1.3a retain the same selectivity, we performed *in situ* titration in dissociated hippocampal neuronal cultures using peptides DynA13, ME and  $\beta$ -endorphin. As expected,  $\kappa$ Light1.3a showed high selectivity to DynA13 over the other two endogenous peptides (Extended Data Fig. 4g). Immunoreactivity studies have shown abundant dynorphin stored in dentate granule cells, dynorphin dynamics in CA3 have also been shown to have an association with stress under various behavior paradigms, and dynorphins have been shown to inhibit excitatory neurotransmission and prevent the induction of long-term potentiation in hippocampus<sup>43–45</sup>. We sparsely expressed  $\kappa$ Light1.3a in CA3 by delivering AAV1-CAG-DIO- $\kappa$ Light1.3a in combination with AAV1-*hSyn*-Cre (Fig. 3g). After 3 weeks of expression, we observed bright labeling of neurons in CA3 and dentate gyrus with clear processes in the basal state and distribution of responses in the field of view using two-photon imaging (Fig. 3h).

Next, we evaluated the responses of  $\kappa$ Light1.3a to a range of electrical stimuli parameters applied locally via a stimulating electrode in CA3. Trains of electrical stimuli (1 s at 50 Hz, 0.5-s interstimulus interval) produced sustained fluorescence increases that rapidly decayed upon cessation of the stimulus (Fig. 3i), with an increasing number of stimuli driving larger maximum fluorescence responses (15 stimulations: 14.3%  $\pm$  2.4%, 10 stimulations: 8.39%  $\pm$  1.9%, 5 stimulations: 4.28%  $\pm$  0.6%, 1 stimulation: 2.12%  $\pm$  3.3%; Fig. 3k).

The response to 15 stimuli was strongly attenuated by the addition of the  $\kappa$ OR antagonist nor-BNI (100  $\mu$ M,  $\Delta F/F = 1.57\% \pm 1.2\%$ ), consistent

with the observed fluorescence increase resulting from activation by endogenous peptide. In the presence of  $\delta$ OR antagonist ICI 174864 (100  $\mu$ M), the responses were decreased but not statistically significant (Fig. 3j,k;  $\Delta F/F = 6.44\% \pm 0.3\%$ ).

### Probing the effect of receptor-selective opioid ligands *in vivo*

We next determined if  $\kappa$ Light and  $\delta$ Light can be activated by systemic administration of exogenous small-molecule drugs *in vivo*. We injected AAV9-*hSyn* encoding  $\kappa$ Light1.3 or  $\delta$ Light, and  $\kappa$ Light0 or  $\delta$ Light0 in the arcuate nucleus (ARC) of the hypothalamus<sup>46</sup>, hippocampal CA3 region<sup>43</sup> and NAc<sup>30</sup>, areas abundant in  $\kappa$ OR and  $\delta$ OR. We next implanted fiber-optic ferrules above each injection site and recorded the fluorescence of  $\kappa$ Light and  $\delta$ Light upon intraperitoneal (i.p.) injection of opioid receptor-selective ligands using fiber photometry (Fig. 4a and Extended Data Fig. 4h–j).

In each case, we observed dose-dependent fluorescence increases in response to systemic drug i.p. treatment, which were blocked by the nonselective opioid receptor antagonist naloxone. In the ARC,  $\kappa$ Light1.3 responded to the  $\kappa$ OR-selective agonist U69,593 with a robust increase in fluorescence within a few minutes of drug injection (1 mg per kg body weight:  $z\text{-score}_{\text{peak}} = 7.0 \pm 1.9$ , 3 mg per kg body weight:  $z\text{-score}_{\text{peak}} = 15.9 \pm 3.05$ ). Co-injection of naloxone (4 mg per kg body weight) drastically attenuated the response to U69,593 (3 mg per kg body weight; U69,593 + naloxone  $z\text{-score}_{\text{peak}} = 0.39 \pm 0.59$ ; Fig. 4b). In CA3, the  $\kappa$ OR-selective agonist U50,488 similarly activated  $\kappa$ Light1.3 in a dose-dependent manner. Again, the response to U50,488 (10 mg per kg body weight) was completely blocked by co-injecting naloxone (10 mg per kg body weight; 5 mg per kg body weight:  $z\text{-score}_{\text{peak}} = 2.68 \pm 1.8$ ; 10 mg per kg body weight:  $z\text{-score}_{\text{peak}} = 11.1 \pm 3.2$ ; U50,488 + naloxone:  $z\text{-score}_{\text{peak}} = -2.86 \pm 0.83$ ; Fig. 4c).

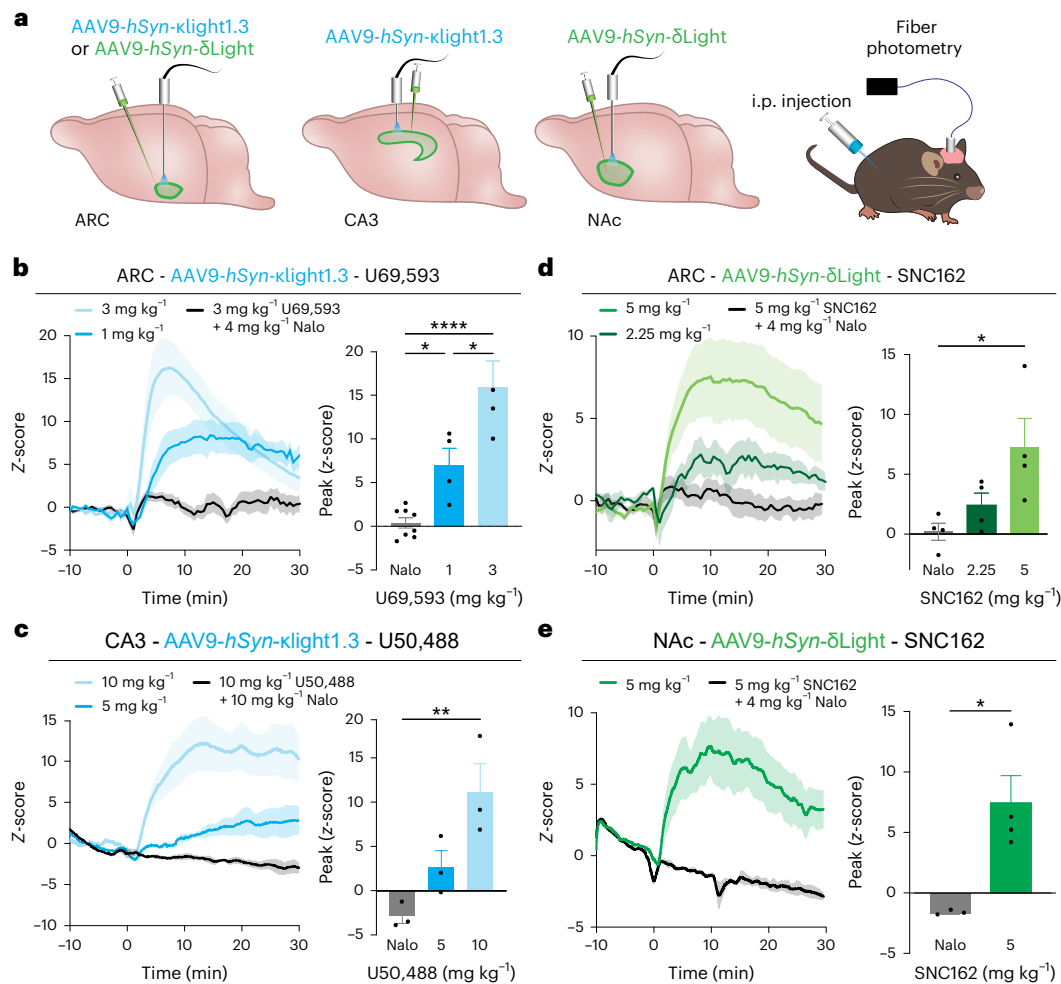
In the ARC, SNC162 administration produced increases in  $\delta$ Light fluorescence (2.25 mg per kg body weight:  $z\text{-score}_{\text{peak}} = 2.4 \pm 1.0$ ; 5 mg per kg body weight:  $z\text{-score}_{\text{peak}} = 7.28 \pm 2.4$ ) that were blocked by naloxone (4 mg per kg body weight) co-injected with SNC162 (5 mg per kg body weight; SNC162 + naloxone:  $z\text{-score}_{\text{peak}} = 0.19 \pm 0.72$ ; Fig. 4d). In the NAc, the administration of SNC162 (5 mg per kg body weight) also increased  $\delta$ Light fluorescence (SNC162:  $z\text{-score}_{\text{peak}} = 7.45 \pm 2.20$ ), and this was again blocked by naloxone (4 mg per kg body weight; SNC162 + naloxone:  $z\text{-score}_{\text{peak}} = -1.66 \pm 0.11$ ; Fig. 4e).

Importantly, we did not observe fluorescence changes in response to agonist when the non-functional mutant sensors  $\kappa$ Light0 or  $\delta$ Light0 were expressed in the ARC, CA3 and NAc (Extended Data Fig. 4k,l). These results suggest that both sensors can be faithfully activated by receptor-specific agonists *in vivo* and ensure a good dynamic range, adequate expression and fiber-expression alignments as a foundation for the following optogenetic and behavioral experiments.

### Measuring dynorphin release via circuit-specific photostimulation

Although optogenetics has been broadly used to trigger neuro-modulator release and neural activity, direct monitoring of peptide release triggered by optogenetic stimulation *in vivo*, especially in a circuit-specific manner with high temporal resolution, has not been measured optically. NAc contains abundant dynorphin, and previous studies have demonstrated that targeting the Dyn- $\kappa$ OR system in the nucleus accumbens shell (NAcSh) can modulate both rewarding and aversive behaviors<sup>47,48</sup>. Furthermore, previous work has demonstrated the ability to measure the optogenetically evoked release of dynorphin in the NAcSh using *in vivo* opto-dialysis<sup>30</sup>. Studies have also shown that the basolateral amygdala (BLA) sends dense, functional excitatory projections to the NAcSh and that these terminals are sensitive to modulation by Dyn- $\kappa$ OR<sup>49,50</sup>. We, therefore, set out to determine if  $\kappa$ Light can detect photostimulated release *in vivo* in BLA to NAcSh projections.

To detect dynorphin signaling at  $\kappa$ OR-expressing neurons, we injected  $\kappa$ OR-Cre mice with AAV5-CAG-DIO- $\kappa$ Light1.3a and implanted



**Fig. 4 | In vivo drug pharmacology imaged with  $\kappa$ Light and  $\delta$ Light.**

**a**, Experimental schematics of  $\kappa$ Light1.3 and  $\delta$ Light injection in the hypothalamus (ARC), the hippocampal CA3 and the NAc, followed by imaging with fiber photometry during drug injection. **b**,  $\kappa$ Light1.3 response in ARC to different doses of U69,593, 3 mg per kg body weight (light blue), 1 mg per kg body weight (blue) and 3 mg per kg body weight U69,593 + 4 mg per kg body weight naloxone (black);  $n = 7$  animals. Solid lines represent the mean, and the shaded area represents the s.e.m. Bar graph indicating the peak z-score of each response, 3 mg per kg body weight + naloxone:  $0.4\% \pm 0.6\%$ , 1 mg per kg body weight:  $7.0\% \pm 1.9\%$ , 3 mg per kg body weight:  $15.9\% \pm 3.1\%$ , ordinary one-way ANOVA with Tukey's multiple-comparisons test, 1 versus 3  $*P = 0.012$ , 1 versus Nalo  $*P = 0.029$ , 3 versus Nalo  $****P < 0.0001$ . **c**,  $\kappa$ Light1.3 response to different doses of U50,488 in CA3, 10 mg per kg body weight (light blue), 5 mg per kg body weight (blue) and 10 mg per kg body weight U50,488 + 10 mg per kg body weight naloxone (black)

in CA3;  $n = 3$  animals. Solid lines represent the mean, and shaded areas represent the s.e.m. Bar graph indicating the peak z-score of each response, 10 mg per kg body weight + naloxone:  $-2.9\% \pm 0.8\%$ , 5 mg per kg body weight:  $2.7\% \pm 1.8\%$ , 10 mg per kg body weight:  $11.1\% \pm 3.2\%$ , ordinary one-way ANOVA with Dunnett's multiple-comparisons test,  $**P = 0.0072$ . **d, e**,  $\delta$ Light response to different doses of SNC162 in ARC (**d**) and NAc (**e**), 5 mg per kg body weight (light green), 2.25 mg per kg body weight (green) and 5 mg per kg body weight SNC162 + 4 mg per kg body weight naloxone (black) in ARC and NAc;  $n = 4$  animals. Solid lines represent the mean, and shaded areas represent the s.e.m. Bar graph indicating the peak z-score of each response; in ARC:  $0.2\% \pm 0.7\%$ , 2.25 mg per kg body weight:  $2.4\% \pm 1.0\%$ , 5 mg per kg body weight:  $7.3\% \pm 2.4\%$ , ordinary one-way ANOVA with Tukey's multiple-comparisons test,  $*P = 0.0258$ ; in NAc:  $1.7 \pm 0.1\%$ , 5 mg per kg body weight:  $7.5\% \pm 2.2\%$ ; two-tailed unpaired  $t$ -test,  $*P = 0.0185$ . In **b–e**, error bars represent the s.e.m.

optical fibers in the NAcSh. A subset of mice was also injected with the red-shifted opsin ChRimson (AAV5-DIO-*EF1a*-ChRimson-tdTomato) in the BLA (Fig. 5a–c and Extended Data Fig. 5a); ChRimson-lacking mice served as a negative control to determine if optical stimulation produced artifactual dynamics in  $\kappa$ Light1.3a fluorescence. We first examined the response of  $\kappa$ Light1.3a to the agonist U50,488 in these mice (Fig. 5d). U50,488 (10 mg per kg body weight; i.p.) administration resulted in a rapid, sustained and robust increase in the fluorescence of  $\kappa$ Light1.3a. This increase was significantly attenuated when the animals were pretreated with the short-acting, reversible  $\kappa$ OR antagonist JNJ-67953964 (ref. 51; aticaprant, 3 mg per kg body weight; i.p.;  $P = 0.034$ , paired  $t$ -test), demonstrating the selectivity of  $\kappa$ Light1.3a responses in vivo (normalized peak,  $P = 0.0344$ , paired  $t$ -test, normalized area under the curve (AUC),  $P = 0.0138$ , paired  $t$ -test; Fig. 5e–h).

Next, we tested whether  $\kappa$ Light1.3a can detect endogenous dynorphin release in the NAc evoked via stimulation of glutamatergic BLA terminals, known to densely innervate the NAc<sup>49</sup>. A 1-s, 20-Hz, 5-ms pulse-width stimulation produced a brief artifact, followed by a significant increase in  $\kappa$ Light1.3a fluorescence (Extended Data Fig. 5b,c). Importantly, this stimulus artifact was present to the same extent in all animals, with and without ChRimson expression in the BLA terminals (Extended Data Fig. 5d). However, the subsequent increase in  $\kappa$ Light1.3a fluorescence was present only in the animals expressing ChRimson in BLA, suggesting that this elevation is due to the BLA terminal stimulation-evoked release of dynorphin ( $P < 0.0001$ , Welch's  $t$ -test; Extended Data Fig. 5e). To determine the appropriate stimulation parameters for stimulation-evoked dynorphin release, we performed a battery of experiments modulating stimulation number (1–5), laser intensity (0.5–5 mW) and stimulation time (1–30 s) within the same



session in a randomized order (Extended Data Fig. 5f–h). Varying the length of stimulation from 1 s to 5 s revealed, somewhat paradoxically, that 1 s of photostimulation produced the most κLight1.3a activation, while the magnitude of the artifact (fluorescence minimum) remained constant throughout ( $P = 0.0082$ , Brown–Forsythe and Welch ANOVA test; Extended Data Fig. 5i,j). Based on these results, we performed all our subsequent experiments using 1-s, 20-Hz, 5-ms pulse-width stimulation.

We then determined the pharmacological selectivity of BLA terminal stimulation-evoked κLight1.3a activation. We first pretreated animals with vehicle or aticaprant (3 mg per kg body weight; i.p.), followed by ten trials per animal of BLA terminal stimulation while simultaneously monitoring κLight1.3a fluorescence. We observed that κOR antagonism significantly decreased stimulation-evoked κLight1.3a activity in vivo (normalized peak,  $P = 0.0365$ , paired  $t$ -test; normalized AUC,  $P < 0.0001$ , paired  $t$ -test; Fig. 5i–l). We then posited that if this is due to κOR antagonism, wherein the antagonist prevents endogenous dynorphin from binding κLight1.3a, we should obtain a similar result following κOR agonism due to κLight1.3 occupancy by U50,488. Hence, we injected animals with vehicle or U50,488 (10 mg per kg body weight; i.p.) and performed the aforementioned recordings of stimulation-evoked κLight1.3 activity. As with aticaprant, we found that U50,488 significantly blunted evoked-κLight1.3a activation (normalized peak,  $P = 0.0022$ , paired  $t$ -test; normalized AUC,  $P = 0.0072$ , paired  $t$ -test; Fig. 5m–p). This suggests that U50,488 occupied and competed for the binding of evoked endogenous dynorphin to κLight1.3a. Next, to determine whether κLight1.3 activity was specific to dynorphin, we performed similar BLA terminal stimulation-evoked experiments in DYN-knockout (KO) mice, or WT controls (Extended Data Fig. 5k,l). As expected, injection of the exogenous receptor-specific agonist U50,488 (10 mg per kg body weight, i.p.) elicited comparable increases in κLight1.3 activity (Extended Data Fig. 5m–p). Importantly, whereas BLA stimulation-evoked κLight1.3 activity increased in WT controls, it was significantly diminished in DYN-KO animals (Extended Data Fig. 5q–t). Altogether, these results demonstrate that we can use optogenetics to trigger and measure terminal-stimulated dynorphin release with κLight in a circuit-specific manner.

### Monitoring behavior-triggered endogenous opioid release in vivo

After successfully detecting optogenetically evoked dynorphin release, we next sought to use κLight and δLight to monitor longitudinal opioid peptide signaling dynamics in behaving animals under fear-inducing and rewarding conditions. Previous studies have demonstrated that dynorphin neurons in ventral and dorsal NAcSh subregions

(vNAc and dNAc, respectively) have a distinct role in aversive and reward behavior<sup>47</sup>. Furthermore, subregion-specific dynorphin and enkephalin release have been measured in vNAc versus dNAc using an opto-dialysis method<sup>30</sup>. We thus decided to examine the utility of κLight1.3 and δLight in probing subregion-specific release of opioid peptides in the NAc during fear learning. To do so, AAV9-*hSyn*-κLight1.3 or AAV9-*hSyn*-δLight was injected in the dNAc and the vNAc, followed by fiber implantation. Three weeks after surgery, we measured peptide transients during an auditory fear conditioning experiment consisting of 30 presentations of a 30-s tone co-terminating with a 1.5-s foot shock (0.5 mA; Fig. 6a and Extended Data Fig. 6a). In the case of κLight, both dNAc and vNAc, we observed a quick rise in fluorescence intensity after the onset of the tone, which was sustained during tone presentation, followed by a small dip at the onset of the shock and a large rise immediately after the foot shock. The fluorescence signal then gradually decreased to the baseline after ~40 s (Tau - κLight1.3 in dNAc = 28.7 s; Tau - κLight1.3 in vNAc = 21.7 s; Fig. 6b,c). To assess differences in release between NAc subregions, we calculated the AUC of individual trials. The AUC to the tone was similar between dNAc and vNAc, whereas the AUC of the post-shock response was significantly higher in the dNAc compared to the vNAc (AUC dNAc,  $194 \pm 24$ ; AUC vNAc,  $135 \pm 15$ ,  $P = 0.0355$ , unpaired  $t$ -test; Fig. 6d). We did not observe fluorescence changes during fear learning when AAV1-*hSyn*-κLight0 was expressed either in the dNAc or the vNAc (Extended Data Fig. 6b–d).

In the case of δLight in the dNAc, we observed a brief increase in fluorescence triggered by the tone that gradually decreased to the baseline during tone presentation. The foot shock also triggered a large fluorescence increase followed by a sharp decay over 10 s after the shock (Tau - δLight in dNAc = 9.9 s; Tau - δLight in vNAc = 3.6 s; Fig. 6e,f). Although the AUC of the tone-evoked response in the vNAc was slightly larger in amplitude than in the dNAc, the difference was not significant. Again, the AUC of the shock-evoked response in the dNAc was significantly higher than in the vNAc (AUC dNAc;  $18 \pm 1.8$ , AUC vNAc;  $13 \pm 1.4$ ,  $P = 0.0276$ , unpaired  $t$ -test; Fig. 6g). We observed significantly attenuated fluorescence changes to the tone and shock in the animals expressing the control sensor δLight0 (Extended Data Fig. 6e,f).

Together, these data suggest κLight and δLight can faithfully report the subregional differences in endogenous opioid peptide release triggered during fear learning. More interestingly, the post-shock signals from κLight were much larger and longer lasting in early trials, and the response gradually shifted from the shock to tone as the number of trials increased (Fig. 6b,c). We did not observe this pattern of signal shifting from shock to tone in δLight (Fig. 6e,f), which suggests that opioid peptide, such as dynorphin, might actively track fear state in the NAcSh.

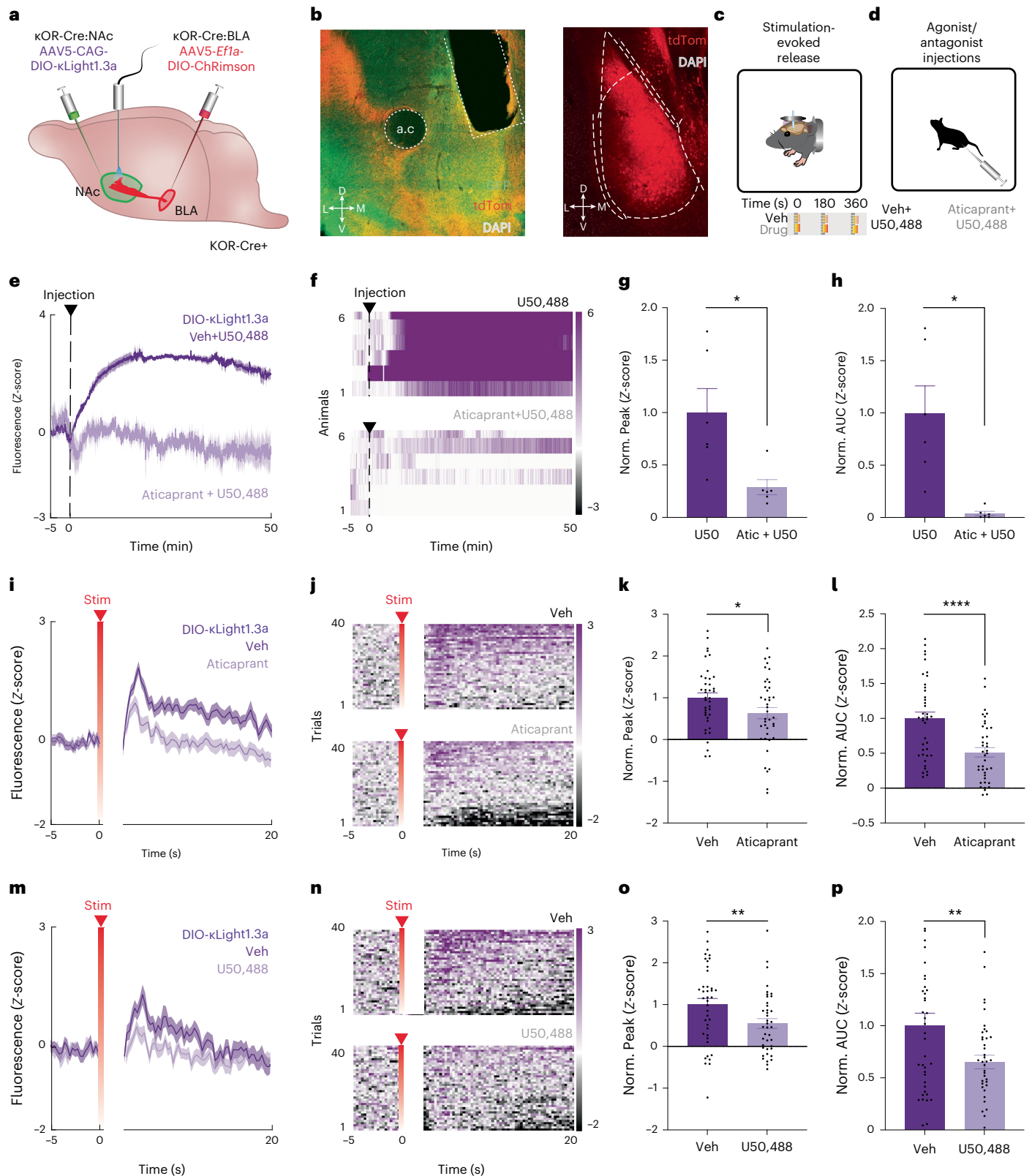
### Fig. 5 | Imaging optogenetically stimulated dynorphin release with κLight1.3a.

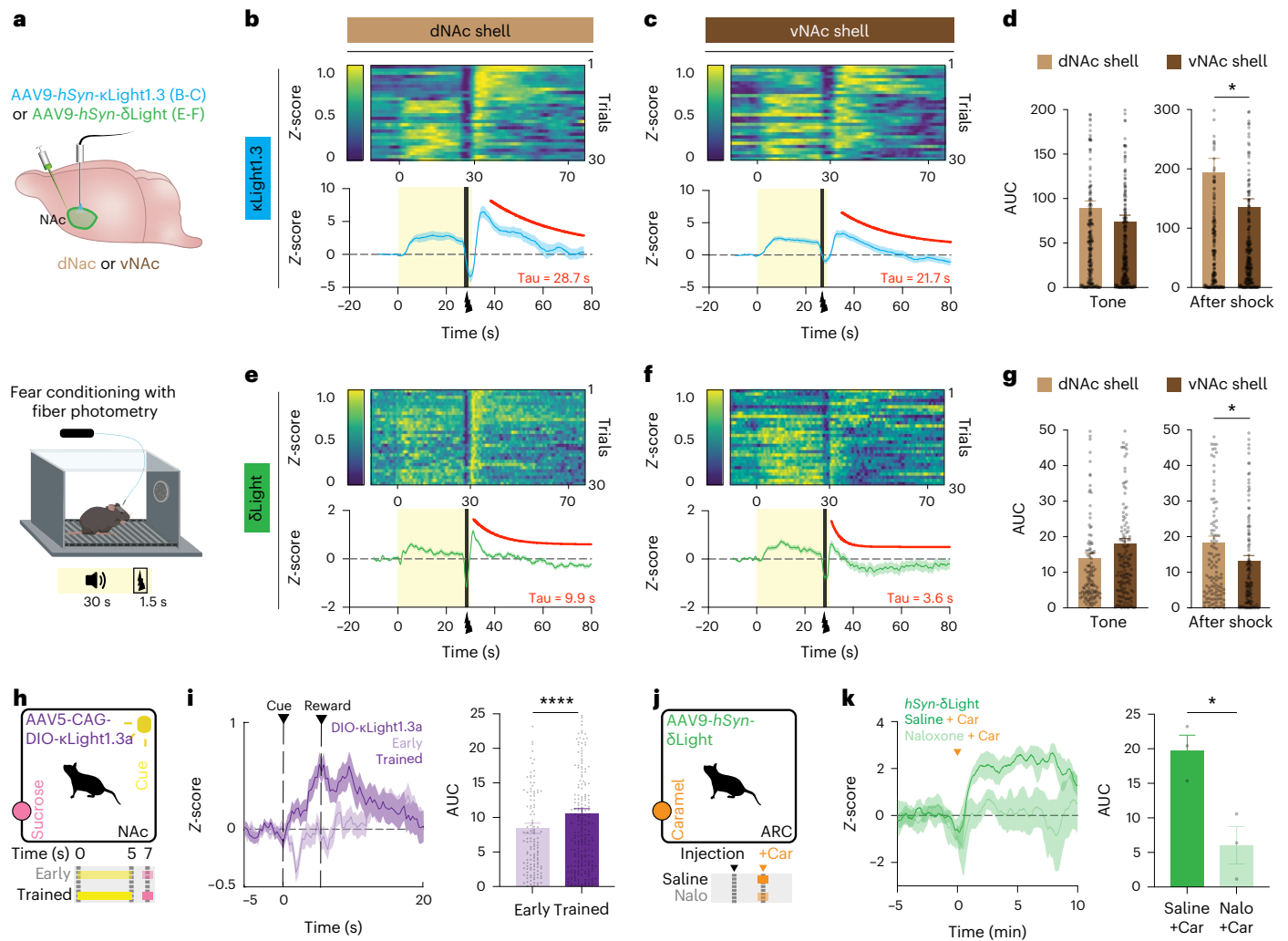
**a**, Schematic showing κLight1.3a-expressed NAcSh and ChRimson into the BLA of κOR-Cre<sup>+</sup> mice. **b**, Representative ×20 coronal image (left) showing expression of κLight1.3a (green), ChRimson (red), DAPI (white) and fiber placement in the NAcSh (left; scale bar, 200 μm), and ChRimson (red) and DAPI (white) in the BLA (right; scale bar, 200 μm) from six animals, which showed similar results. **c,d**, Schematic of in vivo head-fixed stimulation-evoked dynorphin release (stimuli occurred at 0, 180 and 360 s; **c**) and agonist/antagonist drug injection (10 mg per kg body weight U50,488 and 3 mg per kg body weight aticaprant + 10 mg per kg body weight U50,488; **d**) experiments. **e,f**, Mean (**e**) and heat map (**f**) of κLight1.3a activity either averaged across all animals (**e**) or from individuals (**f**) following i.p. injections of vehicle (veh) + U50,488 (dark) and aticaprant + U50,488 (light;  $n = 6$  animals). Solid lines represent the mean, and shaded areas represent the s.e.m. **g,h**, Normalized peak fluorescence (**g**) and AUC (**h**) of single trials during the injection period (0–50 min; U50:  $1 \pm 0.23$ , Atic + U50:  $0.29 \pm 0.07$ ; two-tailed paired  $t$ -test,  $*P = 0.034$ ,  $*P = 0.014$ ,  $n = 6$  animals). Data are represented as the mean ± s.e.m. Atic, aticaprant; U50, U50,488. **i**, Mean κLight1.3a activity averaged across all

trials following vehicle (dark) and aticaprant (light) treatment during ChRimson stimulation-evoked trials ( $n = 4$  animals). Solid lines represent the mean, and shaded areas represent the s.e.m. **j**, Heat map raster plot of κLight1.3a activity averaged across all trials following vehicle (top) and aticaprant (bottom) treatment during ChRimson stimulation-evoked trials ( $n = 4$  animals) displayed in ascending trial order by average activity across trials. ‘Stim’ indicates the time of stimulus application. **k,l**, Normalized peak fluorescence (**k**) and AUC of single trials (**l**) across vehicle and aticaprant treatment during all ChRimson stimulation-evoked trials (0–20 s; veh:  $1 \pm 0.12$ , Atic:  $0.63 \pm 0.14$ ; two-tailed paired  $t$ -test,  $*P = 0.037$ ,  $****P < 0.000$ ,  $n = 4$  animals). Data are represented as the mean ± s.e.m. **m,n**, Mean (**m**) and heat map raster plot (**n**) of recorded κLight1.3a activity averaged across all trials following vehicle (dark) and U50,488 (light) treatment during ChRimson stimulation-evoked trials ( $n = 4$  animals). Solid lines represent the mean, and shaded areas represent the s.e.m. **o,p**, Normalized peak fluorescence (**o**) and AUC of single trials (**p**) across vehicle and U50,488 treatment during all ChRimson stimulation-evoked trials (0–20 s; veh:  $1 \pm 0.15$ , U50:  $0.55 \pm 0.12$ ; two-tailed paired  $t$ -test,  $**P = 0.002$ ,  $**P = 0.007$ ,  $n = 4$  animals). Data are represented as the mean ± s.e.m.

To determine the utility of  $\kappa$ Light to probe reward-trigger endogenous dynorphin release, we first recorded the response of  $\kappa$ Light1.3a to Pavlovian conditioning in the NAc (Fig. 6h). To target  $\kappa$ OR-expressing neurons, we again injected CAG-DIO- $\kappa$ Light1.3a into the NAc of  $\kappa$ OR-Cre mice and trained these animals using classical reward conditioning. Although reward delivery during early trials did not produce fluorescence increases, we found a significant increase

in  $\kappa$ Light1.3a fluorescence during reward delivery and consumption following conditioning, as animals increased their reward consumption across training (AUC early:  $8.4 \pm 0.739$ , AUC trained:  $10.51 \pm 0.77$ ,  $P < 0.0001$ , paired  $t$ -test; Fig. 6i). These results suggest that endogenous dynorphin is released during reward reinforcement, supporting our prior work showing that subpopulations of dynorphin neurons in the NAcSh are reinforcing<sup>47</sup>.





**Fig. 6 | Imaging dynorphin and enkephalin dynamics during aversive and rewarding behavior.** **a**, Schematics show expression of  $\kappa$ Light1.3 or  $\delta$ Light in the dNac shell or the vNac shell (top), followed by a fear conditioning protocol during fiber photometry recording. **b,c**,  $\kappa$ Light1.3 response in the dNac (**b**) and the vNac (**c**): Top, sorted shock trials averaged across animals from top to bottom in chronological order (trial 1 at the top, trial 30 at the bottom). Bottom, average trace of  $\kappa$ Light1.3 response (blue) during fear conditioning, tone (0–30 s, yellow shaded area) and shock (27.5–29 s, black). Solid blue line represents the mean, and the shaded area represents the s.e.m. dNac,  $n = 7$  animals; vNac,  $n = 8$  animals. One-phase decay fit from 35 s to 80 s (red). Tau indicates the decay constant. **d**, AUC of single trials in **b** and **c** during tone and after shock. Tone AUC in dNac:  $89 \pm 8.5$ , tone AUC in vNac:  $74 \pm 7$ , two-tailed unpaired  $t$ -test,  $P = 0.1829$ , NS. Post-shock AUC in dNac:  $194 \pm 24$ , post-shock AUC in vNac:  $135 \pm 15$ , two-tailed unpaired  $t$ -test,  $*P = 0.0355$ . **e,f**,  $\delta$ Light response in the dNac (**e**) and the vNac (**f**). Experimental details same in **b** and **c**. dNac,  $n = 4$  animals; vNac,  $n = 5$  animals. One-phase decay fit from 31 s to 80 s (red). **g**, AUC of single trials in **e** and **f** during tone and after shock. Tone AUC in the dNac:  $14 \pm 1.4$ , tone AUC in the vNac:  $18 \pm 1.5$ ,

two-tailed unpaired  $t$ -test,  $P = 0.0582$ , NS. Post-shock AUC in the dNac:  $18 \pm 1.8$ , post-shock AUC in vNac:  $13 \pm 1.4$ , two-tailed unpaired  $t$ -test,  $*P = 0.0276$ . Error bars represent the s.e.m. In **d** and **g**, all single trial AUCs are plotted and compared for tone (0–25 s) and after shock (30–70 s) from  $n = 4$  animals for  $\delta$ Light response in the dNac and  $n = 5$  animals for  $\delta$ Light response in the vNac. **h**, Schematic shows classical Pavlovian conditioning. **i**, Left, mean  $\kappa$ Light1.3a activity averaged across all trials during day 1 (early; light purple) and day 7 (trained; dark purple) of Pavlovian conditioning ( $n = 6$  animals). Solid lines represent the mean, and shaded areas represent the s.e.m. Right, AUC of single trials across early and trained stages of Pavlovian conditioning; early:  $8.4 \pm 0.74$ , trained:  $10.51 \pm 0.77$ , two-tailed paired  $t$ -test,  $****P < 0.0001$ . Error bars represent the s.e.m. **j**, Schematic shows caramel retrieval experiment. **k**, Left, averaged  $\delta$ Light activity upon caramel retrieval after injection of saline (dark green) or 4 mg per kg body weight naloxone (light green;  $n = 3$  animals). Solid line represents the mean, and shaded area represent the s.e.m. Right, AUC of single trials compared between saline and naloxone conditions, saline:  $20 \pm 2.3$ , naloxone:  $6 \pm 2.7$ ,  $*P = 0.0197$ , two-tailed unpaired  $t$ -test. Error bars represent the s.e.m.

Similarly, we monitored  $\delta$ Light fluorescence in the ARC while mice retrieved caramel rewards (Fig. 6j). We observed elevated  $\delta$ Light signals in animals injected with saline following caramel retrieval, and this response was blocked when naloxone (4 mg per kg body weight) was injected before caramel retrieval (AUC saline:  $20 \pm 2.3$ , AUC naloxone:  $6 \pm 2.7$ ,  $P = 0.0197$ , unpaired  $t$ -test; Fig. 6k). We did not observe an increase in  $\delta$ Light0 in response to caramel retrieval under either condition (Extended Data Fig. 6g). Together, these results suggest that  $\kappa$ Light and  $\delta$ Light can faithfully track dynamic changes in endogenous opioid release during the full course of aversive and rewarding behaviors in vivo.

## Discussion

In this study, we develop and characterize genetically encoded opioid receptor sensors for high-resolution tracking of opioid peptides under various experimental settings. G-protein-coupled-receptor-based sensors have been valuable in monitoring neuromodulator signals in awake animals<sup>52,53</sup>, initially for biogenic amines and acetylcholine<sup>35,54–60</sup>, and more recently for NPs including oxytocin, orexin and others<sup>42,61–63</sup>. The development of opioid sensors addresses a crucial need in the neuroscience toolkit due to opioids' widespread significance.

All three sensors,  $\mu$ Light,  $\kappa$ Light and  $\delta$ Light, collectively respond to a wide range of opioid ligands, including endogenous opioid NPs,

with  $\kappa$ Light and  $\delta$ Light retaining the pharmacological selectivity of the parent receptor. These sensors can detect and differentiate conformational changes of the receptor induced by various peptides, which is difficult to do using traditional radioligand binding assays. The systematic characterization of pharmacological profiles provided by these sensors could open new doors for imaging-based high-throughput screening of a chemical library targeting opioid signaling. However,  $\mu$ Light is weakly activated by small-molecule drugs like morphine and fentanyl and has a lower binding efficacy for endogenous peptides. In fact, oxycodone was observed to suppress  $\mu$ Light fluorescence, which could indicate oxycodone activates  $\mu$ OR with a different conformation. This could lead to the application of performing drug screening to select for compounds that activate  $\mu$ OR in a desired conformation. Structural studies of  $\mu$ ORs in active and inactive states revealed that conformational changes of TM5 and TM6 depend on an allosteric coupling between ligand-binding pockets and G-proteins<sup>64</sup>. As cpGFP was inserted into ICL3, it is possible that cpGFP insertion decreased such coupling. Future optimization of  $\mu$ Light is crucial for reliably detecting  $\mu$ OR-selective NP  $\beta$ -endorphin.

NP receptors can be expressed at a considerable distance ( $\mu\text{m}$ – $\text{mm}$ ) from putative peptide release sites, suggesting volume transmission as one mode of neuropeptidergic transmission, enabling small amounts of NPs to widely impact brain function. We used  $\kappa$ Light with spatially restricted peptide photorelease to measure DynA8 in the dStr, indicating that it can signal via volume transmission to activate receptors over 100  $\mu\text{m}$  away within seconds, with an apparent diffusion coefficient of 1.4  $\mu\text{m}^2 \text{s}^{-1}$ . Diffusion coefficients for NPs and similar molecules vary greatly depending on peptide type and brain region, peptidase content, as well as tissue tortuosity<sup>8,62,65–67</sup>. We measured diffusion in the striatum, a tortuous region with myelinated fiber bundles and patch-matrix microcircuits; peptides may exhibit higher mobility in less tortuous regions. Although peptide uncaging has advantages, it doesn't target endogenous release sites and may release larger quantities than dense-core vesicles. Additionally, confining sensor expression to  $\kappa$ OR-expressing cells could improve sensitivity to endogenous peptide release by minimizing background fluorescence from neurons potentially unexposed to locally released peptide, which can further enhance the accuracy of measurement. Further studies on endogenously released peptide spread are needed.

Understanding the neural activity patterns required for evoking NP release remains a decades-long challenge. Monitoring NP release in response to electrical or optogenetic stimulation *ex vivo* or *in vivo* offers a powerful method for identifying these activity patterns. We demonstrated  $\kappa$ Light's utility in determining electrical parameters to trigger endogenous release in hippocampal slices; this overcomes the challenge of using electrophysiological assays for endogenous receptor activation.

Identifying conditions that support endogenous peptide release may be most appropriately addressed *in vivo*, where neural circuits remain fully intact and endogenous neuromodulatory tone remains unaltered by brain slicing. To demonstrate circuit and cell-type-specific release, rather than stimulating dynorphinergic cells within the NAC directly, we optogenetically stimulated their glutamatergic inputs arising from the BLA. Prior work has established that optogenetic stimulation of BLA terminals in the NAC reliably drives action potentials in striatal neurons in brain slices, as well as facilitate reward-seeking behavior<sup>49</sup>. In addition, synaptic stimulation of action potentials in peptidergic neurons via strong glutamatergic drive can activate metabotropic glutamate receptors, which have been implicated as gatekeepers for dynorphin secretion from striatal neurons in brain slices<sup>68</sup>. Using this optogenetic approach, we successfully identified stimulation conditions that result in  $\kappa$ Light activation, presumably via dynorphin secretion from striatal neurons, as BLA neurons themselves express little to no prodynorphin mRNA (Allen Brain Atlas ISH data). Paradoxically, we found that increasing the duration of the

stimulus beyond 1 s decreased the degree of  $\kappa$ Light activation. This is likely due to the stimulation artifact generated by red light, as evidenced by the comparable minima observed in the animals expressing ChRimson and the controls that lack it (Extended Data Fig. 5b–d). Furthermore, increasing stimulation number also increased the width of the artifact (Extended Data Fig. 5f–h). While our data strongly suggest that this paradoxical suppression is likely due to stimulation artifacts induced by red light, future studies are required to explore the possibility of recruitment of additional neurochemical signaling processes during sustained stimulation that may suppress dynorphin release. Moreover,  $\kappa$ OR-mediated suppression of BLA synaptic output, via dynorphin– $\kappa$ OR signaling at BLA terminals following sustained stimulation, resulting in the dampening of further synaptic activation of NAC dynorphin neurons requires further study. Additionally, whether prolonged stimulation of opioid release, either via optogenetics, or in response to strong behavioral stimuli such as foot shock, results in the transient quenching of sensor activity also warrants future exploration.

In this study, we further demonstrated the utility of  $\kappa$ Light and  $\delta$ Light sensors in tracking rapid dynamic changes in endogenous opioid peptide release triggered by both reward and aversion, which can vary between subregions. Collectively,  $\kappa$ Light and  $\delta$ Light respond to most endogenous opioid NPs, including various dynorphin forms and enkephalins. However, the promiscuity among opioid receptors and peptides presents a disadvantage in specificity, as the sensors cannot reliably distinguish between the endogenous peptides that might activate them—indeed many brain areas are rich in multiple opioid NPs. While our data using DYN-KO animals suggest a good degree of specificity for  $\kappa$ Light to detect endogenous dynorphin (Extended Data Fig. 5m–t), further engineering efforts combined with structural analysis may make it possible to reduce such promiscuity. We expect broad application of these opioid sensors to enable a new understanding of how endogenous opioid peptide signaling contributes to various physiological and pathological conditions, including pain, stress, reward and drug addiction. Monitoring circuit-specific peptide release in behaving animals may reveal new opioid functions in behavioral state transitions and associative learning. Detecting discrete peptide release events, evoked optogenetically or behaviorally, can help identify differences in opioid secretion under various pharmacological, behavioral or disease states. While pharmacology, photopharmacology and optogenetics have contributed substantially to opioid receptor signaling knowledge, these sensors enable a shift from focusing on receptor activation consequences to exploring endogenous NP secretion's impact on the brain's complex and diverse functions.

## Online content

Any methods, additional references, Nature Portfolio reporting summaries, source data, extended data, supplementary information, acknowledgements, peer review information; details of author contributions and competing interests; and statements of data and code availability are available at <https://doi.org/10.1038/s41593-024-01697-1>.

## References

1. Greco, M. A. et al. Opioidergic projections to sleep-active neurons in the ventrolateral preoptic nucleus. *Brain Res.* **1245**, 96–107 (2008).
2. Hökfelt, T. et al. Neuropeptide and small transmitter coexistence: fundamental studies and relevance to mental illness. *Front. Neural Circuits* **12**, 106 (2018).
3. Holden, J. E., Jeong, Y. & Forrest, J. M. The endogenous opioid system and clinical pain management. *AACN Clin. Issues* **16**, 291–301 (2005).
4. Klenowski, P., Morgan, M. & Bartlett, S. E. The role of  $\delta$ -opioid receptors in learning and memory underlying the development of addiction. *Br. J. Pharmacol.* **172**, 297–310 (2015).

5. Nummenmaa, L. & Tuominen, L. Opioid system and human emotions. *Br. J. Pharmacol.* **175**, 2737–2749 (2018).
6. Russo, A. F. Overview of neuropeptides: awakening the senses? *Headache* **57**, 37–46 (2017).
7. Fricker, L. D. Analysis of mouse brain peptides using mass spectrometry-based peptidomics: implications for novel functions ranging from non-classical neuropeptides to microproteins. *Mol. Biosyst.* **6**, 1355–1365 (2010).
8. van den Pol, A. N. Neuropeptide transmission in brain circuits. *Neuron* **76**, 98–115 (2012).
9. Burns, J. A. et al. Molecular imaging of opioid and dopamine systems: insights into the pharmacogenetics of opioid use disorders. *Front. Psychiatry* **10**, 626 (2019).
10. Corder, G., Castro, D. C., Bruchas, M. R. & Scherrer, G. Endogenous and exogenous opioids in pain. *Annu. Rev. Neurosci.* **41**, 453–473 (2018).
11. Franchi, S., Moschetti, G., Amodeo, G. & Sacerdote, P. Do all opioid drugs share the same immunomodulatory properties? A review from animal and human studies. *Front. Immunol.* **10**, 2914 (2019).
12. Higginbotham, J. A., Markovic, T., Massaly, N. & Morón, J. A. Endogenous opioid systems alterations in pain and opioid use disorder. *Front. Syst. Neurosci.* **16**, 1014768 (2022).
13. Le Merrer, J., Becker, J. A., Befort, K. & Kieffer, B. L. Reward processing by the opioid system in the brain. *Physiol. Rev.* **89**, 1379–1412 (2009).
14. Machelska, H. & Celik, M. Ö. Advances in achieving opioid analgesia without side effects. *Front. Pharmacol.* **9**, 1388 (2018).
15. Pathan, H. & Williams, J. Basic opioid pharmacology: an update. *Br. J. Pain* **6**, 11–16 (2012).
16. Gomes, I. et al. Biased signaling by endogenous opioid peptides. *Proc. Natl Acad. Sci. USA* **117**, 11820–11828 (2020).
17. Machelska, H. & Celik, M. Ö. Opioid receptors in immune and glial cells—implications for pain control. *Front. Immunol.* **11**, 300 (2020).
18. Mansour, A. et al. Mu, delta, and kappa opioid receptor mRNA expression in the rat CNS: an in situ hybridization study. *J. Comp. Neurol.* **350**, 412–438 (1994).
19. McGinty, J. F., van der Kooy, D. & Bloom, F. E. The distribution and morphology of opioid peptide immunoreactive neurons in the cerebral cortex of rats. *J. Neurosci.* **4**, 1104–1117 (1984).
20. van Steenbergen, H., Eikemo, M. & Leknes, S. The role of the opioid system in decision making and cognitive control: a review. *Cogn. Affect. Behav. Neurosci.* **19**, 435–458 (2019).
21. Kosten, T. R. & George, T. P. The neurobiology of opioid dependence: implications for treatment. *Sci. Pract. Perspect.* **1**, 13–20 (2002).
22. Al-Hasani, R. & Bruchas, M. R. Molecular mechanisms of opioid receptor-dependent signaling and behavior. *Anesthesiology* **115**, 1363–1381 (2011).
23. Bruchas, M. R. et al. Stress-induced p38 mitogen-activated protein kinase activation mediates kappa-opioid-dependent dysphoria. *J. Neurosci.* **27**, 11614–11623 (2007).
24. Hoyer, D. & Bartfai, T. in *Encyclopedia of Neuroscience* (ed. Squire, L. R.) 801–810 (Academic Press, 2009).
25. Fricker, L. D., Margolis, E. B., Gomes, I. & Devi, L. A. Five decades of research on opioid peptides: current knowledge and unanswered questions. *Mol. Pharmacol.* **98**, 96–108 (2020).
26. Castro, D. C. et al. An endogenous opioid circuit determines state-dependent reward consumption. *Nature* **598**, 646–651 (2021).
27. Ma, X. et al. In vivo photopharmacology with a caged mu opioid receptor agonist drives rapid changes in behavior. *Nat. Methods* **20**, 682–685 (2023).
28. Smith, S. J. et al. Single-cell transcriptomic evidence for dense intracortical neuropeptide networks. *eLife* **8**, e47889 (2019).
29. Banghart, M. R. & Sabatini, B. L. Photoactivatable neuropeptides for spatiotemporally precise delivery of opioids in neural tissue. *Neuron* **73**, 249–259 (2012).
30. Al-Hasani, R. et al. In vivo detection of optically-evoked opioid peptide release. *eLife* **7**, e36520 (2018).
31. Mitsui, S., Saito, M., Hayashi, K., Mori, K. & Yoshihara, Y. A novel phenylalanine-based targeting signal directs telencephalin to neuronal dendrites. *J. Neurosci.* **25**, 1122–1131 (2005).
32. Stockklauser, C., Ludwig, J., Ruppertsberg, J. P. & Klöcker, N. A sequence motif responsible for ER export and surface expression of Kir2.0 inward rectifier K<sup>+</sup> channels. *FEBS Lett.* **493**, 129–133 (2001).
33. Lim, S. T., Antonucci, D. E., Scannevin, R. H. & Trimmer, J. S. A novel targeting signal for proximal clustering of the Kv2.1K<sup>+</sup> channel in hippocampal neurons. *Neuron* **25**, 385–397 (2000).
34. Tandon, N., Thakkar, K. N., LaGory, E. L., Liu, Y. & Giaccia, A. J. Generation of stable expression mammalian cell lines using lentivirus. *Bio Protoc.* **8**, e3073 (2018).
35. Dong, C. et al. Psychedelic-inspired drug discovery using an engineered biosensor. *Cell* **184**, 2779–2792.e18 (2021).
36. Nichols, A. L. et al. Fluorescence activation mechanism and imaging of drug permeation with new sensors for smoking-cessation ligands. *eLife* **11**, e74648 (2022).
37. Gomes, I., Filipovska, J. & Devi, L. A. Opioid receptor oligomerization. Detection and functional characterization of interacting receptors. *Methods Mol. Med.* **84**, 157–183 (2003).
38. Gomes, I., Ijzerman, A. P., Ye, K., Maillet, E. L. & Devi, L. A. G-protein-coupled receptor heteromerization: a role in allosteric modulation of ligand binding. *Mol. Pharmacol.* **79**, 1044–1052 (2011).
39. Banghart, M. R., He, X. J. & Sabatini, B. L. A caged enkephalin optimized for simultaneously probing mu and delta opioid receptors. *ACS Chem. Neurosci.* **9**, 684–690 (2018).
40. He, X. J. et al. Convergent, functionally independent signaling by mu and delta opioid receptors in hippocampal parvalbumin interneurons. *eLife* **10**, e69746 (2021).
41. Toll, L. et al. Standard binding and functional assays related to medications development division testing for potential cocaine and opiate narcotic treatment medications. *NIDA Res. Monogr.* **178**, 440–466 (1998).
42. Ino, D., Tanaka, Y., Hibino, H. & Nishiyama, M. A fluorescent sensor for real-time measurement of extracellular oxytocin dynamics in the brain. *Nat. Methods* **19**, 1286–1294 (2022).
43. Shirayama, Y. et al. Stress increases dynorphin immunoreactivity in limbic brain regions and dynorphin antagonism produces antidepressant-like effects. *J. Neurochem.* **90**, 1258–1268 (2004).
44. Wagner, J. J., Terman, G. W. & Chavkin, C. Endogenous dynorphins inhibit excitatory neurotransmission and block LTP induction in the hippocampus. *Nature* **363**, 451–454 (1993).
45. Weisskopf, M. G., Zalutsky, R. A. & Nicoll, R. A. The opioid peptide dynorphin mediates heterosynaptic depression of hippocampal mossy fibre synapses and modulates long-term potentiation. *Nature* **362**, 423–427 (1993).
46. Romero-Picó, A. et al. Hypothalamic kappa-opioid receptor modulates the orexigenic effect of ghrelin. *Neuropsychopharmacology* **38**, 1296–1307 (2013).
47. Al-Hasani, R. et al. Distinct subpopulations of nucleus accumbens dynorphin neurons drive aversion and reward. *Neuron* **87**, 1063–1077 (2015).
48. Castro, D. C. & Berridge, K. C. Opioid hedonic hotspot in nucleus accumbens shell: mu, delta, and kappa maps for enhancement of sweetness ‘liking’ and ‘wanting’. *J. Neurosci.* **34**, 4239–4250 (2014).

49. Stuber, G. D. et al. Excitatory transmission from the amygdala to nucleus accumbens facilitates reward seeking. *Nature* **475**, 377–380 (2011).
50. Tejada, H. A. et al. Pathway- and cell-specific kappa-opioid receptor modulation of excitation-inhibition balance differentially gates D1 and D2 accumbens neuron activity. *Neuron* **93**, 147–163 (2017).
51. Page, S. et al. Behavioral pharmacology of novel kappa opioid receptor antagonists in rats. *Int. J. Neuropsychopharmacol.* **22**, 735–745 (2019).
52. Dong, C. et al. Fluorescence imaging of neural activity, neurochemical dynamics, and drug-specific receptor conformation with genetically encoded sensors. *Annu. Rev. Neurosci.* **45**, 273–294 (2022).
53. Wu, Z., Lin, D. & Li, Y. Pushing the frontiers: tools for monitoring neurotransmitters and neuromodulators. *Nat. Rev. Neurosci.* **23**, 257–274 (2022).
54. Borden, P. M. et al. A fast genetically encoded fluorescent sensor for faithful in vivo acetylcholine detection in mice, fish, worms and flies. Preprint at *bioRxiv* <https://doi.org/10.1101/2020.02.07.939504> (2020).
55. Jing, M. et al. An optimized acetylcholine sensor for monitoring in vivo cholinergic activity. *Nat. Methods* **17**, 1139–1146 (2020).
56. Patriarchi, T. et al. Ultrafast neuronal imaging of dopamine dynamics with designed genetically encoded sensors. *Science* **360**, eaat4422 (2018).
57. Patriarchi, T. et al. An expanded palette of dopamine sensors for multiplex imaging in vivo. *Nat. Methods* **17**, 1147–1155 (2020).
58. Sun, F. et al. Next-generation GRAB sensors for monitoring dopaminergic activity in vivo. *Nat. Methods* **17**, 1156–1166 (2020).
59. Unger, E. K. et al. Directed evolution of a selective and sensitive serotonin sensor via machine learning. *Cell* **183**, 1986–2002 (2020).
60. Wan, J. et al. A genetically encoded sensor for measuring serotonin dynamics. *Nat. Neurosci.* **24**, 746–752 (2021).
61. Duffet, L. et al. A genetically encoded sensor for in vivo imaging of orexin neuropeptides. *Nat. Methods* **19**, 231–241 (2022).
62. Qian, T. et al. A genetically encoded sensor measures temporal oxytocin release from different neuronal compartments. *Nat. Biotechnol.* **41**, 944–957 (2023).
63. Wang, H. et al. A tool kit of highly selective and sensitive genetically encoded neuropeptide sensors. *Science* <https://doi.org/10.1126/science.abq8173> (2023).
64. Sounier, R. et al. Propagation of conformational changes during  $\mu$ -opioid receptor activation. *Nature* **524**, 375–378 (2015).
65. Drake, C. T. et al. Dynorphin opioids present in dentate granule cells may function as retrograde inhibitory neurotransmitters. *J. Neurosci.* **14**, 3736–3750 (1994).
66. Nicholson, C. & Tao, L. Hindered diffusion of high molecular weight compounds in brain extracellular microenvironment measured with integrative optical imaging. *Biophys. J.* **65**, 2277–2290 (1993).
67. Xiong, H. et al. Probing neuropeptide volume transmission in vivo by simultaneous near-infrared light-triggered release and optical sensing. *Angew. Chem. Int. Ed.* <https://doi.org/10.1002/anie.202206122> (2022).
68. Atwood, B. K., Kupferschmidt, D. A. & Lovinger, D. M. Opioids induce dissociable forms of long-term depression of excitatory inputs to the dorsal striatum. *Nat. Neurosci.* **17**, 540–548 (2014).

**Publisher's note** Springer Nature remains neutral with regard to jurisdictional claims in published maps and institutional affiliations.

**Open Access** This article is licensed under a Creative Commons Attribution 4.0 International License, which permits use, sharing, adaptation, distribution and reproduction in any medium or format, as long as you give appropriate credit to the original author(s) and the source, provide a link to the Creative Commons licence, and indicate if changes were made. The images or other third party material in this article are included in the article's Creative Commons licence, unless indicated otherwise in a credit line to the material. If material is not included in the article's Creative Commons licence and your intended use is not permitted by statutory regulation or exceeds the permitted use, you will need to obtain permission directly from the copyright holder. To view a copy of this licence, visit <http://creativecommons.org/licenses/by/4.0/>.

© The Author(s) 2024

<sup>1</sup>Department of Biochemistry and Molecular Medicine, School of Medicine, University of California Davis, Davis, CA, USA. <sup>2</sup>Center for the Neurobiology of Addiction, Pain, and Emotion, Departments of Anesthesiology and Pharmacology, University of Washington, Seattle, WA, USA. <sup>3</sup>Department of Neurobiology, School of Biological Sciences, University of California, San Diego, La Jolla, CA, USA. <sup>4</sup>Department of Pharmacological Sciences, Icahn School of Medicine at Mount Sinai, New York City, NY, USA. <sup>5</sup>Unit on Neuromodulation and Synaptic Integration, National Institute of Mental Health, National Institutes of Health, Bethesda, MD, USA. <sup>6</sup>Department of Neuroscience and Pharmacology, Iowa Neuroscience Institute, Roy J. and Lucille A. Carver College of Medicine, University of Iowa, Iowa City, IA, USA. <sup>7</sup>Department of Pharmacology, University of California San Francisco, San Francisco, CA, USA. <sup>8</sup>College of Biological Sciences, University of California Davis, Davis, CA, USA. <sup>9</sup>Cold Spring Harbor Laboratory, New York, NY, USA. <sup>10</sup>Center for Neuroscience, University of California Davis, Davis, CA, USA. <sup>11</sup>Present address: Max Planck Florida Institute for Neuroscience, Jupiter, FL, USA. <sup>12</sup>These authors contributed equally: Chunyang Dong, Raajaram Gowrishankar. <sup>13</sup>These authors jointly supervised this work: Yihan Jin, Xinyi Jenny He. ✉e-mail: [mbruchas@uw.edu](mailto:mbruchas@uw.edu); [mbanghart@ucsd.edu](mailto:mbanghart@ucsd.edu); [lin.tian@mphi.org](mailto:lin.tian@mphi.org)

## Methods

### Animals

Animals were housed in ventilated home cages with at most five mice per cage. Animals were housed in a vivarium with a 12-h light and 12-h dark standard light cycle, with a temperature of 68–79 °F and humidity of 30–70%. All housing and experimental procedures involving animals were approved by the Institutional Animal Care and Use Committee at the University of California, Davis, the University of California San Diego, the University of Washington, the University of Iowa Cold Spring Harbor Laboratory and the National Institute of Mental Health or Icahn School of Medicine and adhered to principles described in the National Institutes of Health (NIH) Guide for the Care and Use of Laboratory Animals. The University of California Davis, the University of California San Diego, the University of Washington, the University of Iowa, Cold Spring Harbor Laboratory, the National Institute of Mental Health and Icahn School of Medicine are accredited by the Association for Assessment and Accreditation of Laboratory Animal Care International (AAALAC).

### Reagent and key resources

All reagent, software and equipment are summarized in Supplementary Table 1.

### Sensor development and characterization

**Development of κLight, δLight and μLight.** All constructs were designed using circular polymerase extension cloning, restriction cloning and gBlock gene fragments (Integrated DNA Technologies)<sup>69</sup>. Sequences coding for a FLAG epitope were placed at the 5′-end of the construct as previously described<sup>70</sup>. *HindIII* and *NotI* cut sites were placed at the 5′- and 3′ ends, respectively, for cloning into pCMV (Addgene) to generate all pCMV constructs. *BamHI* and *HindIII* sites were introduced via PCR for final subcloning onto pAAV.hSynapsin1 vectors (Addgene). To maximize coupling between conformational changes and chromophore fluorescence, we chose to use a cpGFP module (LSS-LE-cpGFP-LP-DQL) from GCaMP6 (ref. 71) for insertion into the human OPRK1 (κOR), OPRD1 (δOR) and OPRM1 (μOR) using circular polymerase extension cloning.

For screening linker variants, we generated linker libraries by first creating an insert DNA carrying a randomized two-amino-acid linker on each side of cpGFP (LSS-xx-cpGFP-xx-DQL). Cloned constructs were amplified and purified with the Qiagen PCR purification kit before NEB 5-α competent *Escherichia coli* transformation. Competent cells were plated onto kanamycin-containing agar plates. After allowing for 24 h of growth at 37 °C, single colonies were manually picked and grown overnight as described previously<sup>72</sup>. Plasmids from the colonies were purified using the Qiagen miniprep kit. Top variants were sequenced by Genewiz. For the iteration of κLight variants, κLight1.1 was discovered after linker screen and resulted in linker GI-PH. κLight1.2a: V164K from κLight1.1. κLight1.2b is κLight1.2a with ER2 tag. κLight1.2c is κLight1.2b with T603K. κLight1.3 is κLight1.2a with T1cnC, PRC and ER2 tag. κLight0 is κLight1.2a with D128N. δLight has linker GI-PH, p.Val154Lys mutation with PRC and ER2 tag. δLight0 has p.Asp128Asn mutation. μLight has linker sequence CI-SH, p.Val175Gln mutation with PRC and ER2 tags. To make AAV plasmids, NEB stable competent cells were transformed with pAAV plasmids. After growth on an agar plate at 30 °C, a single colony was selected. After sequencing confirmed the presence of the sensor gene, the cells were expanded at 30 °C in 100 ml of growth medium (2xYT) and purified with a Qiagen Endo-free Plasmid Maxi Kit and sent to the UC Davis Virus Packaging Core for virus production.

**Tissue culture.** HEK293T cells were grown in DMEM, supplemented with FBS and penicillin–streptomycin. Cells were transfected with Effectene according to the manufacturer's instructions. Before imaging, cells were washed with Hank's Balanced Salt Solution (HBSS) supplemented with 2 mM MgCl<sub>2</sub> and 2 mM CaCl<sub>2</sub>. All images were collected in HBSS containing Mg<sup>2+</sup> and Ca<sup>2+</sup> (HBSS+).

**Transient transfection.** HEK293T cells were plated and transfected concurrently 24 h before each experiment using the Qiagen Effectene Transfection Reagent kit according to the manufacturer's protocol.

**Displacement binding assays.** Membranes were prepared from μLight, δLight, κLight cells or CHO-μOR cells as described previously<sup>37</sup>. Displacement binding assays were carried out with membranes (100 μg), [<sup>3</sup>H]diprenorphine (3 nM final concentration) and different ligands (0–10 μM final concentration) as described previously<sup>16,38</sup>, except that the assay buffer consisted of 50 mM Tris-Cl (pH 7.4) containing 100 mM NaCl, 10 mM MgCl<sub>2</sub>, 0.2 mM EGTA and protease inhibitor cocktail (Sigma-Aldrich, P2714), and incubation was carried out for 1 h at 30 °C.

**Micro-confocal high-throughput imaging experiments.** Glass-bottom 96-well plates (P96-1.5H-N, Cellvis) were coated with 50 μg ml<sup>-1</sup> of poly-D-lysine (Sigma, P6407-5MG) and 10 μg ml<sup>-1</sup> of laminin (Sigma, L2020) overnight in an incubator (37 °C, 5% CO<sub>2</sub>). Plates were washed with Dulbecco's PBS (Thermo Fisher, 14190-250) and PSYLI2 cells were suspended in DMEM (Fisher, 11995073) containing 10% FBS (Fisher, 26-140-079) with 5% penicillin–streptomycin (Fisher, 15140-163) and plated at a density of 40,000 cells per well 24 h before each experiment. Immediately before an experiment, stock solutions of drugs in dimethylsulfoxide (10 mM) were diluted at a 1:100 ratio in imaging media distributed across an empty 96-well plate (treatment plate) in triplicate following a randomized plate map. The imaging media consisted of 1× HBSS (Fisher, 14175103) containing 0.5 M MgCl<sub>2</sub> (Sigma, M8266-1KG) and 0.5 M CaCl<sub>2</sub> (Sigma, C5670-50G). Cells grown in a separate 96-well plate (assay plate) were gently washed 3× with imaging media, and the wells were filled with an appropriate volume of imaging media for the respective experiment (see below).

**HEK cell titration.** For titration experiments, 50 μl of imaging medium was added to each well of the assay plate. Wells were then imaged with ImageXpress Micro Confocal High-Content Imaging System at ×40 (N.A., 0.6) with four regions of interest (ROIs) taken per well with no bias to location and no overlap of the ROIs (exposure, 300 ms) with MetaXpress software. Next, 50 μl from the treatment plate was transferred to the assay plate containing a double desired final concentrations. As for titration dose and controls, ligand of interest from 1 pM to 100 μM (final) dissolved in HBSS+ as vehicle were used. Blank controls with vehicles were present on every plate with randomized locations. After 5 min of incubation, the same sites were reimaged using the same settings.

Once imaging was complete, the images were exported and analyzed using a self-written MATLAB script. The script will be deposited in GitHub. In short, segmentation was performed on individual images and a mask highlighting the membrane of the HEK293T cells was generated. Pixel intensities were obtained from the mask-highlighted area and exported into Excel. The ΔF/F values for each well were calculated using the following equation:

$$\frac{(\text{average fluorescence after drug} - \text{average fluorescence before drug})}{\text{average fluorescence before drug}}$$

These values were then used to obtain the triplicate mean ( $n = 3$ ). SNR values are calculated by:

$$\frac{(\text{average fluorescence after drug} - \text{average fluorescence before drug})}{\sqrt{\text{average fluorescence before drug}}}$$

**Schild regression analysis.** A treatment plate was prepared by premixing various concentrations of antagonists with increasing concentrations of the sensors' specific agonist. The agonist and antagonist were premixed in doubled concentrations in a treatment plate in HBSS+.

Wells were first imaged with 50  $\mu$ l HBSS+ in the well, and 50  $\mu$ l of the mix of ligands from the treatment plate was then added to the imaging plate, and the wells were imaged again under the same settings.

**cAMP assay.** HEK293 cells (American Type Culture Collection), maintained in DMEM (Invitrogen, 11965118) supplemented with 10% FBS (Clontech), were transfected in 10-cm dishes with 1  $\mu$ g of Flag- $\kappa$ Light 1.3,  $\delta$ Light, Flag- $\delta$ OR or Flag- $\kappa$ OR construct cloned into pcDNA3.0, together with 2  $\mu$ g of pGloSensor-20F plasmid (Promega), using Lipofectamine 2000 (Thermo Fisher, 11668019) per the manufacturer's instructions. Twenty-four hours after transfection, cells were lifted using TrypLE Express (Thermo Fisher, 12604021), pelleted (500g for 5 min) and resuspended at 100,000 cells per ml in phenol red-free DMEM (Invitrogen, 31053028) supplemented with 30 mM HEPES and 250  $\mu$ g per ml luciferin (Biogold). Then, 150  $\mu$ l of the suspension was added to each well of a 96-well dish, and cells were maintained for 45–60 min in a 37 °C incubator. Cells were then assayed using a scanning plate-reading luminometer (Tecan Spark) at 37 °C. Baseline luminescence was measured over 5 min. Forskolin and dynorphin A (1-17; Anaspec, A24298) were used to assess  $\kappa$ Light1.3 relative to  $\kappa$ OR, and forskolin and DADLE (DADLE [D-Ala<sup>2</sup>, D-Leu<sup>5</sup>]-enkephalin; Sigma-Aldrich, E7131) were used to assess  $\delta$ Light relative to  $\delta$ OR. Forskolin and each opioid agonist peptide were added together to each well in a volume of 50  $\mu$ l, adjusted to achieve a final concentration of 10  $\mu$ M forskolin and the indicated concentration of opioid agonist. Luminescence measurement was resumed for 10 min and a maximum baseline-subtracted value was used to determine the cellular cAMP response. Each condition was measured in triplicate wells and values reported were averages from four to five independent experiments.

**$\beta$ -Arrestin recruitment assay.** HEK293 cells were transfected in 6-well dishes with 200 ng of Flag- $\kappa$ Light1.3, Flag- $\delta$ Light, Flag- $\kappa$ OR or Flag- $\delta$ OR constructs cloned into pcDNA3.0, 100 ng LargeBit-CAAX and 500 ng SmallBit  $\beta$ -Arrestin1 (ref. 73), using Lipofectamine 2000 per the manufacturer's instructions. Twenty-four hours after transfection, cells were lifted, washed by centrifugation as above and resuspended to a density of  $0.5\text{--}1 \times 10^6$  cells per ml in phenol red-free DMEM supplemented with 30 mM HEPES and 5  $\mu$ M coelenterazine-H (Research Products International). Cells were distributed in a 96-well dish at 150  $\mu$ l per well, incubated for 15 min at 37 °C to load coelenterazine-H and then a 5-min baseline was measured in the luminometer at 37 °C. Following this, 1  $\mu$ M of dynorphin A (1-17; for  $\kappa$ Light/ $\kappa$ OR assessment) or DADLE (for  $\delta$ Light/ $\delta$ OR assessment) was added, and measurement was resumed for an additional 30 min. The maximum baseline-subtracted luminescence was used to determine recruitment values. Each condition was measured in triplicate wells and values reported are averages from three independent experiments.

### Slice experiments

**Stereotaxic intracranial injection.** Male and female C57/B6J mice (postnatal day 0–3) were anesthetized with isoflurane and placed in a small animal stereotaxic frame (David Kopf Instruments). After puncturing the skin and skull under aseptic conditions, AAVs were injected (0.5–1  $\mu$ l total volume) bilaterally through a pulled glass pipette at a rate of 100 nl min<sup>-1</sup> using a UMP3 microsyringe pump (World Precision Instruments). Depending on the size of the mouse, injection coordinates ranged from 0 mm to +0.5 mm from bregma, 0.5 mm to 1.0 mm lateral and 1.8 mm to 2.3 mm below pia for dStr. For targeting hippocampus to study buffering, injection coordinates were +0.3 mm to 0.5 mm from lambda, 2.2 mm to 2.5 mm lateral and 1.4 mm to 2.0 mm below pia. After surgical procedures, mice were returned to their home cage for >30 days to allow for maximal gene expression. For CA3 injection in hippocampus for electrical stimulation, we used the coordinates: -1.7 mm AP, 1.75 mm ML, -2.3 mm DV. To achieve sparse labeling of neurons in CA3, we injected AAV1-CAG-DIO- $\kappa$ Light1.3a into

CA3 with a 1:1,000 dilution of AAV1-*hSyn*-Cre virus. Male and female C57/B6J mice were injected 8–10 weeks postnatally.

**Brain slice preparation.** P30–60 mice were anesthetized with isoflurane and killed, and the brains were removed, blocked and mounted in a VT1000S vibratome (Leica Instruments). For striatal imaging experiments, coronal slices (300  $\mu$ m) were prepared in 34 °C artificial cerebrospinal fluid (aCSF) containing 127 mM NaCl, 2.5 mM KCl, 25 mM NaHCO<sub>3</sub>, 1.25 mM NaH<sub>2</sub>PO<sub>4</sub>, 2 mM CaCl<sub>2</sub>, 1 mM MgCl<sub>2</sub> and 25 mM glucose, with osmolarity of 307, equilibrated with 95% O<sub>2</sub>/5% CO<sub>2</sub>. For hippocampal electrophysiology recordings, horizontal slices (300  $\mu$ m) were prepared in ice-cold choline-aCSF containing 25 mM NaHCO<sub>3</sub>, 1.25 mM NaH<sub>2</sub>PO<sub>4</sub>, 2.5 mM KCl, 7 mM MgCl<sub>2</sub>, 25 mM glucose, 1 mM CaCl<sub>2</sub>, 110 mM choline chloride, 11.6 mM ascorbic acid and 3.1 mM pyruvic acid, equilibrated with 95% O<sub>2</sub>/5% CO<sub>2</sub>. Slices were transferred to a holding chamber with oxygenated aCSF and incubated at 32 °C for 30 min and then left at room temperature until recordings were performed.

**Fluorescence imaging with peptide uncaging.** All video recordings were performed within 5 h of slicing in a submerged slice chamber perfused with aCSF warmed to 32 °C and equilibrated with 95% O<sub>2</sub>/5% CO<sub>2</sub>. Sensor-expressing tissue in the dStr was located and imaged through an eGFP filter cube (Semrock, GFP-3035D-OMF) under a  $\times 60$ , 0.8-NA objective using a SciCam CCD camera (Scientifica) and illumination with the 470-nm LED (CoolLED). Ocular image acquisition software (QImaging) was used to acquire videos using a 100-ms exposure time at a frame rate of 1 Hz. For uncaging trials, 5  $\mu$ M of CYD8 was circulated in the bath before beginning video acquisition. During uncaging trials, ScanImage was used to trigger video acquisition and the UV laser. Uncaging was carried out using 50-ms flashes of light from a 355-nm laser (DPSS Lasers). For full-field uncaging (Fig. 3c,d and Extended Data Fig. 3b,c), a 70- $\mu$ m-diameter area of tissue was illuminated with collimated UV light at a power density of 5  $\mu$ W/ $\mu$ m<sup>2</sup>, as measured in the sample plane. When measuring DynA8 diffusion, a 25- $\mu$ m-diameter area of focused 355-nm light at a power density of 39  $\mu$ W/ $\mu$ m<sup>2</sup> was applied near the edge of the imaging field.

**Electrophysiology.** All recordings were performed within 5 h of slicing in a submerged slice chamber perfused with aCSF warmed to 32 °C and equilibrated with 95% O<sub>2</sub>/5% CO<sub>2</sub>. Whole-cell voltage-clamp recordings were obtained with an Axopatch 700B amplifier (Molecular Devices). Data were sampled at 10 kHz, filtered at 3 kHz and acquired using National Instruments acquisition boards and a custom version of ScanImage written in MATLAB (Math Works). Cells were rejected if holding currents exceeded -200 pA or if the series resistance (<25 M $\Omega$ ) changed during the experiment by more than 20%. For recordings measuring inhibitory synaptic transmission in mouse hippocampus, patch pipettes (2.8–3.5 M $\Omega$ ) were filled with an internal solution containing 135 mM CsMeSO<sub>3</sub>, 10 mM HEPES, 1 mM EGTA, 3.3 mM QX-314 (Cl<sup>-</sup> salt), 4 mM Mg-ATP, 0.3 mM Na-GTP and 8 mM Na<sub>2</sub> phosphocreatine (pH 7.3, 295 mOsm kg<sup>-1</sup>). Cells were held at 0 mV to produce outward currents. Excitatory transmission was blocked by the addition to the aCSF of NBQX (2,3-dioxo-6-nitro-7-sulfamoyl-benzo[f]quinoxaline, 10  $\mu$ M) and CPP (3-(2-carboxypiperazin-4-yl)propyl-1-phosphonic acid, 10  $\mu$ M). To electrically evoke IPSCs, stimulating electrodes pulled from theta glass with -5- $\mu$ m tip diameters were placed at the border between stratum pyramidale and stratum oriens nearby the recorded cell (-50–150  $\mu$ m), and two brief pulses (0.5 ms, 50–300  $\mu$ A, 50-ms interval) were delivered every 20 s. Uncaging was carried out using 5-ms flashes of collimated full-field illumination with a 355-nm laser at different power densities, which were measured at the sample plane.

**Data analysis.** Video acquisition data were first analyzed in ImageJ and subsequently plotted in Igor Pro (Wave Metrics). The mean brightness of each frame was divided by the average baseline fluorescence of the



first minute to calculate  $\Delta F/F$ . Then, the first minute before uncaging was fit with a bi-exponential curve to estimate the rate of bleaching during the video acquisition. The fitted bleaching curve was then subtracted from the recorded traces to correct for bleaching. A 3,800  $\mu\text{m}^2$  circle ROI was drawn at the center of the uncaging field and the mean brightness of this ROI was plotted per frame. Electrophysiology data were analyzed in Igor Pro (Wave Metrics). Peak current amplitudes were calculated by averaging over a 2-ms window around the peak IPSC. To determine the magnitude of modulation by DynA8 photorelease (the percentage of IPSC suppression), the IPSC peak amplitude measured immediately after a flash was divided by the average peak amplitude of the three IPSCs preceding the light flash. To determine the time constant of recovery ( $\tau_{\text{off}}$ ), the IPSC amplitudes were fit to a mono-exponential function starting at the point of maximal IPSC suppression to the point at which the IPSC amplitude returned to baseline.

**Diffusion coefficient calculation.** Based on a derivation of Fick's law of diffusion that yields  $\gamma^2 = 4D^*(t_i + t_0)$  (ref. 66),  $D^*$  is the slope of the linear regression between  $\gamma^2/4$ , where  $\gamma$  is the half-width of the spatial fluorescence profile, and time ( $t$ ), as demonstrated by diffusion of dextrans molecules or quantum dots in the cortex<sup>74</sup>. To reduce noise, we averaged 50 pixels in the  $y$  axis around the center line of the image plane (parallel to the uncaging spot).

**Brain slices for two-photon imaging.** Three to four weeks after viral injection, samples from adult mice were anesthetized with 2.5% avertin and perfused in ice-cold carbogen (95%  $\text{O}_2$  and 5%  $\text{CO}_2$ ) gassed cutting NMDG-HEPES aCSF solution that contained: 92 mM NMDG, 2.5 mM KCl, 1.25 mM  $\text{NaH}_2\text{PO}_4$ , 30 mM  $\text{NaHCO}_3$ , 20 mM HEPES, 24 mM D-glucose, 2 mM thiourea, 5 mM sodium ascorbate, 3 mM sodium pyruvate, pH adjusted to 7.3–7.4 mM and supplemented with 0.5 mM  $\text{CaCl}_2$  and 10 mM  $\text{MgCl}_2$ , before decapitation. Brains were quickly extracted and were cut (300  $\mu\text{m}$ ) with a vibratome (VI200, Leica) in ice-cold oxygenated NMDG-HEPES aCSF. Brain slices were incubated at 34–36 °C for 10 min before transferring to HEPES holding aCSF that contained 92 mM NaCl, 2.5 mM KCl, 1.25 mM  $\text{NaH}_2\text{PO}_4$ , 30 mM  $\text{NaHCO}_3$ , 20 mM HEPES, 25 mM D-glucose, 2 mM thiourea, 5 mM sodium ascorbate and 3 mM sodium pyruvate, pH adjusted to 7.3–7.4 and supplemented with and 2 mM  $\text{CaCl}_2$  and 2 mM  $\text{MgCl}_2$ , saturated with 95%  $\text{O}_2$  and 5%  $\text{CO}_2$  (ref. 75). Imaging was carried out at room temperature using a two-photon microscope. The sensor was excited at 920 nm with a titanium–sapphire laser (Ultra II, Coherent) that was focused by an Olympus  $\times 40$ , 0.8-NA water immersion objective. Emitted fluorescence was separated by a 525/50-nm filter set, and detected by a photomultiplier (H7422PA-40, Hamamatsu). Data were acquired and collected with ScanImage5 software. Electrical stimulation was performed with a bipolar stimulating electrode (Array of 2 SNEX-100 PI concentric electrodes epoxied side-by-side, MicroProbes). The area within approximately 20  $\mu\text{m}$  of the electrode was imaged. Rectangular voltage pulses were applied through a nine-channel programmable pulse stimulator (Master-9, A.M.P. Instruments) and a stimulus isolation unit (Analog Stimulus Isolator, A-M Systems). Imaging and electrical stimulation were controlled by an Axon Digidata 1550B. Field potentials were applied at 1, 5, 10 and 15 trains with an interstimulus interval of 0.5 s, where one single stimulus is one train at 5 V, 50 Hz with a duration of 1 s. Experiments were carried out at a scan rate of 30 Hz (512  $\times$  512 pixels). Drugs were dissolved as a stock solution in imaging HBSS buffer and diluted to final concentration before application in the perfusion system.

Fluorescence intensities from video acquisition for two-photon field stimulation recording were performed with ImageJ. Due to the long-range diffusion nature of NPs, whole two-photon field-of-view fluorescence intensity was extracted instead of applying segmentation for fine cellular components.  $\Delta F/F$  were calculated by (fluorescence intensity per frame – average base line fluorescence intensity) / average

base line fluorescent intensity), where baseline is defined as first 2 min for each recording. The peak intensities were determined by averaging the  $\Delta F/F$  values from frames at the plateau of elevated signals following stimulation.

The z-score image was processed by  $\Delta F/\text{s.d. (baseline)}$ ; baseline is the average intensity of the first 500 frames without stimulation, and  $\Delta F$  is calculated as the difference between averaged fluorescence intensity across frames at responses plateau and baseline. Data were averaged per stimulation condition and plotted by Prism.

## In vivo recordings

**Experimental subjects and stereotaxic surgery.** Adult (25–35 g), 12- to 16-week-old  $\kappa\text{OR-Cre}$  mice or C57/B6J mice were group housed, given access to food pellets and water ad libitum and maintained on a 12-h:12-h light–dark cycle (lights on at 7:00). All animals were kept in a sound-attenuated, isolated holding facility in the lab 1 week before surgery, after surgery and during the behavioral assays to minimize stress.

For surgery, mice were anesthetized in an induction chamber (2–4% isoflurane) and placed into a stereotaxic frame (Kopf Instruments, 1900) where they were maintained at 1–2% isoflurane. Male and female mice were anesthetized, following which we performed a craniotomy and unilaterally injected as described below, using a blunt neural syringe (65457-01, Hamilton Company). For photostimulation experiments and  $\kappa\text{Light}$  Pavlovian conditioning experiments: 300–400 nl of AAV5-DIO-ChrimsonR-tdTomato (UW NAPE Center Viral Vector Core, viral titer  $5 \times 10^{12}$  viral genomes (vg) per ml) into the BLA (stereotaxic coordinates from bregma: –1.3 mm [AP],  $\pm 3.2$  mm [ML], –4.6 mm [DV]), and AAV-DIO- $\kappa\text{Light1.3}$  (UC Davis Viral Core, viral titer  $3.6 \times 10^{13}$  vg per ml) followed immediately by fiber-optic implantation into the NAcSh (stereotaxic coordinates from bregma: +1.3 mm [AP],  $\pm 0.5$  mm [ML], –4.5 mm [DV]). For experiments involving the DYN-KO, AAV5-DIO-ChrimsonR-tdTomato and AAV-DIO- $\kappa\text{Light1.3}$  were mixed with AAV-DIO-Cre at a 1:1 dilution and injected and implanted in the aforementioned regions using the same coordinates. For fear conditioning experiments: 300–400 nl of AAV9- $h\text{Syn-}\kappa\text{Light1.3}$  (Canadian Neurophotonics, viral titer  $1 \times 10^{13}$  vg per ml) and AAV9- $h\text{Syn-}\delta\text{Light}$  (Canadian Neurophotonics, viral titer  $3.3 \times 10^{12}$  vg per ml) were injected separately into the dorsal NAcsh (dNAcsh, +1.3 mm [AP],  $\pm 0.5$  mm [ML], –4.5 mm [DV]) and ventral NAcsh (vNAcsh, +1.3 mm [AP],  $\pm 0.5$  mm [ML], –5 mm [DV]). For fear conditioning control experiments: 300–400 nl of AAV1- $h\text{Syn-}\kappa\text{Light0}$  (Canadian Neurophotonics, viral titer  $7.8 \times 10^{12}$  vg per ml) and AAV1- $h\text{Syn-}\delta\text{Light0}$  (Canadian Neurophotonics, viral titer  $9.5 \times 10^{12}$  vg per ml) were injected into vNAcsh as controls. For  $\delta\text{Light}$  caramel reward retrieval experiments: 300–500 nl virus (AAV9- $h\text{Syn-}\delta\text{Light}$ , AAV-syn- $\delta\text{Light0}$ ) was injected bilaterally in the mediobasal hypothalamus (ARC, –1.25 mm [AP],  $\pm 0.25$  mm [ML], –5.6 mm [DV]) from the surface of the brain using a pulled glass pipette (Drummond Scientific, Wiretrol) controlled by a micromanipulator (Narishige). A fiber cannula was then implanted at the injection site, and the implants were secured using two bone screws and a dental cement head cap (Lang Dental). ([AP] values were measured from bregma, and [ML] values were measured from the skull at bregma unless otherwise noted.)

**Fiber photometry.** For fiber photometry studies, recordings were obtained throughout the entirety of drug injection, Pavlovian conditioning and head-fixed sessions as previously described<sup>76</sup>. Before recording, an optic fiber was attached to the implanted fiber using a ferrule sleeve (Doric, ZR\_2.5). Two LEDs were used to excite  $\kappa\text{Light1.3}$ . A 531-Hz sinusoidal LED light (Thorlabs, LED light: M470F3; LED driver: DC4104) was bandpass filtered ( $470 \pm 20$  nm, Doric, FMC4) to excite  $\kappa\text{Light1.3}$  and evoke emission. A 211-Hz sinusoidal LED light (Thorlabs, LED light: M405FP1; LED driver: DC4104) was bandpass filtered ( $405 \pm 10$  nm, Doric, FMC4) to evoke isosbestic control emission. Laser intensity for the 470-nm- and 405-nm-wavelength bands were

measured at the tip of the optic fiber and adjusted to 50  $\mu$ W before each day of recording.  $\kappa$ Light1.3 fluorescence traveled through the same optic fiber before being bandpass filtered ( $525 \pm 25$  nm, Doric, FMC4), transduced by a femtowatt silicon photoreceiver (Newport, 2151) and recorded by a real-time processor (TDT, RZ5P). The envelopes of the 531-Hz and 211-Hz signals were extracted in real time by the TDT program Synapse at a sampling rate of 1,017.25 Hz. For the ChrimsonR stimulation experiments, a 625-nm laser was used at 2 mW of intensity to deliver red light through the tip of the same optic fiber used to excite BLA terminals for stimulation-evoked dynorphin release.

**Drug injection.** Mice were pretreated with either vehicle (17:1:1 ratio of saline:dimethylsulfoxide:corn oil:ethanol) or aticaprant (Eli Lilly) at 3 mg per kg body weight of body weight i.p. for 30 min. Mice were then tethered to a photometry cable and placed in a chamber. Following a 5-min baseline recording, mice were injected with either saline or U50,488 (Sigma-Aldrich) at 10 mg per kg body weight body weight i.p. Recordings were conducted for a total of 1 h.

**Pavlovian behavior paradigm.** Mice were initially food deprived to 90% of their body weight and trained in a Pavlovian behavioral paradigm for a total of 7 days with a modular test chamber ( $17.8 \times 15.2 \times 18.4$  cm; Med Associates), as previously described<sup>76</sup>. Mice were tethered to a photometry cable and habituated to an operant chamber in which there is a house light and pellet receptacle. The house light illuminates as the conditioned stimulus (CS) and sucrose pellets (20 mg, BioServe) are the unconditioned stimulus (US). Each trial consists of 5 s of CS presentation and a single sucrose pellet dropped 7 s after CS onset. The intertrial interval was randomized between 60 and 120 s. The total session was 1 h.

**Stimulation-evoked release.** Mice were restrained at the head in a custom-made head-fixation device<sup>77</sup> and tethered to a photometry cable. For initial parameter determination experiments, mice received 20-Hz, 5-ms pulse-width laser stimulation in a randomized order varying the stimulus intensity, duration or pulse number, separated by an intertrial interval of 5 min resulting in five trials per mouse per condition, every session. For drug pretreatment experiments, mice were injected with aticaprant at 3 mg per kg body weight or U50,488 at 10 mg per kg body weight body weight i.p. using the aforementioned vehicle 30 min before stimulation sessions. Mice received ten trials per mouse with an intertrial interval of 5 min.

**Fear conditioning paradigm.** Mice were placed into a fear conditioning chamber (Med Associates) with a patch cord connected for photometric recordings. A Doric fiber photometry system was used in this study with 465 nm and 405 nm of light (LED,  $\sim 30$   $\mu$ W) used for generating the signal and as an isosbestic control, respectively. Each animal received 15 presentations of a 27-s tone (3,000 Hz) co-terminating with a foot shock (0.5 mA for 1.5 s) delivered at 2-min intervals. Each animal received 15 tone-foot shock pairings over the course of 40 min, and the responses for these trials were averaged to create a single trace per animal. Data analysis was performed with custom-written script in MATLAB. In brief, 405-nm traces were fit with a bi-exponential curve, and then the fit was subtracted from the signal to correct for baseline drift.  $\Delta F/F\%$  was calculated as  $[100 \times (465 \text{ signal} - \text{fitted signal})/\text{fitted signal}]$ . Traces were then z-scored. A heat map was plotted using a custom MATLAB script by plotting normalized single trials of traces from all animals tested per brain region.

**Photometry analysis.** Custom MATLAB scripts were developed for analyzing fiber photometry data in the context of mouse behavior. The isosbestic 405-nm excitation control signal was subtracted from the 470-nm excitation signal to remove movement artifacts. Baseline drift was evident in the signal due to slow photobleaching artifacts,

particularly during the first several minutes of each recording session. A double exponential curve was fit to the raw trace and subtracted to correct for baseline drift. After baseline correction, the photometry trace was z-scored relative to the mean and standard deviation of the session. The post-processed fiber photometry signal was analyzed in the context of animal behavior during Pavlovian conditioning and operant task performance. Pearson correlations, one-sample *t*-tests, two-sample *t*-tests and two-way ANOVAs were performed using standard MATLAB functions 'corr', 'ttest', 'ttest2' and 'anovan', respectively. Peak, mean and minimum fluorescence was determined during pre-determined time windows for the injection period (0–5 min), reward period (5–20 s), release period (0–20 s) or artifact period (0–20 s) subtracted from peak, mean or minimum fluorescence values in a baseline window (–5 to 0 s). Code that supports the analysis will be made available from the corresponding author upon reasonable request.

**Perfusion and histology.** The stock Avertin (tribromoethanol) was made by mixing 10 g of 2,2,2-tribromoethyl alcohol and 10 ml of tert-amyl alcohol. The working stock was diluted to 1.2% (vol/vol) with water and shielded from light. Animals were euthanized with 125 mg per kg body weight 1.2% Avertin (i.p.) followed by transcardial perfusion with ice-cold  $1 \times$  PBS and subsequently perfused with ice-cold 4% paraformaldehyde in  $1 \times$  PBS. After extraction of the mouse brains, samples were post-fixed in 4% paraformaldehyde at 4 °C overnight. The mouse brains were cryo-protected by immersion in 10% sucrose in a  $1 \times$  PBS solution overnight. Samples were next placed in 30% sucrose in a  $1 \times$  PBS solution for >1 day, before embedding the samples in O.C.T. Samples were then transferred to a  $-80$  °C freezer for long-term storage or were sliced into 50- $\mu$ m sections on a cryostat (Leica Biosystems) for histology. Histology samples were imaged on a Leica Stellaris 8 confocal microscope.

### Quantification and statistical analysis

Treatments were randomized, and the data were analyzed by experimenters blinded to the treatment conditions. No statistical methods were used to predetermine sample sizes, but our sample sizes are similar to those reported in previous publications<sup>35,54,56,57,59</sup>. Data distribution was assumed to be normal, but this was not formally tested. Statistical analyses were performed using GraphPad Prism 9 unless noted otherwise. Measurements are taken from distinct samples, and the sample size is indicated as *n* numbers. All comparisons were planned before performing each experiment. A  $P < 0.05$  was considered significant. Data are represented as mean  $\pm$  s.e.m., unless otherwise noted, with asterisks indicating significance levels (\* $P < 0.05$ , \*\* $P < 0.01$ , \*\*\* $P < 0.001$  and \*\*\*\* $P < 0.0001$ ). No animals or data points were excluded from the analysis.

### Materials availability

The following plasmids have been deposited in Addgene: pCMV- $\kappa$ Light1.3 (201223), pCMV- $\delta$ Light (201224) and pCMV- $\mu$ Light (201225). The following viral constructs have been deposited at UNC Neurotools: pAAV-*hSyn*- $\kappa$ Light1.3 (NT-23-888), pAAV-CAG-DIO- $\kappa$ Light1.3a (NT-23-724) and pAAV-*hSyn*- $\delta$ Light (NT-23-485).  $\kappa$ Light1.3,  $\delta$ Light and  $\mu$ Light stable cell lines will be available upon request via MTA with UCD.

### Inclusion and ethics statement

In adherence to the principles outlined in the Global Code of Conduct for Research in Resource-Poor Settings, this study engaged local researchers in all phases, ensuring local relevance and shared ownership of data and intellectual property. Local ethical approval was obtained, and roles were clearly defined and agreed upon with local partners to foster capacity building. This research was conducted with high ethical standards, prioritizing the safety and well-being of all participants, and incorporating benefit-sharing measures for the use of local resources and knowledge.

## Reporting summary

Further information on research design is available in the Nature Portfolio Reporting Summary linked to this article.

## Data availability

The following public dataset was used to support this study: Allen Brain Atlas ISH data (<https://mouse.brain-map.org/>). All source data present in this manuscript are available from <https://github.com/lintianlab/OpioidSensors/tree/main/0-SourceData/>.

## Code availability

All custom MATLAB codes are available from <https://github.com/lintianlab/OpioidSensors/tree/main/1-Codes/>.

## References

69. Quan, J. & Tian, J. Circular polymerase extension cloning for high-throughput cloning of complex and combinatorial DNA libraries. *Nat. Protoc.* **6**, 242–251 (2011).
70. Irannejad, R. et al. Conformational biosensors reveal GPCR signalling from endosomes. *Nature* **495**, 534–538 (2013).
71. Chen, T. W. et al. Ultrasensitive fluorescent proteins for imaging neuronal activity. *Nature* **499**, 295–300 (2013).
72. Tian, L. et al. Imaging neural activity in worms, flies and mice with improved GCaMP calcium indicators. *Nat. Methods* **6**, 875–881 (2009).
73. Janetzko, J. et al. Membrane phosphoinositides regulate GPCR- $\beta$ -arrestin complex assembly and dynamics. *Cell* **185**, 4560–4573.e19 (2022).
74. Thorne, R. G. & Nicholson, C. In vivo diffusion analysis with quantum dots and dextrans predicts the width of brain extracellular space. *Proc. Natl Acad. Sci. USA* **103**, 5567–5572 (2006).
75. Ting, J. T., Daigle, T. L., Chen, Q. & Feng, G. in *Patch-Clamp Methods and Protocols* (eds Martina, M. & Taverna, S.) 221–242 (Springer, 2014).
76. Al-Hasani, R. et al. Author correction: ventral tegmental area GABAergic inhibition of cholinergic interneurons in the ventral nucleus accumbens shell promotes reward reinforcement. *Nat. Neurosci.* **24**, 1501 (2021).
77. Piantadosi, S. C. et al. Hyperactivity of indirect pathway-projecting spiny projection neurons promotes compulsive behavior. *Nat. Commun.* <https://doi.org/10.1038/s41467-024-48331-z> (2024).

## Acknowledgements

This work is funded by NIH Brain Initiative (U01NS103522 and U01NS120820 to L.T., U01NS113295 to M. R. Banghart and L.T.). We acknowledge NIDA grants R37DA033396 and R61DA051489 to M. R. Bruchas, and NIDA grant K99058709 to R.G. This research was supported, in part, by NIH grants DA008863 and DA058300 to L.A.D., and DK126740 to D.A. We thank the support from NIMH Intramural Research Program (ZIA-MH002970-04) to H.A.T. We thank M. V. Zastrow (UCSF) and J. Williams (Vollum) for providing key input to design and characterize early versions of sensors. We thank S. Gooding for

assistance in drug injection experiments in vivo. We thank J. Roshgadol (UC Davis) for assisting with the behavior-related experiments and analysis. We thank B. Trainor (UC Davis) for insightful comments.

## Author contributions

L.T. conceived and led the project. G.O.M., K.M. and C.D. developed and optimized the opioid sensors. C.D. designed and performed key experiments, including in vitro sensor characterization, drug screening assays, part of the in vivo drug injection assay and in vivo fear conditioning behavior experiments. C.D. also performed rodent surgeries for two-photon electrical stimulation experiments and in vivo fear conditioning experiments. R.G. worked with M. R. Bruchas to design and perform the optogenetics and Pavlovian conditioning experiments. Y.J. led the design and implementation of the two-photon electrical stimulation experiments. X.J.H. worked closely with M. R. Banghart to design and execute the uncaging experiments and dynorphin diffusion constant measurement. H.W. and R.J.F. characterized sensor variants and control sensors using in vivo fear conditioning experiments with guidance from H.A.T. N.S.-A. played a crucial role in performing the majority of the in vivo drug injection and caramel retrieval experiments with guidance from D.A. A.G. and I.G. performed the radioligand binding assay under the guidance of L.A.D. N.T. assisted on neuronal culture and imaging analysis. R.L. engineered viral vectors encoding sensors. A.M. performed cAMP and  $\beta$ -arrestin assays together with M.V.Z. D.K.L. assisted in vitro characterization. Q.S. and B.L. provided useful and informative discussions. J.L.W. provided compounds and helped design the sensor drug screening assay. L.T., C.D. and M. R. Banghart wrote the manuscript with input from other authors.

## Funding

Open access funding provided by Max Planck Society.

## Competing interests

L.T. is a co-founder of Seven Biosciences. All other authors declare no competing interests.

## Additional information

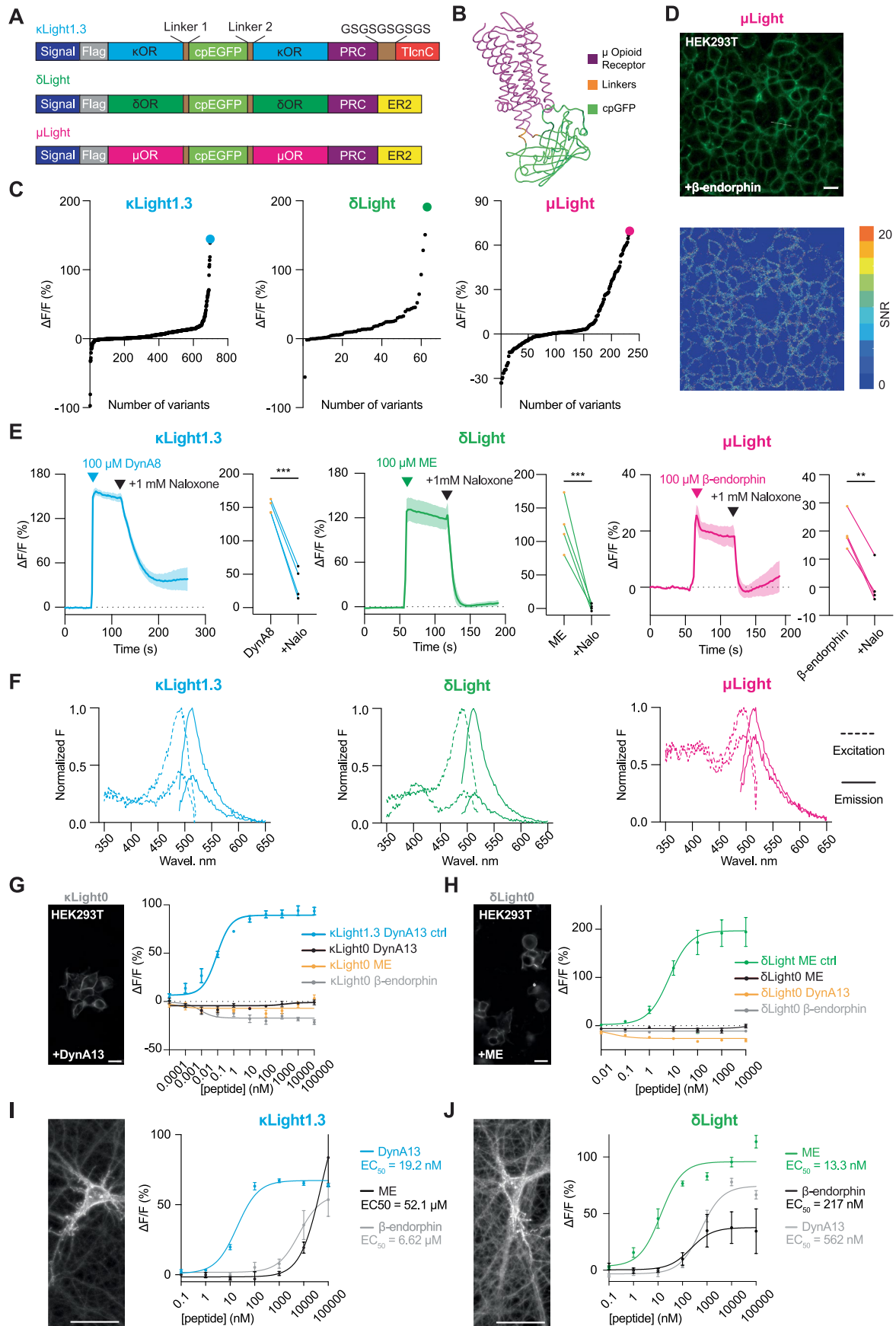
**Extended data** is available for this paper at <https://doi.org/10.1038/s41593-024-01697-1>.

**Supplementary information** The online version contains supplementary material available at <https://doi.org/10.1038/s41593-024-01697-1>.

**Correspondence and requests for materials** should be addressed to Michael R. Bruchas, Matthew R. Banghart or Lin Tian.

**Peer review information** *Nature Neuroscience* thanks the anonymous reviewers for their contribution to the peer review of this work.

**Reprints and permissions information** is available at [www.nature.com/reprints](http://www.nature.com/reprints).

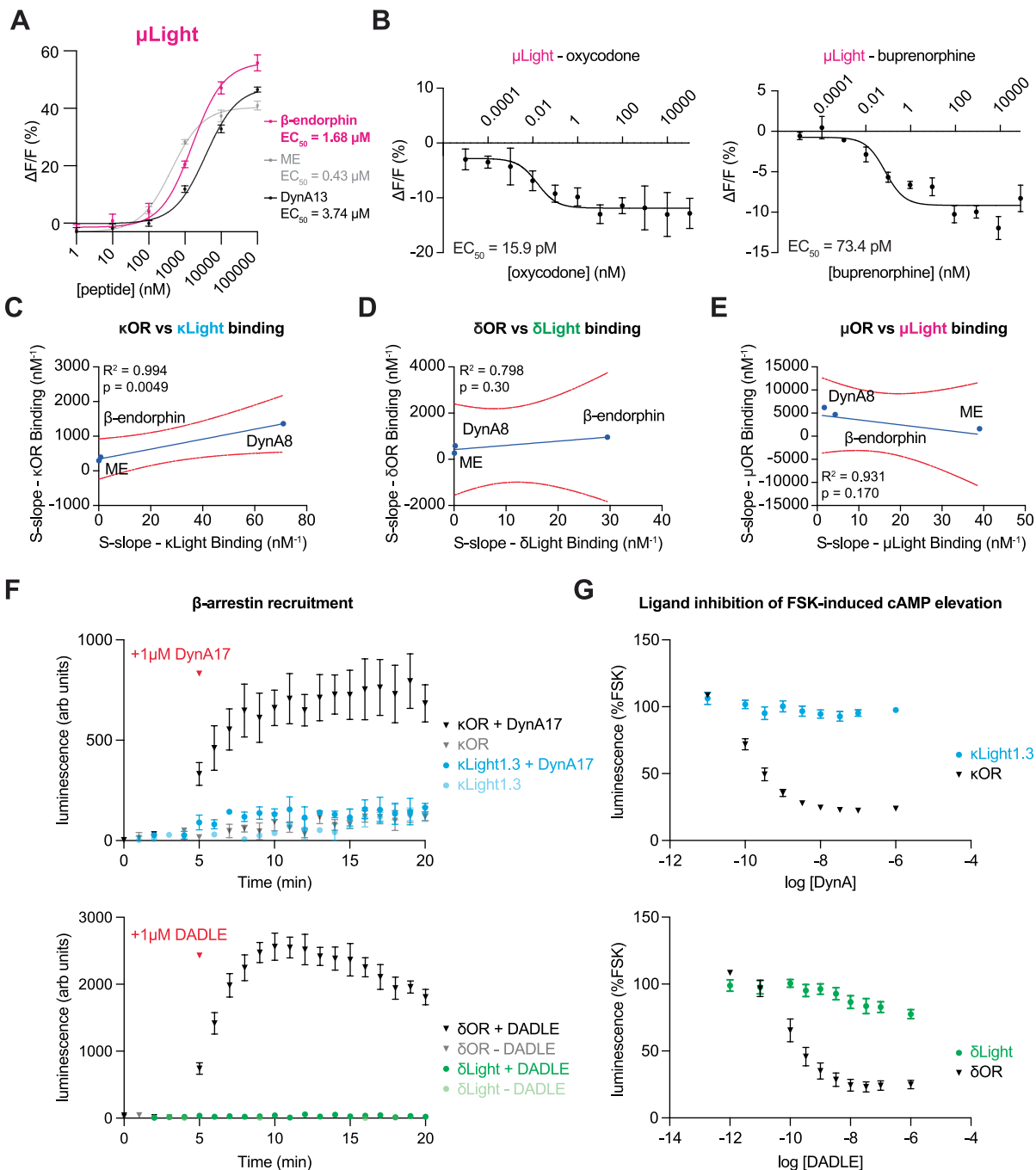


Extended Data Fig. 1 | See next page for caption.

**Extended Data Fig. 1 | Screening and characterization of the opioid sensors.**

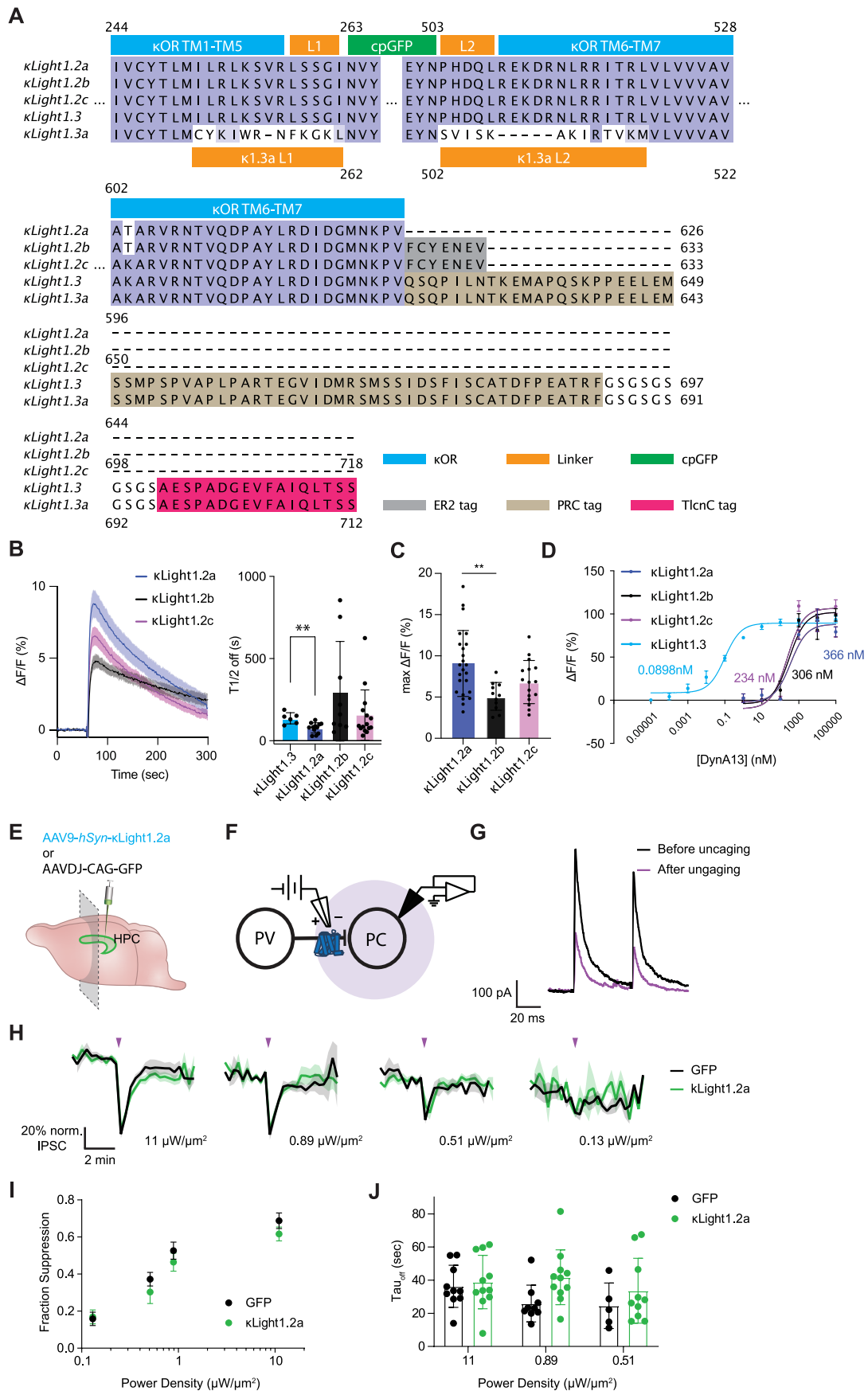
(a) Schematic diagrams showing the components of recombinant DNA for each opioid sensor. (b) Simulated structure of  $\mu$ Light. Mu opioid receptor ( $\mu$ OR, magenta), linkers (orange), cpGFP (light green). (c) Optimization of the opioid sensor variants. Dots representing  $\Delta F/F$  (%) of variants screened along optimizations, including cpGFP insertion sites, linker screening, and point mutations. A ligand concentration of 100  $\mu$ M was used for screening; U50,488 for  $\kappa$ Light (blue), ME for  $\delta$ Light (green) and DAMGO for  $\mu$ Light (magenta). Variants with the highest  $\Delta F/F$  (%) indicated as  $\kappa$ Light1.3 (144.47%) with 698 variants screened;  $\delta$ Light (191%) with 63 variants screened;  $\mu$ Light (69.6%) with 233 variants screened. (d) (Top) Representative image of 4 independent transient transfection of  $\mu$ Light in HEK293T cells. (Bottom) Heatmap indicating signal-to-noise-ratio (SNR) upon addition of 100  $\mu$ M  $\beta$ -endorphin. Scale bar, 20  $\mu$ m. (e) (Left) Agonist (100  $\mu$ M DynA8) and antagonist (1 mM naloxone) response of  $\kappa$ Light1.3 transiently expressed in dissociated hippocampal neuron cultures.  $n = 4$  wells. Solid blue line represents the mean, and shaded area represents SEM.  $\Delta F/F$  (%) comparison between two states: agonist response ( $151 \pm 5.0$  %), + antagonist response ( $36.9 \pm 11.7$  %), two-tailed unpaired  $t$  test,  $***p = 0.0001$ . Nalo = Naloxone. (middle) Agonist (100  $\mu$ M ME) and antagonist (1 mM naloxone) response of  $\delta$ Light transiently expressed in dissociated hippocampal neuron cultures.  $n = 4$  wells. Solid green line represents the mean, and the shaded area represents SEM.  $\Delta F/F$  (%) comparison between two states: agonist response ( $123 \pm 19.4$  %), + antagonist response ( $1.82 \pm 2.4$  %), two-tailed unpaired  $t$  test,  $***p = 0.0008$ . (right) Agonist (100  $\mu$ M  $\beta$ -endorphin) and antagonist (1 mM naloxone) response of  $\mu$ Light transiently expressed in dissociated hippocampal neuron cultures.  $n = 4$  wells. Solid magenta line represents the mean, and the shaded area represents SEM.  $\Delta F/F$  (%) comparison between two states: agonist

response ( $19.6 \pm 3.2$  %), + antagonist response ( $0.75 \pm 3.6$  %), two-tailed unpaired  $t$  test,  $***p = 0.0082$ . (Right). (f) Excitation-emission spectra of the three opioid sensors under both bound (upper lines, 100  $\mu$ M DynA8 for  $\kappa$ Light -blue, 100  $\mu$ M ME for  $\delta$ Light -green, and 100  $\mu$ M  $\beta$ -endorphin for  $\mu$ Light -magenta) and unbound (lower lines) states. Excitation (dotted lines) of all three sensors peaks at  $\sim 490$  nm, and emission (solid lines) of all three sensors peaks at  $\sim 515$  nm. (g) (Left) representative imaging showing  $\kappa$ Light0-expressing HEK293T cells, scale bar 20  $\mu$ m. (Right)  $\kappa$ Light0-expressing HEK293T cells respond to ligands in a concentration-dependent manner plotted together with  $\kappa$ Light1.3 (DynA13- $\kappa$ Light1.3 - blue, DynA13- $\kappa$ Light0 - black,  $\beta$ -endorphin- $\kappa$ Light0 - gray, ME- $\kappa$ Light0 - yellow). Error bars represent SEM.  $n = 4$  wells each. Dyn = dynorphin, ME = met-enkephalin. (h) (Left) representative imaging showing  $\delta$ Light0-expressing HEK293T cells, scale bar 20  $\mu$ m. (Right)  $\delta$ Light0-expressing HEK293T cells respond to ligands in a concentration-dependent manner plotted together with  $\delta$ Light (ME- $\delta$ Light - green, ME- $\delta$ Light0 - black,  $\beta$ -endorphin- $\delta$ Light0 - gray, DynA13- $\delta$ Light0 - yellow). Error bars represent SEM.  $n = 4$  wells each. Dyn = dynorphin, ME = met-enkephalin. (i) (Left) representative imaging showing  $\kappa$ Light1.3-expressing dissociated hippocampal neurons, scale bar 50  $\mu$ m. (Right)  $\kappa$ Light1.3-expressing dissociated hippocampal neurons respond to ligands in a concentration-dependent manner (DynA13 - blue,  $\beta$ -endorphin - gray, ME - black). Error bars represent SEM.  $n = 4$  wells each. Dyn = dynorphin, ME = met-enkephalin. (j) (Left) representative imaging showing  $\delta$ Light-expressing dissociated hippocampal neurons, scale bar 50  $\mu$ m. (Right)  $\delta$ Light-expressing dissociated hippocampal neurons respond to ligands in a concentration-dependent manner (ME - green, DynA13 - gray,  $\beta$ -endorphin - black). Error bars represent SEM.  $n = 4$  wells each. Dyn = dynorphin, ME = met-enkephalin, scale bar, 50  $\mu$ m.



**Extended Data Fig. 2 | Binding studies of selected compounds on the opioid sensors and receptors.** (a) Concentration-response curves of  $\mu$ Light-expressing HEK293T cells to three peptide ligands ( $\beta$ -endorphin – magenta, ME – gray, DynA13 – black). Error bars represent SEM. (b) Concentration-response curve of  $\mu$ Light-expressing HEK293T cells to oxycodone and buprenorphine. Error bars represent SEM. (c) Linear regression plot between the s-slope (maximum displacement / IC<sub>50</sub>, in nM<sup>-1</sup>) for  $\kappa$ OR (S-slope -  $\kappa$ OR Binding) and  $\kappa$ Light1.3 (S-slope -  $\kappa$ Light Binding) measured with a radio-ligand binding assay. Red curves indicate 95 % confidence interval. (d) Linear regression plot between the s-slope (maximum displacement / IC<sub>50</sub>, in nM<sup>-1</sup>) for  $\delta$ OR (S-slope -  $\delta$ OR Binding) and  $\delta$ Light (S-slope -  $\delta$ Light Binding) measured from radio-ligand binding assay. Red curves indicate 95 % confidence interval. (e) Linear regression plot between the

s-slope (maximum displacement / IC<sub>50</sub>, in nM<sup>-1</sup>) for  $\mu$ OR (S-slope -  $\mu$ OR Binding) and  $\mu$ Light (S-slope -  $\mu$ Light Binding) measured from radio-ligand binding assay. Red curves indicate 95 % confidence interval. (f) NanoBIT assay ( $\kappa$ OR /  $\kappa$ Light1.3 or  $\delta$ OR /  $\delta$ Light + SmBiT- $\beta$ arr1 + LgBiT-CAAX) measuring  $\beta$ arrestin1 translocation to plasma membrane upon stimulation with 1  $\mu$ M DynA17 (top:  $\kappa$ OR + DynA17 (black),  $\kappa$ OR (gray),  $\kappa$ Light1.3 + DynA17 (blue),  $\kappa$ Light1.3 (light blue), 1  $\mu$ M DynA17 added at 5 min) or 1  $\mu$ M DADLE (bottom:  $\delta$ OR + DADLE (black),  $\delta$ OR (gray),  $\delta$ Light + DADLE (green),  $\delta$ Light (light green), 1  $\mu$ M DADLE added at 5 min), n = 3 for each experiment, error bars represent SEM. (g) GloSensor cAMP assay measuring DynA17 inhibition of forskolin (FSK)-induced cAMP elevation between top:  $\kappa$ OR (black) and  $\kappa$ Light1.3 (blue), n = 5, and bottom:  $\delta$ OR (black) and  $\delta$ Light (green), n = 4, error bars represent SEM.

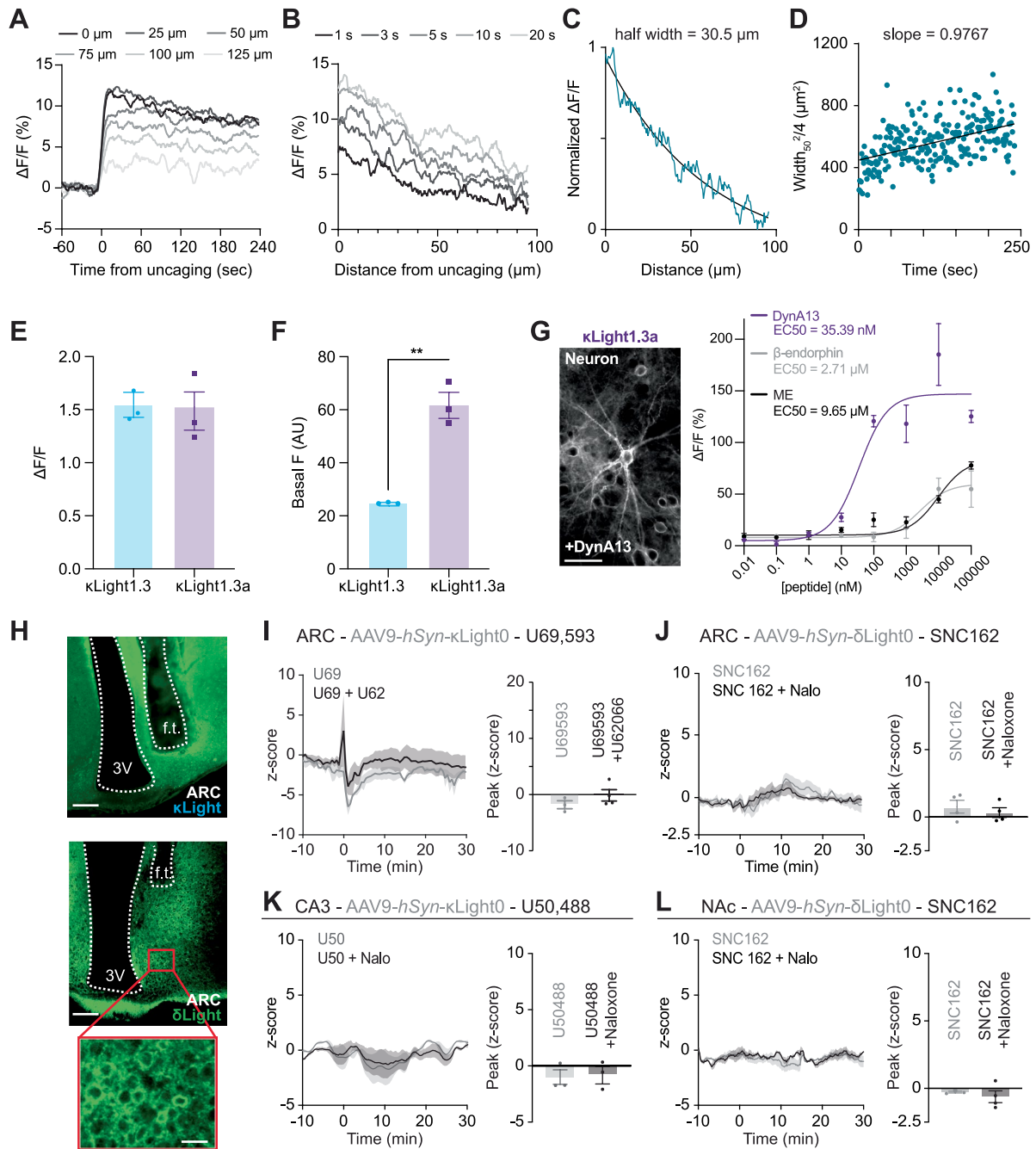


Extended Data Fig. 3 | See next page for caption.

**Extended Data Fig. 3 | Comparison of top  $\kappa$ Light variants and buffering effect study.** (a) Sequence alignment of  $\kappa$ Light1.2a,  $\kappa$ Light1.2b,  $\kappa$ Light1.2c,  $\kappa$ Light1.3, and  $\kappa$ Light1.3a. Purple indicates the same residues across all variants. Blank indicates different residues. Blue color indicates  $\kappa$ OR sequence. Orange indicates linkers. Green indicates cpGFP sequences. Gray indicates the sequence for the ER2 tag. Khaki indicates the sequence for the PRC tag, and magenta indicates the TlcnC tag. (b) (left) CYD8 uncaging response comparison between  $\kappa$ Light1.2a (dark blue,  $n = 12$  videos),  $\kappa$ Light1.2b (black  $n = 9$  videos), and  $\kappa$ Light1.2c (magenta,  $n = 15$  videos) expressed in dStr in acute brain slices. The solid line represents the mean, and the shaded area represents SEM. (right)  $\kappa$ Light1.2a showed faster T1/2 off dynamics compared to  $\kappa$ Light1.3 ( $\kappa$ Light1.3 T1/2 extracted from Fig. 3c,  $137 \pm 14$ ,  $n = 6$ ;  $\kappa$ Light1.2a,  $79 \pm 8.9$ ,  $n = 12$ ;  $\kappa$ Light1.2b,  $301 \pm 101$ ,  $n = 9$ ;  $\kappa$ Light1.2c,  $156 \pm 40$ ,  $n = 15$ ,  $**p = 0.001$ , one-way ANOVA). Error bars represent SEM. (c) Max  $\Delta F/F$  (%) at the peak of the CYD8 uncaging responses for  $\kappa$ Light1.2a (blue,  $n = 24$  videos),  $\kappa$ Light1.2b (black,  $n = 11$  videos), and  $\kappa$ Light1.2c (magenta,  $n = 16$  videos).  $\kappa$ Light1.2a:  $9.09 \pm 0.8\%$ ,  $\kappa$ Light1.2b:  $5.1 \pm 0.5\%$ ,  $\kappa$ Light1.2c:  $6.84 \pm 0.7\%$ .  $**p = 0.0027$ , ordinary one-way ANOVA with Dunnett's multiple comparisons test. Error bars represent SEM. (d) Dose response curves for DynA13 at  $\kappa$ Light1.2a (dark blue,  $n = 3$  wells,  $EC_{50} = 366$  nM),  $\kappa$ Light1.2b (black,  $n = 5$  wells,  $EC_{50} = 306$  nM),  $\kappa$ Light1.2c (magenta,  $n = 4$  wells,  $EC_{50} = 234$  nM), and reused  $\kappa$ Light1.3 trace from Fig. 1e (blue,  $n = 4$  wells,  $0.0898$  nM). Error bars represent SEM. (e) Schematic indicating injection of C57/B6J pups with AAV1-*hSyn*- $\kappa$ Light1.2a or AAV-DJ-CAG-GFP in the hippocampus followed by 3 weeks of expression prior to preparation of acute brain slices for electrophysiology. (f) Schematic of the electrophysiological recording configuration. Whole-cell voltage-clamp recordings are obtained from pyramidal cells (PCs) held at 0 mV

while parvalbumin (PV) basket cell axons are preferentially stimulated with a narrow-tipped theta-glass-based bipolar stimulating electrode. Two electrical stimuli are applied 50 ms apart to drive synaptic inhibition. A 5 ms flash of 355 nm light (semitransparent purple circle) is applied to photorelease DynA8, which acts on presynaptic mu and delta opioid receptors on the PV cell to suppress the synaptic output. (g) Example inhibitory post-synaptic currents (IPSCs) before (black) and after (purple) DynA8 photorelease. (h) Time-course of IPSC suppression in response to DynA8 photorelease in slices expressing  $\kappa$ Light1.2a ( $n = 13$  cells from 3 mice, green) or GFP ( $n = 10$  cells from 3 mice, black) using different intensities of UV light. Traces indicate the mean peak IPSC (normalized to 100%) over time, which was probed every 20 sec. Purple arrows indicate the application of UV light. The solid lines represent the mean, and the shaded areas represent SEM. (i) Power-response curve summarizing the fraction of the baseline IPSC suppressed by DynA8 photorelease in slices expressing  $\kappa$ Light1.2a ( $n = 13$  cells from 3 mice, green) or GFP ( $n = 10$  cells from 3 mice, black). No significant differences were detected at different power densities (Two tailed multiple Mann-Whitney tests between GFP and  $\kappa$ Light1.2a at different power densities:  $0.13 \mu W/\mu m^2$ :  $p = 0.91$ ,  $0.51 \mu W/\mu m^2$ :  $p = 0.71$ ,  $0.89 \mu W/\mu m^2$ :  $p = 0.71$ ,  $11 \mu W/\mu m^2$ :  $p = 0.70$ , non-significant). (j) Average time constant of IPSC recovery after DynA8 photorelease in slices expressing  $\kappa$ Light1.2a ( $n = 3$  mice, green) or GFP ( $n = 3$  mice, black). No significant differences were detected (Two tailed multiple Mann-Whitney tests between GFP and  $\kappa$ Light1.2a at different power densities:  $0.51 \mu W/\mu m^2$ :  $\kappa$ Light1.2a  $n = 10$  cells, GFP  $n = 5$  cells,  $p = 0.52$ ;  $0.89 \mu W/\mu m^2$ :  $\kappa$ Light1.2a  $n = 11$  cells, GFP  $n = 9$  cells,  $p = 0.04$ ;  $11 \mu W/\mu m^2$ :  $\kappa$ Light1.2a  $n = 11$  cells, GFP  $n = 10$  cells,  $p = 0.56$ , non-significant). Error bars represent SEM.

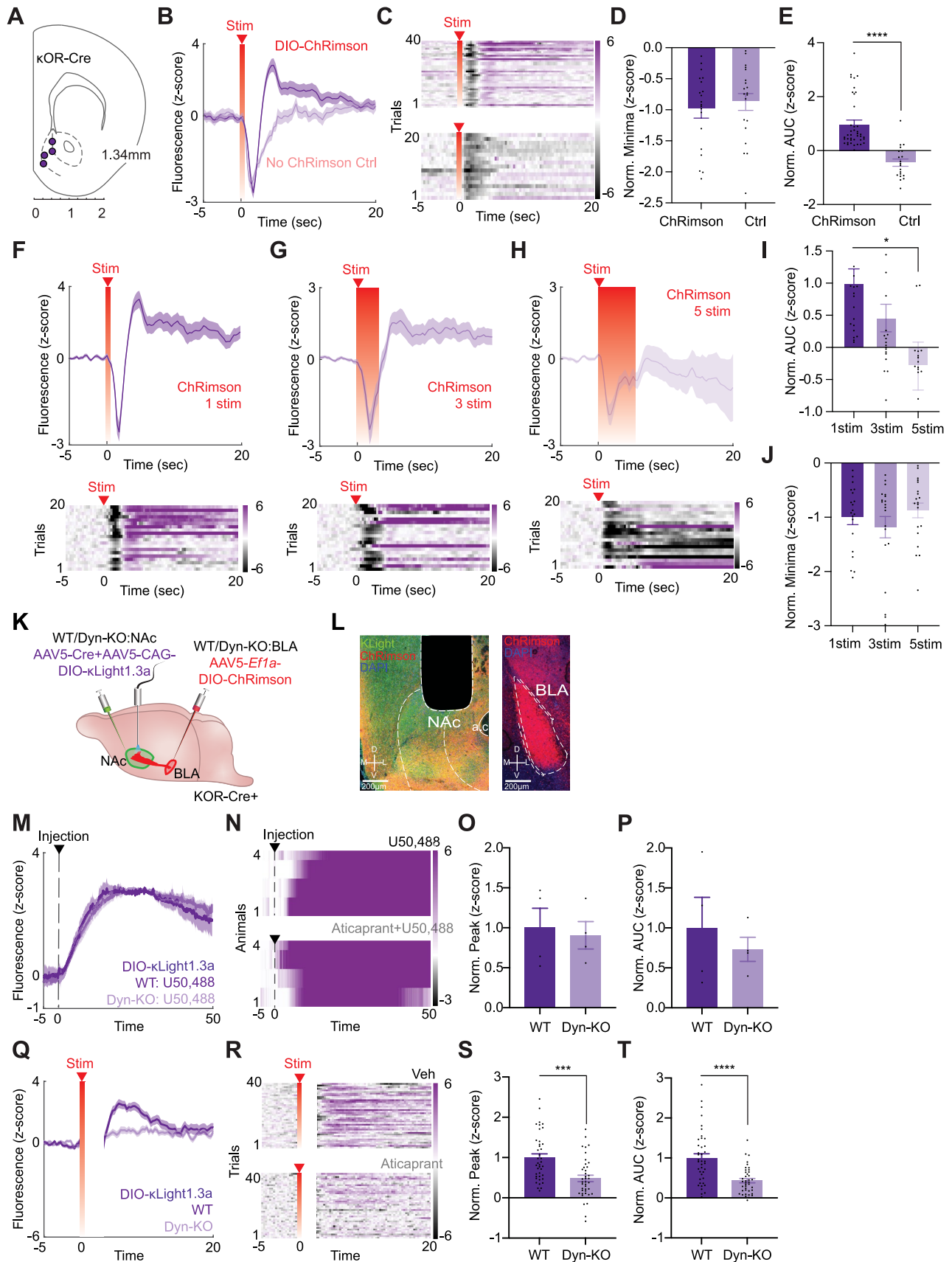




Extended Data Fig. 4 | See next page for caption.

**Extended Data Fig. 4 | Dynorphin diffusion analysis and in vivo pharmacology with control sensors.** (a) Representative example of the fluorescence response of  $\kappa$ Light1.2a for single pixels along the center of the imaging field at various distances from the site of DynA8 photorelease. (b) Representative examples of fluorescence profile as a function of distance from the uncaging site at differing time points after uncaging. (c) Representative example of a fluorescence profile at a single time (5 sec, as in Extended Data Fig. 4b), normalized and fit to an exponential function in order to extract the half width (30.5  $\mu$ m). (d) Representative plot of the half-width squared/4 vs. time for determination of the apparent diffusion coefficient  $D^*$ . The fluorescence profile fits (for example Extended Data Fig. 4c) were repeated in 1 second time bins to extract the half-width. The slope of this linear regression is the apparent diffusion coefficient  $D^*$ . (e) Fluorescence response ( $\Delta F/F$ ) to U50,488 (100  $\mu$ M) compared between  $\kappa$ Light1.3 (blue,  $n = 3$  wells), and  $\kappa$ Light1.3a (magenta,  $n = 3$  wells).  $\kappa$ Light1.3:  $1.56 \pm 0.12$ ,  $\kappa$ Light1.3a:  $1.474 \pm 0.18$ , two tailed unpaired t test,  $p = 0.724$ , non-significant. Error bar represents SEM. (f) Basal fluorescence compared between  $\kappa$ Light1.3 (blue,  $n = 3$  wells), and  $\kappa$ Light1.3a (magenta,  $n = 3$  wells).  $\kappa$ Light1.3:  $25.0 \pm 0.08$ ,  $\kappa$ Light1.3a:  $61.01 \pm 4.49$ , two tailed unpaired t test,  $**p = 0.0013$ . Error bar represents SEM. (g) (Left) representative imaging showing  $\kappa$ Light1.3a-expressing dissociated hippocampal neurons, scale bar 50  $\mu$ m. (Right)  $\kappa$ Light1.3a-expressing dissociated hippocampal neurons respond to ligands in a concentration-dependent manner (DynA13 – magenta,  $\beta$ -endorphin – gray, ME – black). Error bars represent SEM.  $n = 4$  wells each. Dyn = dynorphin, ME = met-enkephalin. (h) Representative images showing  $\kappa$ Light (top),  $\delta$ Light (middle), and zoomed-in image for  $\delta$ Light (bottom) expression in ARC.

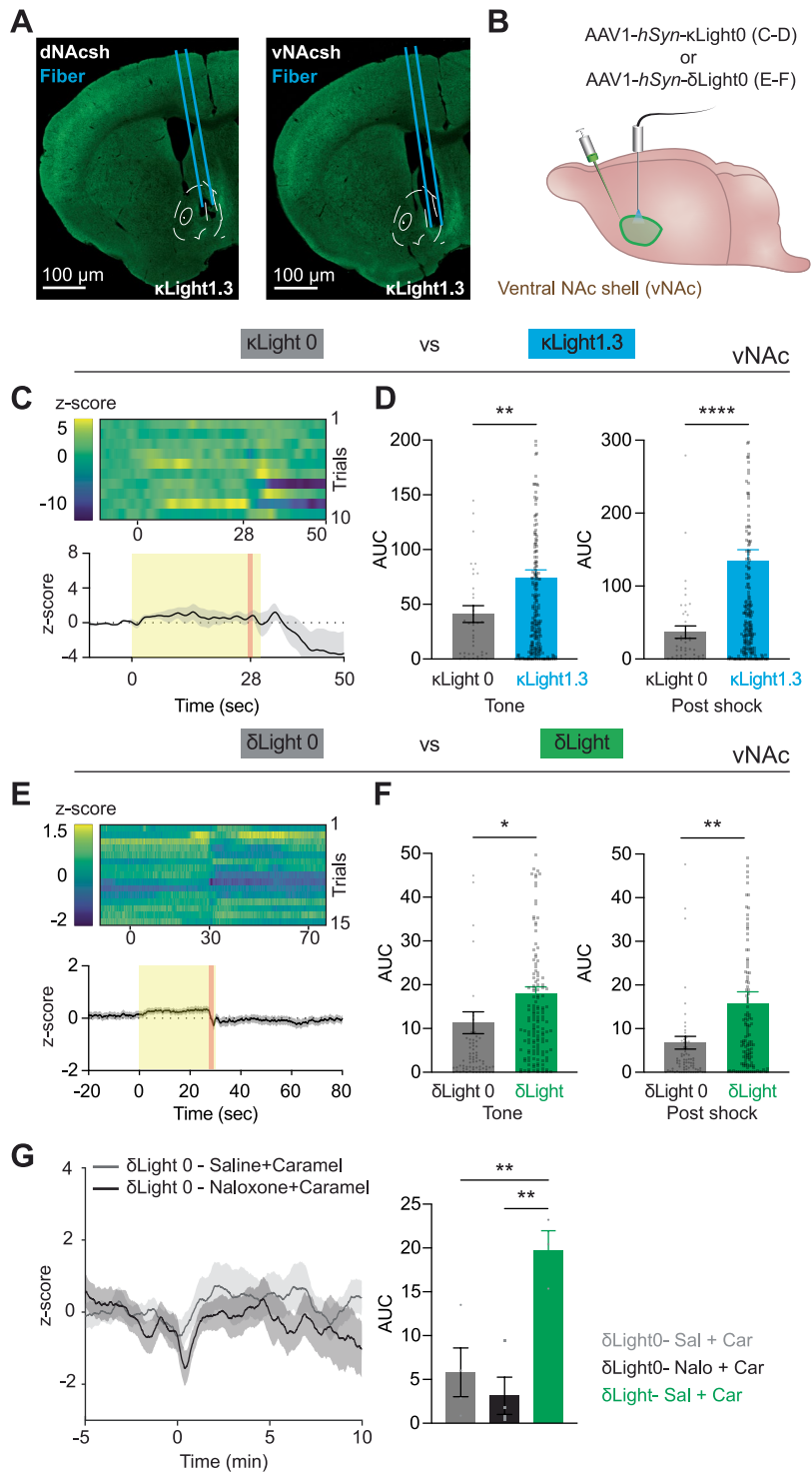
Scale bar 150  $\mu$ m for both  $\kappa$ Light and  $\delta$ Light.  $\delta$ Light zoomed insert has scale bar = 30  $\mu$ m. Abbreviations: ventricle (3 V), fiber track (f.t.). (i) (Left)  $\kappa$ Light0 response to 3 mg/kg U69,593 (gray,  $n = 3$  animals), and 3 mg/kg U69,593 + 1 mg/kg U62,066 (black,  $n = 4$  animals) in ARC. Solid lines represent the mean, and shaded areas represent SEM. (Right) bar graph indicating the peak z-score of each response, U69,593:  $-1.9 \pm 0.7\%$ , U69,593 + U62,066:  $-0.2 \pm 1\%$ , unpaired t test,  $p = 0.2625$ , non-significant. U69 = U69,593, U62 = U62,066. Error bars represent SEM. (j) (Left)  $\delta$ Light0 response to 5 mg/kg SNC162 (gray,  $n = 4$  animals), and 5 mg/kg SNC162 + 4 mg/kg naloxone (black,  $n = 4$  animals) in ARC. Solid lines represent the mean, and shaded areas represent SEM. (Right) bar graph indicating the peak z-score of each response, SNC162:  $0.77 \pm 0.5\%$ , SNC162 + naloxone:  $0.33 \pm 0.4\%$ , unpaired t test,  $p = 0.4948$ , non-significant. Nalo = Naloxone. Error bars represent SEM. (k) (Left)  $\kappa$ Light0 response to 10 mg/kg U50,488 (gray,  $n = 3$  animals), and 10 mg/kg U50,488 + 10 mg/kg naloxone (black,  $n = 3$  animals) in CA3. Solid lines represent the mean, and shaded areas represent SEM. (Right) bar graph indicating the peak z-score of each response, U50,488:  $-1 \pm 0.7\%$ , U50,488 + naloxone:  $-0.75 \pm 0.8\%$ , two tailed unpaired t test,  $p = 0.8123$ , non-significant. U50 = U50,488, Nalo = Naloxone. Error bars represent SEM. (l) (Left)  $\delta$ Light0 response to 5 mg/kg SNC162 (gray,  $n = 4$  animals), and 5 mg/kg SNC162 + 4 mg/kg naloxone (black,  $n = 3$  animals) in ARC. Solid lines represent the mean, and shaded areas represent SEM. (Right) bar graph indicating the peak z-score of each response, SNC162:  $-0.61 \pm 0.4\%$ , SNC162 + naloxone:  $-0.27 \pm 0.07\%$ , two tailed unpaired t test,  $p = 0.5451$ , non-significant. Nalo = Naloxone. Error bars represent SEM.



Extended Data Fig. 5 | See next page for caption.

**Extended Data Fig. 5 | Controls for in vivo fiber photometry with optogenetics and other stimulation parameters.** (a) Coronal brain schematic showing photometry fiber placements in the NAcSh of  $\kappa$ OR-Cre<sup>+</sup> mice. (b) Mean recorded  $\kappa$ Light1.3a fluorescence averaged across all stimulation-evoked trials in ChRimson-injected (dark purple;  $n = 4$  mice) or control mice (light purple;  $n = 2$  mice). Solid lines represent the mean, and shaded areas represent SEM. (c) Heatmap raster plot of recorded  $\kappa$ Light1.3a fluorescence averaged across all stimulation-evoked trials in ChRimson-injected (top;  $n = 4$  mice) or control mice (bottom;  $n = 2$  mice). (d) Normalized fluorescence minima during all stimulation-evoked trials (0-20 sec; ChRimson -  $n = 4$  animals:  $-1 \pm 0.14$ , Control -  $n = 2$  animals:  $-0.87 \pm 0.14$ , two tailed unpaired t test,  $p = 0.51$ , non-significant). Data represented as mean  $\pm$  SEM. (e) Normalized fluorescence area under the curve of single trails during all stimulation-evoked trials (0-20 sec; ChRimson -  $n = 4$  animals:  $0.98 \pm 0.15$ , Control -  $n = 2$  animals:  $-0.45 \pm 0.13$ , two tailed unpaired t test, \*\*\*\* $p < 0.0001$ ). Data represented as mean  $\pm$  SEM. (f) Mean trace and heatmap raster plot of recorded  $\kappa$ Light1.3a fluorescence averaged across all 1 second stimulation-evoked trials in ChRimson-injected mice ( $n = 4$  animals). Stim indicates the time of stimulus application. Solid lines represent the mean, and shaded areas represent SEM. (g) Mean trace and heatmap raster plot of recorded  $\kappa$ Light1.3a fluorescence averaged across all 3 second stimulation-evoked trials in ChRimson-injected mice ( $n = 4$  animals). Stim indicates the time of stimulus application. Solid lines represent the mean, and shaded areas represent SEM. (h) Mean trace and heatmap raster plot of recorded  $\kappa$ Light1.3a fluorescence averaged across all 5 second stimulation-evoked trials in ChRimson-injected mice ( $n = 4$  animals). Stim indicates the time of stimulus application. Solid lines represent the mean, and shaded areas represent SEM. (i) Normalized fluorescence area under the curve of single trails during all stimulation-evoked trials (0-20 sec; 1 stim (dark purple):  $1 \pm 0.22$ , 3 stim (medium purple):  $0.46 \pm 0.22$ , 5 stim (light purple):  $-0.29 \pm 0.37$ , ordinary one-way ANOVA with Dunnett's multiple comparisons test, \* $p = 0.0167$ ,  $n = 4$  animals). Data represented as mean  $\pm$  SEM. (j) Normalized fluorescence minima during all stimulation-evoked trials (0-20 sec; 1 stim (dark purple):  $-1 \pm 0.14$ , 3 stim (medium purple):  $-1.18 \pm 0.2$ , 5 stim (light purple):  $-0.87 \pm 0.14$ , ordinary one-way ANOVA with

Dunnett's multiple comparisons test,  $p > 0.05$ ,  $n = 4$  animals). Data represented as mean  $\pm$  SEM. (k) Schematic of viral injection sites for  $\kappa$ Light1.3a into NAcSh and ChRimson into BLA of WT or DYN-KO mice. (l) Representative 20X coronal image (left panel) showing expression of  $\kappa$ Light1.3a (green), ChRimson (red), DAPI (blue), and fiber placement in NAcSh (left; scalebar - 200  $\mu$ m), and ChRimson (red) and DAPI (blue) in BLA (right; scalebar - 200  $\mu$ m) from 6 animals and showed similar results. (m) Mean recorded  $\kappa$ Light1.3a activity averaged across all animals following i.p injections of U50,488 in WT (dark;  $n = 4$  animals) and DYN-KO (light;  $n = 4$  animals). Solid lines represent the mean, and shaded areas represent SEM. (n) Heatmap raster plot of recorded  $\kappa$ Light1.3a activity averaged across all animals following i.p injections of U50,488 in WT (dark;  $n = 4$  animals) and DYN-KO (light;  $n = 4$  animals) displayed in animal ascending order by average activity following injection. (o) Normalized peak fluorescence during injection period (0-50 min; WT:  $1 \pm 0.24$ , DYN-KO:  $0.9 \pm 0.17$ ; two tailed paired t test,  $p = 0.8078$ ,  $n = 4$  animals). Data represented as mean  $\pm$  SEM. U50 = U50,488. (p) Normalized fluorescence area under the curve of single trails during injection period (0-50 min; WT:  $1 \pm 0.38$ , DYN-KO:  $0.73 \pm 0.3$ ; two tailed paired t test,  $p = 0.6123$ ,  $n = 4$  animals). Data represented as mean  $\pm$  SEM. U50 = U50,488. (q) Mean recorded  $\kappa$ Light1.3a activity averaged across all trials during ChRimson stimulation-evoked trials in WT and DYN-KO ( $n = 4$  animals). Solid lines represent the mean, and shaded areas represent SEM. Stim indicates the time of stimulus application. (r) Heatmap raster plot of recorded  $\kappa$ Light1.3a activity averaged across all trials during ChRimson stimulation-evoked trials in WT and DYN-KO ( $n = 4$  animals) displayed in ascending trial order by average activity across trials. Stim indicates the time of stimulus application. (s) Normalized peak fluorescence across vehicle and aticaprant treatment during all ChRimson stimulation-evoked trials (0-20 sec; WT:  $1 \pm 0.09$ , DYN-KO:  $0.48 \pm 0.08$ ; two tailed paired t test, \*\*\*\* $p = 0.0004$ ,  $n = 4$  animals). Data represented as mean  $\pm$  SEM. (t) Normalized fluorescence area under the curve of single trails across vehicle and aticaprant treatment during all ChRimson stimulation-evoked trials (0-20 sec; WT:  $1 \pm 0.1$ , DYN-KO:  $0.43 \pm 0.05$ ; two tailed paired t test, \*\*\*\* $p < 0.0001$ ,  $n = 4$  animals). Data represented as mean  $\pm$  SEM.



Extended Data Fig. 6 | See next page for caption.

**Extended Data Fig. 6 | In vivo fiber photometry during aversive and rewarding behaviors with control sensors.**

**(a)** Representative images indicating  $\kappa$ Light1.3 expression in dNacsh from 7 animals (left) and vNacsh from 8 animals (right) showing similar results. Blue lines indicate the fiber tract. Scale bar = 100  $\mu$ m. **(b)** Experimental schematic indicating injection of  $\kappa$ Light0 and  $\delta$ Light0 into vNac individually, followed by fear conditioning protocol (30 sec tone, co-terminated with 1.5 sec shock, as described in Fig. 6a), recorded with fiber photometry. **(c)**  $\kappa$ Light0 response in vNac: (Top) Sorted shock trials averaged across animals from top to bottom in chronological order (trial 1 at the top, trial 10 at the bottom). (Bottom) Average trace of  $\kappa$ Light0 response (black) during fear conditioning, tone (0–30 sec, yellow shade), shock, (27.5–29 sec, orange). Solid line represents the mean, and shaded areas represent SEM.  $n = 5$  animals. **(d)** Area under the curve of single trails in (Extended Data Fig. 6c) and (Fig. 6c) during tone and post-shock. Tone AUC  $\kappa$ Light0 (gray):  $41 \pm 7.6$ , tone AUC  $\kappa$ Light1.3 (blue):  $74 \pm 7$ , two tailed unpaired t test,  $**p = 0.0016$ . Post-shock AUC  $\kappa$ Light0 (gray):  $37 \pm 8.5$ , post-shock AUC  $\kappa$ Light1.3 (blue):  $135 \pm 15$ , two tailed unpaired t test,  $****p = 0.0001$ .  $\kappa$ Light1.3 bar graph data reused from Fig. 6d. Error bars represent SEM. Plotted and compared all single trial AUCs for tone (0–25 sec) and post-shock (30–70 sec) from  $n = 5$  animals for  $\kappa$ Light0 and  $n = 8$  animals for  $\kappa$ Light1.3. **(e)**  $\delta$ Light0 response in vNac: (Top) Sorted shock trials averaged across animals from top to down in chronological order (trial 1 at the

top, trial 15 at the bottom). (Bottom) Average trace of  $\delta$ Light response (black) during fear conditioning, tone (0–30 sec, yellow shade), shock, (27.5–29 sec, orange). Solid line represents the mean, and shades represent SEM.  $n = 5$  animals. **(f)** Area under the curve of single trails in (Extended Data Fig. 6e) and (Fig. 6f) during tone and post-shock. Tone AUC  $\delta$ Light0 (gray):  $11 \pm 2.5$ , tone AUC  $\delta$ Light (green):  $18 \pm 1.5$ , two tailed unpaired t test,  $*p = 0.025$ . Post-shock AUC  $\delta$ Light0 (gray):  $6.8 \pm 1.5$ , post-shock AUC  $\delta$ Light (green):  $16 \pm 2.7$ , two tailed unpaired t test,  $**p = 0.0034$ .  $\delta$ Light bar graph data reused from Fig. 6g. Error bars represent SEM. Plotted and compared all single trial AUCs for tone (0–25 sec) and post-shock (30–70 sec) from  $n = 5$  animals for  $\delta$ Light0 and  $n = 5$  animals for  $\delta$ Light. **(g)** (Left) Averaged  $\delta$ Light0 fluorescence upon caramel retrieval after injection of saline (gray) or 4 mg/kg naloxone (black) ( $n = 4$  animals). Solid lines represent the mean, and shaded areas represent SEM. (Right) Area under the curve of single trails between  $\delta$ Light0-saline,  $\delta$ Light0-naloxone, and  $\delta$ Light-saline conditions,  $\delta$ Light0-saline (gray):  $5.8 \pm 2.8$ ,  $\delta$ Light0-naloxone (black):  $3.1 \pm 2.1$ ,  $\delta$ Light-saline (green):  $20 \pm 2.3$ ,  $\delta$ Light-saline vs  $\delta$ Light0-saline  $**p = 0.0088$ ,  $\delta$ Light-saline vs  $\delta$ Light0-naloxone  $**p = 0.0032$ , ordinary one-way ANOVA with Dunnett's multiple comparisons test.  $\delta$ Light-saline bar graph data reused from Fig. 6k. Error bars represent SEM. Abbreviations: saline (Sal), naloxone (Nalo), caramel (Car).

Extended Data Table 1 | Drug activation and affinity parameters in κLight, δLight, and μLight cells

| Compound       | κLight       |          | δLight        |          | μLight       |          |
|----------------|--------------|----------|---------------|----------|--------------|----------|
|                | ΔF/F max (%) | EC50 (M) | ΔF/F max (%)  | EC50 (M) | ΔF/F max (%) | EC50 (M) |
| β-endorphin    | 126.9±8.55   | 1.77E-06 | 147.9±4.07    | 4.18E-07 | 54.9±2.78    | 1.61E-06 |
| BAM18          | 99.5±1.70    | 3.56E-08 | 155.0±1.73    | 1.82E-07 | 13.2±2.17    | 1.86E-07 |
| β-neoendorphin | 92.0±1.40    | 2.59E-08 | 157.5±3.66    | 3.31E-08 | 14.2±4.45    | 6.31E-06 |
| Buprenorphin   | 58.6±3.31    | 1.58E-08 | 253.8±29.88   | 8.10E-10 | -8.3±1.63    | 7.34E-11 |
| DAMGO          | 52.9±2.09    | 1.34E-06 | 101.5±22.50   | 1.51E-05 | 50.5±1.95    | 5.05E-07 |
| Deltorhin I    | 37.8±7.27    | 2.17E-09 | 253.8±29.88   | 7.36E-09 | 43.1±9.43    | 7.38E-06 |
| DPDPE          | 20.5±1.67    | 1.66E-10 | 17.1±4.08     | 1.93E-10 | n/a          | n/a      |
| DynA17         | 94.0±6.42    | 9.20E-10 | 167.4±3.65    | 1.96E-07 | n/a          | n/a      |
| DynA13         | 93.6±3.93    | 8.98E-11 | 232.6 ± 6.82  | 2.13E-07 | 45.6 ± 0.83  | 3.74E-06 |
| DynA8          | 112.6±2.21   | 1.05E-08 | 231.6 ± 15.57 | 1.97E-08 | 24.8 ± 0.63  | 6.51E-06 |
| DynB9          | 177.2±3.94   | 1.00E-08 | 217.1±20.88   | 1.99E-08 | 42.3±3.28    | 3.76E-06 |
| Endomorphin I  | 41.7±6.31    | 4.96E-08 | 11.6±1.074    | 1.75E-10 | 26.6±4.37    | 1.01E-07 |
| Fentanyl       | 103.9±11.88  | 2.09E-07 | 134.1±5.97    | 6.00E-07 | 13.9±2.20    | 3.58E-08 |
| LE             | 95.9±3.55    | 5.01E-06 | 214.9±5.53    | 7.22E-09 | 27.0±3.68    | 2.84E-06 |
| ME             | 80.3±1.79    | 6.64E-06 | 246.1±4.56    | 6.58E-09 | 40.0±1.55    | 4.27E-07 |
| Methadone      | 149.9±2.96   | 6.79E-06 | 146.7±3.20    | 1.80E-05 | 26.7±5.31    | 3.77E-06 |
| Metorpinimide  | 105.3±8.15   | 1.52E-08 | 161.3±2.69    | 9.55E-08 | 40.9±1.55    | 6.39E-08 |
| Morphine       | 40.1±2.78    | 3.77E-08 | 26.7±1.25     | 1.18E-10 | n/a          | n/a      |
| Nalfurafine    | 199.4±25.33  | 9.61E-12 | 39.7±3.24     | 3.22E-10 | -12.8±1.33   | 1.16E-09 |
| Oxycodone      | 34.5±4.44    | 1.08E-08 | 45.0±6.45     | 6.97E-08 | -12.8±2.78   | 1.59E-11 |
| SNC162         | 12.2±2.39    | 8.28E-06 | 152.1±5.20    | 1.03E-08 | 2.9±1.69     | 8.73E-08 |
| SNC80          | 42.4±3.39    | 6.65E-09 | 209.4±5.29    | 1.82E-07 | 38.8±0       | 1.52E-06 |
| U50,488        | 189.7±2.79   | 5.29E-08 | 36.1±0.87     | 4.1E-5   | 13.4±1.61    | 1.08E-05 |
| U69,593        | 163.4±4.97   | 2.78E-07 | 23.9±1.59     | 2.14E+10 | 30.8±9.63    | 2.43E-12 |

Dose-response assays from (1pM–100μM) of each compound screened on κLight, δLight, μLight stable cell lines. ΔF/F max values are sensor responses at 100μM of each compound. EC50 values were calculated with the mean of ΔF/F values at each concentration of compounds. Data are represented by mean±SEM, n/a = not applicable.

Extended Data Table 2 | Displacement binding parameters in κLight, δLight, and μLight cells

| Compound       | κLight                |                  | δLight                |                  | μLight                |                  |
|----------------|-----------------------|------------------|-----------------------|------------------|-----------------------|------------------|
|                | IC <sub>50</sub> [nM] | % bound at 10 μM | IC <sub>50</sub> [nM] | % bound at 10 μM | IC <sub>50</sub> [nM] | % bound at 10 μM |
| ME             | 130±3                 | 10±5             | 947±1                 | 77±4             | 2±2                   | 77±3             |
| LE             | 14±3                  | 13±8             | 343±1                 | 65±3             | 67±2                  | 70±2             |
| β-endorphin 31 | 81±2                  | 62±4             | 2±2                   | 59±2             | 12±4                  | 46±3             |
| DynA8          | 1±2                   | 71±3             | 222±1                 | 51±3             | 48±2                  | 58±2             |
| DynA17         | 47±2                  | 74±4             | 47±2                  | 47±2             | 15±2                  | 60±2             |
| DynB13         | 6±2                   | 76±2             | 178±2                 | 58±4             | 10±2                  | 61±2             |
| Metorphamide   | 13±2                  | 28±3             | 56±1                  | 53±3             | 1490±2                | 40±3             |
| BAM 18         | 243±2                 | 66±3             | 32±3                  | 32±3             | 14±2                  | 82±2             |
| Peptide E      | 252±2                 | 40±2             | 2278±2                | 51±7             | 154±2                 | 65±2             |
| Peptide F      | 18±3                  | 21±6             | 901±2                 | 40±4             | 13±3                  | 34±2             |
| α-neoendorphin | 6±3                   | 42±4             | n.t.                  | n.t.             | n.t.                  | n.t.             |
| β-neoendorphin | 13±2                  | 25±5             | n.t.                  | n.t.             | n.t.                  | n.t.             |
|                |                       |                  |                       |                  |                       |                  |
| DAMGO          | n.t.                  | n.t.             | n.t.                  | n.t.             | 2±2                   | 79±3             |
| Morphine       | n.t.                  | n.t.             | n.t.                  | n.t.             | 2249±2                | 77±2             |
| Oxycodone      | n.t.                  | n.t.             | n.t.                  | n.t.             | 103±2                 | 32±3             |
| Fentanyl       | n.t.                  | n.t.             | n.t.                  | n.t.             | 2587±2<br>1±2*        | 62±3<br>88±4*    |
|                |                       |                  |                       |                  |                       |                  |
| Deltorphan II  | n.t.                  | n.t.             | 53±2                  | 72±2             | n.t.                  | n.t.             |
| DPDPE          | n.t.                  | n.t.             | 215±2                 | 83±2             | n.t.                  | n.t.             |
| SNC80          | n.t.                  | n.t.             | 246±2                 | 88±3             | n.t.                  | n.t.             |
|                |                       |                  |                       |                  |                       |                  |
| U69,593        | 110±2                 | 72±2             | n.t.                  | n.t.             | n.t.                  | n.t.             |

Displacement binding assays were carried out with membranes (100 μg) from μLight, δLight or κLight cells, [<sup>3</sup>H] diprenorphine (3 nM final concentration) and different ligands (0- 10 μM final concentration) as described in Methods. Data are Mean±SE of 3 experiments in triplicate. Binding in the absence of cold ligand was taken as 100% bound. Binding in the presence of 10 μM ligand was taken as non-specific binding. % Specific binding at 10 μM = Total binding – non-specific binding. n.t.= not tested. \* Displacement binding assays were carried out with CHO-MOR membranes (100 μg).



## Reporting Summary

Nature Portfolio wishes to improve the reproducibility of the work that we publish. This form provides structure for consistency and transparency in reporting. For further information on Nature Portfolio policies, see our [Editorial Policies](#) and the [Editorial Policy Checklist](#).

### Statistics

For all statistical analyses, confirm that the following items are present in the figure legend, table legend, main text, or Methods section.

- | n/a                                 | Confirmed  |
|-------------------------------------|--|
| <input type="checkbox"/>            | <input checked="" type="checkbox"/> The exact sample size ( $n$ ) for each experimental group/condition, given as a discrete number and unit of measurement  |
| <input type="checkbox"/>            | <input checked="" type="checkbox"/> A statement on whether measurements were taken from distinct samples or whether the same sample was measured repeatedly  |
| <input type="checkbox"/>            | <input checked="" type="checkbox"/> The statistical test(s) used AND whether they are one- or two-sided<br><i>Only common tests should be described solely by name; describe more complex techniques in the Methods section.</i>   |
| <input checked="" type="checkbox"/> | <input type="checkbox"/> A description of all covariates tested  |
| <input type="checkbox"/>            | <input checked="" type="checkbox"/> A description of any assumptions or corrections, such as tests of normality and adjustment for multiple comparisons  |
| <input type="checkbox"/>            | <input checked="" type="checkbox"/> A full description of the statistical parameters including central tendency (e.g. means) or other basic estimates (e.g. regression coefficient) AND variation (e.g. standard deviation) or associated estimates of uncertainty (e.g. confidence intervals) |
| <input type="checkbox"/>            | <input checked="" type="checkbox"/> For null hypothesis testing, the test statistic (e.g. $F$ , $t$ , $r$ ) with confidence intervals, effect sizes, degrees of freedom and $P$ value noted<br><i>Give <math>P</math> values as exact values whenever suitable.</i>                            |
| <input checked="" type="checkbox"/> | <input type="checkbox"/> For Bayesian analysis, information on the choice of priors and Markov chain Monte Carlo settings  |
| <input checked="" type="checkbox"/> | <input type="checkbox"/> For hierarchical and complex designs, identification of the appropriate level for tests and full reporting of outcomes  |
| <input checked="" type="checkbox"/> | <input type="checkbox"/> Estimates of effect sizes (e.g. Cohen's $d$ , Pearson's $r$ ), indicating how they were calculated  |

*Our web collection on [statistics for biologists](#) contains articles on many of the points above.*

### Software and code

Policy information about [availability of computer code](#)

**Data collection** We have provided a code availability statement. Fiber photometry data collected by Doric Neuroscience Studio V5.4.1.12, Fear behaviors are controlled by Video Freeze V3.0.0.0, Microconfocal HEK cell imaging data was collected by MetaXpress V6.6.3.55, two-photon data was collected by ScanImage 5 run by Matlab R2013b.

**Data analysis** GraphPad Prism 9, Matlab R2022a, and Jupyter Notebook 6.4.6, ImageJ Version:2.1.0/1.53c. Microsoft Excel 16.72, Illustrator 2024. All custom MATLAB codes are available from <https://github.com/lintianlab/OpioidSensors/tree/main/1-Codes>.

For manuscripts utilizing custom algorithms or software that are central to the research but not yet described in published literature, software must be made available to editors and reviewers. We strongly encourage code deposition in a community repository (e.g. GitHub). See the Nature Portfolio [guidelines for submitting code & software](#) for further information.

## Data

Policy information about [availability of data](#)

All manuscripts must include a [data availability statement](#). This statement should provide the following information, where applicable:

- Accession codes, unique identifiers, or web links for publicly available datasets
- A description of any restrictions on data availability
- For clinical datasets or third party data, please ensure that the statement adheres to our [policy](#)

The following public dataset were used to support this study: Allen Brain Atlas ISH data (<https://mouse.brain-map.org>). All source data present in this manuscript are available from <https://github.com/lintianlab/OpioidSensors/tree/main/0-SourceData>.

## Research involving human participants, their data, or biological material

Policy information about studies with [human participants or human data](#). See also policy information about [sex, gender \(identity/presentation\), and sexual orientation](#) and [race, ethnicity and racism](#).

|  |     |
|--|-----|
| Reporting on sex and gender  | n/a |
| Reporting on race, ethnicity, or other socially relevant groupings | n/a |
| Population characteristics   | n/a |
| Recruitment  | n/a |
| Ethics oversight   | n/a |

Note that full information on the approval of the study protocol must also be provided in the manuscript.

## Field-specific reporting

Please select the one below that is the best fit for your research. If you are not sure, read the appropriate sections before making your selection.

Life sciences       Behavioural & social sciences       Ecological, evolutionary & environmental sciences

For a reference copy of the document with all sections, see [nature.com/documents/nr-reporting-summary-flat.pdf](https://www.nature.com/documents/nr-reporting-summary-flat.pdf)

## Life sciences study design

All studies must disclose on these points even when the disclosure is negative.

|                 |  |
|-----------------|--|
| Sample size     | No statistical methods were used to predetermine sample size. However, sample sizes are consistent with those reported in previous publications (35,54-60).  |
| Data exclusions | No data were excluded from this study  |
| Replication     | Each and every experiment was performed with at least n = 3 biological independent cultures or animal subjects. Sample size for each experiment is indicated in the figure legends. All attempts were successful.  |
| Randomization   | Animals and cultures were randomly assigned for transduction and transfection with the different constructs described in the manuscript. Drug testing on stable cell lines are randomly chosen wells on imaging plates to ensure each biological replicates have no plate location influence on results.   |
| Blinding        | Drug screening experiments are done with two person. One prepare the compound treatment plates, and the other do the imaging blindly. Data analysis were done with matlab script to analyze uniformly for data generation. In vivo experiments are done blindly without knowing which animal is expressing which construct until the data is analyzed. |

## Reporting for specific materials, systems and methods

We require information from authors about some types of materials, experimental systems and methods used in many studies. Here, indicate whether each material, system or method listed is relevant to your study. If you are not sure if a list item applies to your research, read the appropriate section before selecting a response.

## Materials &amp; experimental systems

| n/a                                 | Involvement   |
|-------------------------------------|---|
| <input checked="" type="checkbox"/> | <input type="checkbox"/> Antibodies                             |
| <input type="checkbox"/>            | <input checked="" type="checkbox"/> Eukaryotic cell lines       |
| <input checked="" type="checkbox"/> | <input type="checkbox"/> Palaeontology and archaeology          |
| <input type="checkbox"/>            | <input checked="" type="checkbox"/> Animals and other organisms |
| <input checked="" type="checkbox"/> | <input type="checkbox"/> Clinical data                          |
| <input checked="" type="checkbox"/> | <input type="checkbox"/> Dual use research of concern           |
| <input checked="" type="checkbox"/> | <input type="checkbox"/> Plants                                 |

## Methods

| n/a                                 | Involvement                                     |
|-------------------------------------|---|
| <input checked="" type="checkbox"/> | <input type="checkbox"/> ChIP-seq               |
| <input checked="" type="checkbox"/> | <input type="checkbox"/> Flow cytometry         |
| <input checked="" type="checkbox"/> | <input type="checkbox"/> MRI-based neuroimaging |

## Eukaryotic cell lines

Policy information about [cell lines and Sex and Gender in Research](#)

|  |   |
|--|---|
| Cell line source(s)  | HEK293T (ATCC, CRL-3216, <a href="https://www.atcc.org/products/crl-3216">https://www.atcc.org/products/crl-3216</a> ). Three sensor expressing stable cell lines are generated based on HEK293T cells from this study. |
| Authentication   | These cell lines were not authenticated   |
| Mycoplasma contamination   | These cell lines were not tested for mycoplasma contamination.  |
| Commonly misidentified lines<br>(See <a href="#">ICLAC</a> register) | No commonly misidentified cell lines were used in the study   |

## Animals and other research organisms

Policy information about [studies involving animals; ARRIVE guidelines](#) recommended for reporting animal research, and [Sex and Gender in Research](#)

|                         |  |
|-------------------------|--|
| Laboratory animals      | C57/B6J mice (postnatal day 0-3, 8-10 weeks, or 12-16 weeks) were used in this study as described in the manuscript. Adult (25-35 g), 12-16 week old KOR-Cre mice were used for optostimulation experiments. Animals are housed in ventilated home cages with at most five mice per cage. Animals are housed in vivarium with 12 hour light and 12 hour dark standard light cycle, with temperature of 68 – 79 °F and humidity 30 - 70%.   |
| Wild animals            | We did not use wild animals.   |
| Reporting on sex        | Both male and female mice were used in this study.   |
| Field-collected samples | We did not use field-collected samples.  |
| Ethics oversight        | All housing and experimental procedures involving animals were approved by the Institutional Animal Care and Use Committee (IACUC) at the University of California, Davis, the University of California San Diego, the University of Washington, the University of Iowa Cold Spring Harbor Laboratory, the National Institute of Mental Health, or Icahn School of Medicine, and adhered to principles described in the National Institutes of Health Guide for the Care and Use of Laboratory Animals. The University of California, Davis, the University of California San Diego, the University of Washington, the University of Iowa, Cold Spring Harbor Laboratory, the National Institute of Mental Health, and Icahn School of Medicine are accredited by the Association for Assessment and Accreditation of Laboratory Animal Care International (AAALAC). |

Note that full information on the approval of the study protocol must also be provided in the manuscript.